

DRAFT REPORT

# IN-DELTA STORAGE PROGRAM SEISMIC ANALYSIS

*Prepared for*  
Department of Water Resources  
901 P Street  
Sacramento, CA 94236

June 2003

**URS**

URS Corporation  
500 12th Street, Suite 200  
Oakland, CA 94607

26814104

# TABLE OF CONTENTS

---

Section 1	Introduction.....	1-3
	1.1 Purpose.....	1-3
	1.2 Scope of Work .....	1-3
Section 2	Dynamic Response Analysis.....	2-3
	2.1 Data Review.....	2-3
	2.2 Analysis Parameters.....	2-3
	2.2.1 Embankment Cross Sections.....	2-3
	2.2.2 Material Properties.....	2-3
	2.2.3 Reservoir Stages and Slough Water Levels for Analyses.....	2-3
	2.3 Earthquake Loads.....	2-3
	2.3.1 Earthquake Response Spectra.....	2-3
	2.3.2 Spectrally-Matched Time Histories .....	2-3
	2.4 Analysis Results.....	2-3
Section 3	Seismic Stability and Deformation Analysis.....	3-3
	3.1 Methodology.....	3-3
	3.2 Results.....	3-3
	3.2.1 Bench Alternative .....	3-3
	3.2.2 Rock Berm Alternative .....	3-3
Section 4	Estimated Probability of Failure.....	4-3
	4.1 Embankment Fragility Curve.....	4-3
	4.2 Failure Probability .....	4-3
Section 5	Summary and Conclusions .....	5-3
Section 6	References .....	6-3

## Tables

Table 1	Dynamic Soil Parameters Selected for Analysis
Table 2	Summary of Earthquake Records Used in the Dynamic Response Analysis
Table 3	Summary of Calculated Slope Deformations and Failure Probabilities for Cross Section I with Bench Alternative, Peat at -20 Ft (Non-liquefied Case)
Table 4	Summary of Calculated Slope Deformations and Failure Probabilities for Cross Section II with Bench Alternative, Peat at -40 Ft (Non-liquefied Case)
Table 5	Summary of Calculated Slope Deformations and Failure Probabilities for Cross Section I with Bench Alternative, Peat at -20 Ft (Liquefied Case)

# TABLE OF CONTENTS

---

Table 6	Summary of Calculated Slope Deformations and Failure Probabilities for Cross Section II with Bench Alternative, Peat at -40 Ft (Liquefied Case)
Table 7	Summary of Calculated Slope Deformations and Failure Probabilities for Cross Section I with Rock Berm, Peat at -20 Ft (Non-liquefied Case)
Table 8	Summary of Calculated Slope Deformations and Failure Probabilities for Cross Section II with Rock Berm, Peat at -40 Ft (Non-liquefied Case)
Table 9	Summary of Calculated Slope Deformations and Failure Probabilities for Cross Section I with Rock Berm, Peat at -20 Ft (Liquefied Case)
Table 10	Summary of Calculated Slope Deformations and Failure Probabilities for Cross Section II with Rock Berm, Peat at -40 Ft (Liquefied Case)
Table 10A	Summary of Maximum Calculated Deformations, 475-year Earthquake Event
Table 11	Probability of Failure of Cross Section I (Peat at -20 Ft) with Bench Alternative
Table 12	Probability of Failure of Cross Section II (Peat at -40 Ft) with Bench Alternative
Table 13	Probability of Failure of Cross Section I (Peat at -20 Ft) with Rock Berm Alternative
Table 14	Probability of Failure of Cross Section II (Peat at -40 Ft) with Rock Berm Alternative

## Figures

Figure 1	Finite Element Model for Seismic Analysis, Cross Section I (Peat At -20 Ft)
Figure 2	Finite Element Model for Seismic Analysis, Cross Section II (Peat At -40 Ft)
Figure 3	Modulus and Damping Curves for Clay and Peat
Figure 4	Modulus and Damping Curves for Sand
Figure 5	Target Response Spectra for Return Periods of 43, 475 and 2500 Years
Figure 6	Matched Time History for Return Period of 43 Years for 1992 Landers Earthquake at Sta. 24577, 0 Deg. Comp.
Figure 7	Matched Time History for Return Period of 475 Years for 1992 Landers Earthquake at Sta. 24577, 0 Deg. Comp.
Figure 8	Matched Time History for Return Period of 2,500 Years for 1992 Landers Earthquake at Sta. 24577, 0 Deg. Comp.
Figure 9	Matched Time History for Return Period of 43 Years for 1987 Whittier Narrows Earthquake at Sta. 24402, 90 Deg. Comp.
Figure 10	Matched Time History for Return Period of 475 Years for 1987 Whittier Narrows Earthquake at Sta. 24402, 90 Deg. Comp.
Figure 11	Matched Time History for Return Period of 2,500 Years for 1987 Whittier Narrows Earthquake at Sta. 24402, 90 Deg. Comp.
Figure 12	Comparison of Response Spectra for Return Period of 43 Years

# TABLE OF CONTENTS

---

Figure 13	Comparison of Response Spectra for Return Period of 475 Years
Figure 14	Comparison of Response Spectra for Return Period of 2,500 Years
Figure 15	Cross Section I with Bench Alternative (Peat at –20 Ft)
Figure 16	Cross Section II with Bench Alternative (Peat at –40 Ft)
Figure 17	Cross Section I with Rock Berm (Peat at –20 Ft)
Figure 18	Cross Section II with Rock Berm (Peat at –40 Ft)
Figure 19	Average Horizontal Acceleration Time Histories for Sliding Masses, Cross Section I – Non-liquefied Case for Landers Earthquake
Figure 20	Average Horizontal Acceleration Time Histories for Sliding Masses, Cross Section II– Non-liquefied Case for Landers Earthquake
Figure 21	Average Horizontal Acceleration Time Histories for Sliding Masses, Cross Section I – Non-Liquefied Case for Whittier Narrows Earthquake
Figure 22	Average Horizontal Acceleration Time Histories for Sliding Masses, Cross Section II– Non-Liquefied Case for Whittier Narrows Earthquake

## Attachment

1	Earthquake Ground Motion Assessment
---	-------------------------------------

## 1.1 PURPOSE

As part of the feasibility study, the Department of Water Resources requested that URS Corporation (URS) undertake a risk analysis and integrate the physical design with a desirable level of protection through seismic, flooding, operational, environmental and economic analyses. Other objectives were to recommend a desirable level of protection and appropriate factor of safety for the project.

## 1.2 SCOPE OF WORK

The specific scope presented under this Task Order was to address the vulnerability and reliability of the existing conditions and In-Delta Storage Re-engineered project (embankment and integrated facilities) under seismic loads. The work for this Task Order included the evaluation of the existing conditions and the proposed re-engineered reservoir project at Webb Tract and Bacon Island. Specifically, the following subtasks were performed:

- Collected and reviewed existing information.
- Conducted a seismic hazard analysis and evaluated expected ground motions at the reservoir island sites. (The probability seismic hazard analysis is presented in Attachment 1 of this report).
- Performed seismic stability analyses of the existing conditions and the re-engineered project.
- Estimated failure probabilities under seismic loading.

The work was conducted in accordance with all applicable standards and guidelines contained in Standard Agreement No. 4600001747 and in coordination with Department staff.

Dynamic response analyses of the embankments were performed to calculate time histories of seismic-induced inertial force acting on the critical sliding masses. We utilized the computer program QUAD4M (Hudson et al., 1994) for these analyses. QUAD4M is a two-dimensional, plan-strain, finite element code for dynamic response analysis. It uses an equivalent linear procedure (Seed and Idriss, 1970) to model the nonlinear behavior of soils. The softening of the soil stiffness is specified using the shear modulus degradation ( $G/G_{\max}$ ) and damping vs. shear strain curves. QUAD4M also incorporates a compliant base (energy-transmitting base), which can be used to model the elastic half-space.

Our review of the soil data indicates that there are some sections under the perimeter levees where the upper 5 feet of the underlying sand deposits may liquefy during earthquake events. In addition, part of the existing levee, on the island side, may contain loose sands, which have the potential to liquefy when they become saturated during the reservoir filling. One of the consequences of the liquefaction of the loose saturated sand is the reduction in shear resistance along the critical slip surface during earthquake shaking. In the context of this analysis, this translates into lower yield acceleration,  $k_y$ , which in turn, induces larger deformations. Dynamic analyses for both cases involving non-liquefied and liquefied sandy layers were performed. Embankment deformations for these cases were then estimated.

## 2.1 DATA REVIEW

The information from the following studies was reviewed:

- Dynamic Properties of Sherman Island Peat by Boulanger et al. (1997). Report No. UCD/CGM-97/01, Center for Geotechnical Modeling, Department of Civil and Environmental Engineering, University of California at Davis
- Three deep boring logs and geophysical measurements at Webb Tract and Bacon Island obtained from Department of Water Resources
- Nonlinear Dynamic Properties of a Fibrous Organic Soil by Wehling et al. (2001). Paper accepted for publication in ASCE Journal of Geotechnical Engineering
- Seismic Vulnerability of the Sacramento-San Joaquin Delta Levees, December 1998, Calfed Bay-Delta Program, Seismic Vulnerability Sub-Team
- Department of Water Resources, 2002, Draft report on engineering investigations, In-Delta Storage Program, CALFED Bay-Delta Program.

## 2.2 ANALYSIS PARAMETERS

### 2.2.1 Embankment Cross Sections

Two embankment alternatives were considered. The first alternative consists of building the embankment on the island side with a slough-side bench (bench alternative). This alternative results in a relatively off-set embankment from the existing levee, and provides for a flat slough side slope of 4H:1V or flatter. The second alternative consists of building the embankment on the existing levee and placing a rock toe berm on the slough-side slopes with an average slope of 3H:1V (rock berm alternative).

For each of these alternatives, two cross-sections representing the variation in the subsurface conditions were developed for analysis. These cross-sections represent the upper and lower base elevation of the peat underlying the existing levees. Figure 1 shows the finite element model for Cross Section I, where a thinner peat deposit was encountered (peat bottom elevation at –20 feet). The finite element model for Cross Section II with a thicker peat deposit (peat bottom elevation at –40 feet) is illustrated in Figure 2. These cross sections are considered to be representative at both Webb Tract and Bacon Island sites.

## 2.2.2 Material Properties

Dynamic soil parameters used in our previous study (URS, 2000) were reviewed and updated using the more recent information. Specifically, the shear and compressive wave velocities obtained from the geophysical measurements at the Sherman Island (Boulanger, 1997) and at the Webb Tract and Bacon Island (Wehling, 2001) were used. The relationship that relates maximum shear modulus, over consolidation ratio (OCR) and effective pressure proposed by Wehling (2001) for peat was also utilized to account for the dependency of shear modulus (or shear wave velocity) on effective pressure.

The shear modulus degradation ( $G/G_{\max}$ ) and damping curves of Kokusho (1980) and Vucetic and Dobry (1991) were applied for the sandy soils (embankment fill and alluvium) and clay, respectively. For peat, the relationships of Wehling (2001) were utilized. The selected dynamic soil properties used for the response analyses are summarized in Table 1. Plots of the selected  $G/G_{\max}$  and damping vs. shear strain relationships are presented in Figures 3 and 4. It should be noted that analysis results (Section 2.4) showed high seismic induced shear stresses within the peat; i.e., stresses that are higher than the undrained shear strength of the peat. To reduce the calculated stresses from the equivalent linear procedure, the  $G/G_{\max}$  vs. shear strain relationship of Wehling (2001) was slightly lowered at large shear strain values.

For liquefied sand, small-strain shear wave velocities of 300 and 400 ft/sec were used for deposits outside and within the footprint of the embankment, respectively. No shear modulus degradation was applied for the liquefied soil, and the damping values were kept constant at 8% to 10% of the critical damping value.

## 2.2.3 Reservoir Stages and Slough Water Levels for Analyses

Two operating water elevation scenarios were selected to represent the fluctuation of water elevations in the reservoir and the slough, and are as follows (see Embankment Design Analysis Report):

- High Tide and Low Reservoir: a low reservoir and high slough water at elevation +3.5 feet. This condition was assumed to prevail 2/3 of the time.
- Low Tide and High Reservoir: a high reservoir water at elevation +4.0 feet and low slough water at elevation –1 foot. This condition was assumed to prevail 1/3 of the time.

These scenarios represent normal fluctuation in tidal water at the project site. They do not correspond to “extreme” conditions associated with flooding.

**Table 1**  
**Dynamic Soil Parameters Selected for Analysis**

Description		Moist Unit Weight (pcf)	$K_{2max}$	Shear Wave Velocity (ft/sec)	Modulus and Damping Curves
<b>Embankment Materials</b>					
New fills: sand		120	80	-	Sand <sup>1</sup>
Peat	- free-field	70	-	See note <sup>4</sup>	Peat <sup>2</sup>
	- under embankment				Peat <sup>2</sup>
<b>Foundation Materials</b>					
Sand	(non-liquefied)	120-125	80	-	Sand <sup>1</sup>
	(liquefied)	120-125	-	300-400	See Note <sup>5</sup>
Clay		127	-	1000	Clay <sup>3</sup>

- Note:
1. Relationships of Kokusho (1980), function of confining pressure
  2. Relationships of Wehling et al (2001)
  3. Relationships of Vucetic and Dobry (1991) for PI = 50
  4. Shear wave velocity was estimated using the following equations (Wehling et al. (2001):

$$v_s = \sqrt{\frac{G_{max}}{\rho}} \geq 75 \text{ ft / sec}$$

$$\frac{G_{max}}{Pa} = 75.7 \left[ \frac{\sigma'_{1c}}{Pa} \right]^{0.87} OCR^{0.65}$$

Where Pa and  $\sigma'_{1c}$  are the atmospheric and effective vertical pressures, respectively

5. For liquefied sand, no reduction in G is allowed and the damping is fixed at 8%-10% of critical damping.

## 2.3 EARTHQUAKE LOADS

A site-specific probabilistic seismic hazard analysis was performed for the current study to provide estimates of ground motions for future earthquake occurrences. A discussion of the approach, assumptions and results is represented in Attachment 1 to this report.

### 2.3.1 Earthquake Response Spectra

Three seismic events representing a small, a moderate, and a large earthquake in the region are considered. The three selected events correspond to ground motions having probabilities of exceedance in 50 years of about 69%, 10% and 2%. These correspond to ground motions with return periods of about 43 years, 475 years and 2,500 years, respectively. Figure 5 depicts the 5%-damped response spectra of these ground motions. These response spectra represent free-field motions for the outcropping stiff soil site condition. The peak ground accelerations (PGA's) at the site are as follows:

- 43 year return period: 0.14g
- 475 year return period: 0.33g
- 2,500 year return period: 0.52g

### 2.3.2 Spectrally-Matched Time Histories

To perform the dynamic response analyses, earthquake acceleration time histories are needed as input. We have used the same time histories as in the previous URS, 2000 study. These records are from the 1992 **M** 7.3 Landers earthquake, recorded at Fort Irwin station (station #24577), and the **M** 6.0 1987 Whittier Narrows earthquake, recorded at Altadena, Eaton Canyon station (station #24402). Table 2 lists these recorded motions along with their closest distances from the rupture planes and recorded peak accelerations. The site conditions at these recording stations are classified as stiff soil sites. The record from the 1992 Landers earthquake was selected to represent the larger and more distant earthquakes on the San Andreas and Hayward faults. The 1987 Whittier Narrows earthquake was selected to represent seismic events on the local seismic sources.

The response spectral values calculated from the selected acceleration time histories (natural time histories) have peaks and valleys that deviate from the smooth analysis response spectra (target response spectra). To develop acceleration time histories with overall characteristics that match the target response spectra, modifications to the natural time histories were necessary.

The two acceleration time histories were spectrally matched to the selected response spectra (i.e., response spectra for return periods of 43 years, 475 years and 2,500 years) using the method proposed by Lilhanand and Tseng (1988) and modified by Abrahamson (1993). The plots of the acceleration, velocity and displacement time histories of these spectrally matched motions are presented in Figures 6 through 11. The 5% damped response spectra for the modified motions are shown in Figures 12 through 14 along with the target spectra. It can be seen from these figures that the response spectra calculated from the modified time histories closely match the target spectra.

**Table 2**  
**Summary of Earthquake Records Used in the Dynamic Response Analysis**

Earthquake	$M_w$	Recording Station			Comp.	Recorded PGA (g)
		Distance (km)	Station	Site Condition		
1987 Whittier Narrows	6.0	18	Altadena – Eaton Canyon Station	Soil <sup>a</sup>	90°	0.15
1992 Landers	7.3	64	Fort Irwin Station	Soil <sup>a</sup>	0°	0.11

Note : a = Deep stiff soil site

## 2.4 ANALYSIS RESULTS

Dynamic response analyses were performed by using compliant bases at the bottom of the finite element models to prevent total reflection of wave energy at the fixed boundaries. The shear wave velocity for the underlying elastic half space was taken equal to that of the stiff clay deposit beneath the sand layer. The spectrally-matched acceleration time histories were input to the finite element models at an elevation of about -100 feet. These input acceleration time histories were obtained by deconvolving the spectrally matched time histories to that elevation. We used the one-dimensional wave propagation computer program SHAKE (Schnabel et al, 1972) to deconvolve the ground motions at elevation -100 feet.

The results of analyses are expressed in terms of average horizontal acceleration ( $K_{ave}$ ) time histories of the potential (critical) slide masses within the embankments. The critical slide masses for each embankment alternative and for the two cross sections were identified in the static slope stability analyses (Embankment Design Analysis Report), and are presented in Figures 15 through 18. The average horizontal acceleration was calculated by computing the dynamic response of the embankment and averaging various stresses within or close to the sliding surface. Examples of the calculated  $K_{ave}$  time history are presented in Figures 19 through 22 for the 475-year return period ground motion.

Seismic-induced deformations of the embankments were estimated for the three ground motion levels selected for this study. The estimated deformations and their associated ground motion levels were used to evaluate the seismic risk of the proposed embankment alternatives.

### 3.1 METHODOLOGY

Seismic-induced permanent deformations of the embankment slopes were estimated using the Newmark Double Integration Method (1965) and the Makdisi and Seed Simplified Procedure (1978). The Newmark Double Integration Method is based on the concept that deformations of an embankment will result from incremental sliding during the short periods when earthquake inertia forces in the critical slide mass exceed the available resisting forces. This method involves the calculation of the displacement (deformation) increment of a critical slide mass at each time step using the average horizontal acceleration ( $k_{ave}$ ) and the value of yield acceleration ( $k_y$ ) calculated for the slide mass. The development of the  $k_y$  is discussed in the Embankment Design Analysis Report. The displacement increment is calculated by double integrating the difference between  $k_{ave}$  and  $k_y$  values acting on the slide mass. The estimated permanent deformation of the slide mass is then taken as the sum of the displacement increments at the end of ground shaking.

The simplified procedure of Makdisi and Seed (1978) was developed based on observations of dam performance during past earthquakes and analysis results. In this method, the inertial force on the slide mass is represented by the peak average horizontal acceleration ( $k_{max}$ ) induced by the design earthquake. Empirical relationships relating the ratio of  $k_y$  and  $k_{max}$  ( $k_y/k_{max}$ ) and the average deformation were used to estimate embankment deformations.

### 3.2 RESULTS

#### 3.2.1 Bench Alternative

The slope deformations calculated using the Newmark Double Integration Method for non-liquefied sandy soils are tabulated in Tables 3 and 4 for Cross Section I (bottom of peat at elevation -20 feet) and Cross Section II (bottom of peat at elevation -40 feet), respectively. For the non-liquefied cases, the results of the analysis suggest that up to about 1.65 feet and 0.4 feet of slope deformations on the slough and reservoir sides, respectively, can be expected during an earthquake event having a 475-year return period. Under the 43-year return period ground motions, the seismic induced slope deformations are expected to be small. The Simplified Makdisi and Seed procedure was also used to estimate slope deformations for comparison purposes. The comparisons are shown in Tables 3 and 4.

The results for the liquefied cases are tabulated in Tables 5 and 6 for Cross Sections I and II, respectively. As expected, under the 475-year return period event, much larger slope deformations were estimated. For Cross Section I, up to about 3.3 feet and 1.35 feet of deformations were calculated for the slough and reservoir slopes, respectively. Slough side slope deformations of about 9 feet and reservoir side slope deformation of about 2.25 feet were estimated for Cross Section II. Under the smaller ground motions of 43-year return period, maximum deformations of about 0.6 feet and 1.15 feet were calculated for the slough and reservoir slopes, respectively, for Cross Section I. The maximum slope deformations for Cross

Section II were calculated to be about 1.5 feet, for the slough slopes, and 1.35 feet, for the reservoir slopes.

As noted in Tables 3 through 6, convergence was not obtained for some of the cases with larger earthquakes (2500-year and some 475-year events). For these cases, the average horizontal acceleration time histories could not be computed in the QUAD4M runs. These numerical problems were caused by large deformations (shear strain in excess of 40%) calculated in the peat deposits due to large earthquake shaking. The procedure of Makdisi and Seed (1978) was not judged appropriate for these cases where substantial strength loss takes place. For embankments experiencing large seismically induced strains, the average acceleration may not continue to increase with increasing levels of seismic shaking and deformations. However, for the purpose of this study, a deformation of over 12 feet was assumed to have a 95 percent probability of embankment failure. This condition was considered to represent the expected embankment performance under severe earthquake events.

The results of the seismic deformation analyses for the bench alternative are summarized in Table 10A for the 475-year earthquake event.

### 3.2.2 Rock Berm Alternative

For rock berm alternative, the calculated slope deformations considering non-liquefied sandy soils are tabulated in Tables 7 and 8 for Cross Section I (bottom of peat at elevation -20 feet) and Cross Section II (bottom of peat at elevation -40 feet), respectively. For the non-liquefied case, the results of the analysis suggest that up to about 0.4-foot of slope deformation can be expected during an earthquake event having a 475-year return period. Under the 43-year return period ground motions, the seismic induced slope deformations are expected to be small. The Simplified Makdisi and Seed procedure was also used to estimate slope deformations for comparison purposes. The comparisons are shown in Table 7 and 8.

The results for the liquefied cases are tabulated in Tables 9 and 10 for Cross Sections I and II, respectively. As expected, under the 475-year return period event, larger slope deformations were estimated. For Cross Section I, up to about 1.4 feet and 0.6 foot of deformations were calculated for the reservoir and slough slopes, respectively. Maximum deformations of about 2.0 feet were estimated for the reservoir and slough slopes of Cross Section II. Under the smaller ground motions of 43-year return period, maximum reservoir slope deformation of about 1 foot was calculated.

As noted in Tables 7 through 10, convergence was not obtained for some of the cases with larger earthquakes (2500-year and some 475-year events). Similarly to the above discussion, a deformation of over 12 feet was assumed to have a 95 percent probability of embankment failure. This condition was considered to represent the expected embankment performance under severe earthquake events.

The results of the seismic deformation analyses for the rock berm alternative are summarized in Table 10A for the 475-year earthquake event.

This section of the report summarizes the estimated probability of failures for the various cross sections analyzed under the different earthquake scenarios. The modes of failure considered for this study included those caused by an earthquake event, such as seismic-induced slumping, slope failure, liquefaction-induced sliding and lateral spreading and other related secondary failures (i.e., piping through an open crack, etc.).

#### **4.1 EMBANKMENT FRAGILITY CURVE**

The embankment fragility curve developed by the Seismic Vulnerability Sub-Team (CALFED, 1998) was used for this study for both the liquefied and non-liquefied cases. This curve was then utilized to evaluate the probability of failure of an embankment cross section with given earthquake-induced deformations.

#### **4.2 FAILURE PROBABILITY**

Failure probabilities for the two project alternatives (bench and rock berm) and the two embankment cross sections (Cross Section I and II) were calculated by combining the various weights (probabilities) associated with reservoir and slough water levels, earthquake ground motion and liquefaction scenarios. Weights assigned to the reservoir and slough water level scenarios were estimated based on the time percentage of each scenario to occur annually. Weights for the earthquake ground motion scenarios were estimated by assuming a time-independent Poisson process for earthquake occurrence and a project life cycle of 50 years. In estimating the weights for the three ground motion scenarios, we assumed that the 43-year, 475-year and 2,500-year ground motions are represented by ground motions with return periods less than about 130 years, 130 years to about 1,000 years and greater than 1,000 years, respectively. The failure probabilities were calculated considering the contributions from the large/distant and moderate/near earthquakes and critical slide masses on the reservoir and slough sides. Weights for the liquefaction scenarios were selected based on judgment and evaluation of sampler blowcounts recorded in the sandy deposits.

Tables 11 through 14 summarize the contributions of the various scenarios and provide estimates for the total probability of failure for each project alternative and each cross section for a 50-year life cycle. The bench alternative with peat at elevation –20 feet has about 19 percent chance of failure (Table 11), while the cross section with peat at elevation –40 feet has about 28 percent chance of failure (Table 12). For the rock berm alternative, the cross section with peat at elevation –20 feet has about 17 percent chance of failure (Table 13), while the cross section with peat at elevation –40 feet has about 23.5 percent chance of failure (Table 14).

This report presents the results of estimated seismic performance of the two embankment design alternatives, and addresses the probability of earthquake-induced embankment failure.

Table 10A shows that the calculated seismic deformations are large for several conditions for the 475-year earthquake event. The results of the evaluation appear to suggest that the rock berm alternative would provide for a lower probability of failure than the bench alternative. The rock berm alternative is preferable to the bench alternative because it places the embankment over the existing levee and, therefore, makes use of the stronger peat under the levee as opposed to the weaker free-field peat. In addition, the rock berm alternative provides a more stable slough side slope.

Because liquefaction would lead to large deformations that would affect overall stability of the embankment, further investigation and evaluation of the existing levee materials are recommended. Depending on the extent of the potentially liquefiable sands within the existing levee, removal of the loose sands may need to be implemented.

Due to the limitations of the QUAD4M computer program for large earthquake loads, a uniform assumption has been made for estimating the expected embankment deformation. Although this assumption is considered conservative, a more rigorous non-linear analysis would probably be useful and could provide more insight into the deformation patterns associated with large strains under the large earthquake shaking. This analysis could also provide more insight into the comparative performance of the embankment alternatives under the larger earthquakes.

The calculation of the overall risk is presented in the URS Risk Analysis report. The risk analysis combines the probabilities of failure from various events (seismic, operational and flood) and their failure consequences.

- Abrahamson N., 1993, Non-stationary spectral matching program, personnel communication.
- Boulanger R. et al., 1997, Dynamic properties of Sherman Island peat, Report No. UCD/CGM-97/01, Center for Geotechnical Modeling, Department of Civil and Environmental Engineering, University of California at Davis.
- CALFED, 1998, Seismic vulnerability of the Sacramento-San Joaquin Delta Levees, Calfed Bay-Delta Program, Seismic Vulnerability Sub-Team, December.
- Department of Water Resources, 2002, Draft report on engineering investigations, In-Delta Storage Program, CALFED Bay-Delta Program.
- Hudson, M., Idriss, I.M., Beikae, M., 1994, User's Manual for QUAD4M, Center for Geotechnical Modeling, Department of Civil & Environmental Engineering, University of California, Davis, California, May.
- Kokusho T., 1980, Cyclic triaxial test of dynamic soil properties for wide strain range, Soils and Foundations, 20, 45-60.
- Lilhanand, K. and Tseng, W.S., 1988, Development and application of realistic earthquake time histories compatible with multiple-damping design spectra, Proceeding of the 9<sup>th</sup> World Conference on Earthquake Engineering, Tokyo-Kyoto, Japan, August.
- Makdisi, F.I. and Seed, H.B., 1978, Simplified procedure for estimating dam and embankment earthquake-induced deformations', Journal of the Geotechnical Engineering Division, ASCE, Vol. 104, No. GT7, July.
- Newmark N.M., 1965, 'Effects of earthquakes on dams and embankments', Geotechnique, Vol. 15, No. 2, June.
- Schnabel, P.B., Lysmer, J., and Seed, H.B., 1972, 'A computer program for earthquake response analysis of horizontal layered sites', Earthquake Engineering Research Center, Report No. EERC 72-12, December 1972.
- Seed, H.B. and Idriss, I.M., 1970, Soil moduli in damping factors for dynamic response analysis, Report No. EERC 70-10, University of California, Berkeley, December.
- URS, 2000, Geotechnical services report in support of the supplemental EIS/EIS, Report prepared for Jones & Stokes Associates, Inc. March 17.
- Vucetic, M. and Dobry, R., 1991, Effect of soil plasticity on cyclic response, Journal of Geotechnical Engineering, ASCE, Vol. 117, No.1.
- Wehling, T.M. et al., 2001, Nonlinear dynamic properties of a fibrous organic soil, Paper accepted for publication in ASCE Journal of Geotechnical Engineering.

**TABLE 3 - SUMMARY OF CALCULATED SLOPE DEFORMATIONS AND FAILURE PROBABILITIES FOR CROSS SECTION I WITH BENCH ALTERNATIVE, PEAT AT -20FT (NONLIQUEFIED CAS)**

Cross Section	Water Level Scenario	Ground Motion Level	Time History	Sliding Surface <sup>3</sup>	K <sub>y</sub> (g)	K <sub>max</sub> (g)	K <sub>y</sub> /K <sub>max</sub>	Slope Deformation (feet)			Probability of Failure <sup>1</sup> (%)	Probability of Failure for Section <sup>2</sup> (%)	Average Probability of Failure for Section (%)
								Newmark	Makdisi and Seed				
									Best Estimate	Min Estimate			
Cross Section I (Peat at -20 ft)	Low tide high reservoir	43 years	Landers	A	0.125	0.041	3.04	0.03	0.03	0.03	0.03	0.01	0.01
				B	0.138	0.097	1.43	0.03	0.03	0.03	0.03	0.01	
				C	0.094	0.072	1.31	0.03	0.03	0.03	0.03	0.01	
				D	0.095	0.100	0.95	0.03	0.03	0.03	0.03	0.01	
		Whittier Narrows	A	0.125	0.040	3.16	0.03	0.03	0.03	0.03	0.01	0.01	
			B	0.138	0.112	1.23	0.03	0.03	0.03	0.03	0.01		
			C	0.094	0.089	1.05	0.03	0.03	0.03	0.03	0.01		
			D	0.095	0.124	0.76	0.03	0.05	0.03	0.07	0.01		
		475 years	Landers	A	0.125	0.089	1.41	0.03	0.03	0.03	0.03	0.01	0.17
				B	0.138	0.213	0.65	0.12	0.15	0.03	0.26	0.01	
				C	0.094	0.175	0.54	0.23	0.33	0.07	0.59	0.03	
				D	0.095	0.200	0.48	0.50	0.56	0.13	0.98	0.17	
	Whittier Narrows	A	0.125	0.076	1.65	0.03	0.03	0.03	0.03	0.01	0.30		
		B	0.138	0.204	0.68	0.09	0.07	0.03	0.10	0.01			
		C	0.094	0.158	0.60	0.17	0.10	0.03	0.16	0.02			
		D	0.095	0.221	0.43	0.64	0.19	0.05	0.33	0.30			
	2500 years	Landers	A	No Convergence				-	-	-	-	95.00	95.00
			B	No Convergence				-	-	-	-	95.00	
			C	No Convergence				-	-	-	-	95.00	
			D	No Convergence				-	-	-	-	95.00	
	Whittier Narrows	A	No Convergence				-	-	-	-	95.00	95.00	
		B	No Convergence				-	-	-	-	95.00		
		C	No Convergence				-	-	-	-	95.00		
		D	No Convergence				-	-	-	-	95.00		
High tide low reservoir	43 years	Landers	A	0.092	0.030	3.03	0.03	0.03	0.03	0.03	0.01	0.01	
			B	0.135	0.116	1.17	0.03	0.03	0.03	0.03	0.01		
			C	0.115	0.082	1.41	0.03	0.03	0.03	0.03	0.01		
			D	0.108	0.113	0.96	0.03	0.03	0.03	0.03	0.01		
	Whittier Narrows	A	0.092	0.035	2.64	0.03	0.03	0.03	0.03	0.01	0.01		
		B	0.135	0.129	1.05	0.03	0.03	0.03	0.03	0.01			
		C	0.115	0.077	1.49	0.03	0.03	0.03	0.03	0.01			
		D	0.108	0.113	0.95	0.03	0.03	0.03	0.03	0.01			
	475 years	Landers	A	0.092	0.081	1.13	0.03	0.03	0.03	0.03	0.01	0.08	
			B	0.135	0.229	0.59	0.32	0.25	0.07	0.43	0.06		
			C	0.115	0.150	0.77	0.07	0.07	0.03	0.10	0.01		
			D	0.108	0.214	0.50	0.38	0.43	0.10	0.75	0.08		
Whittier Narrows	A	0.092	0.056	1.64	0.03	0.03	0.03	0.03	0.01	0.09			
	B	0.135	0.269	0.50	0.40	0.15	0.03	0.26	0.09				
	C	0.115	0.123	0.94	0.03	0.03	0.03	0.03	0.01				
	D	0.108	0.208	0.52	0.27	0.13	0.03	0.23	0.04				
2500 years	Landers	A	No Convergence				-	-	-	-	95.00	95.00	
		B	No Convergence				-	-	-	-	95.00		
		C	No Convergence				-	-	-	-	95.00		
		D	No Convergence				-	-	-	-	95.00		
Whittier Narrows	A	No Convergence				-	-	-	-	95.00	95.00		
	B	No Convergence				-	-	-	-	95.00			
	C	No Convergence				-	-	-	-	95.00			
	D	No Convergence				-	-	-	-	95.00			

Note: 1 - For no convergence cases, probabilities of failure were estimated based on slope deformations of 8 feet  
 2 - Failure probability of section was taken as the maximum of the 4 sliding surfaces  
 3 - Sliding surfaces A and B are on the reservoir side and C and D are on the slough side

**TABLE 4 - SUMMARY OF CALCULATED SLOPE DEFORMATIONS AND FAILURE PROBABILITIES FOR CROSS SECTION II WITH BENCH ALTERNATIVE, PEAT AT -40FT (NONLIQUEFIED CASE)**

Cross Section	Water Level Scenario	Ground Motion Level	Time History	Sliding Surface <sup>3</sup>	K <sub>y</sub> (g)	K <sub>max</sub> (g)	K <sub>y</sub> /K <sub>max</sub>	Slope Deformation (feet)				Probability of Failure <sup>1</sup> (%)	Probability of Failure for Section <sup>2</sup> (%)	Average Probability of Failure for Section (%)
								Newmark	Makdisi and Seed					
									Best Estimate	Min Estimate	Max Estimate			
Cross Section II (Peat at -40 ft)	Low tide high reservoir	43 years	Landers	A	0.082	0.021	3.90	0.03	0.03	0.03	0.03	0.01	0.01	
				B	0.094	0.077	1.22	0.03	0.03	0.03	0.03	0.01		
				C	0.082	0.124	0.66	0.07	0.13	0.03	0.23	0.01		
				D	0.062	0.093	0.67	0.07	0.13	0.03	0.23	0.01		
			Whittier Narrows	A	0.082	0.020	4.10	0.03	0.03	0.03	0.03	0.01		
				B	0.094	0.071	1.32	0.03	0.03	0.03	0.03	0.01		
				C	0.082	0.124	0.66	0.07	0.10	0.03	0.16	0.01		
				D	0.062	0.094	0.66	0.07	0.10	0.03	0.16	0.01		
		475 years	Landers	A	0.082	0.054	1.52	0.03	0.03	0.03	0.03	0.01	2.62	
				B	0.094	0.173	0.54	0.22	0.41	0.10	0.72	0.03		
				C	0.082	0.273	0.30	1.49	1.46	0.43	2.49	2.62		
				D	0.062	0.200	0.31	1.21	1.46	0.43	2.49	1.55		
	Whittier Narrows	A	0.082	0.035	2.34	0.03	0.03	0.03	0.03	0.01	3.29			
		B	0.094	0.140	0.67	0.23	0.10	0.03	0.16	0.03				
		C	0.082	0.233	0.35	1.63	0.51	0.16	0.85	3.29				
		D	0.062	0.178	0.35	1.56	0.51	0.16	0.85	2.94				
	2500 years	Landers	A	No Convergence				-	-	-	-	95.00	95.00	
			B	No Convergence				-	-	-	-	95.00		
			C	No Convergence				-	-	-	-	95.00		
			D	No Convergence				-	-	-	-	95.00		
	Whittier Narrows	A	No Convergence				-	-	-	-	95.00	95.00		
		B	No Convergence				-	-	-	-	95.00			
		C	No Convergence				-	-	-	-	95.00			
		D	No Convergence				-	-	-	-	95.00			
High tide low reservoir	43 years	Landers	A	0.058	0.021	2.76	0.03	0.03	0.03	0.03	0.01	0.01		
			B	0.070	0.090	0.78	0.03	0.07	0.03	0.10	0.01			
			C	0.110	0.111	0.99	0.03	0.03	0.03	0.03	0.01			
			D	0.078	0.088	0.89	0.03	0.03	0.03	0.03	0.01			
		Whittier Narrows	A	0.058	0.020	2.90	0.03	0.03	0.03	0.03	0.01			
			B	0.070	0.089	0.79	0.03	0.03	0.03	0.03	0.01			
			C	0.110	0.100	1.10	0.03	0.03	0.03	0.03	0.01			
			D	0.078	0.083	0.94	0.03	0.03	0.03	0.03	0.01			
	475 years	Landers	A	No Convergence				-	-	-	-	95.00	95.00	
			B	No Convergence				-	-	-	-	95.00		
			C	No Convergence				-	-	-	-	95.00		
			D	No Convergence				-	-	-	-	95.00		
Whittier Narrows	A	No Convergence				-	-	-	-	95.00	95.00			
	B	No Convergence				-	-	-	-	95.00				
	C	No Convergence				-	-	-	-	95.00				
	D	No Convergence				-	-	-	-	95.00				
2500 years	Landers	A	No Convergence				-	-	-	-	95.00	95.00		
		B	No Convergence				-	-	-	-	95.00			
		C	No Convergence				-	-	-	-	95.00			
		D	No Convergence				-	-	-	-	95.00			
Whittier Narrows	A	No Convergence				-	-	-	-	95.00	95.00			
	B	No Convergence				-	-	-	-	95.00				
	C	No Convergence				-	-	-	-	95.00				
	D	No Convergence				-	-	-	-	95.00				

Note: 1 - For no convergence cases, probabilities of failure were estimated based on slope deformations of 8 feet  
 2 - Failure probability of section was taken as the maximum of the 4 sliding surfaces  
 3 - Sliding surfaces A and B are on the reservoir side and C and D are on the slough side

**TABLE 5 - SUMMARY OF CALCULATED SLOPE DEFORMATIONS AND FAILURE PROBABILITIES FOR CROSS SECTION I WITH BENCH ALTERNATIVE, PEAT AT -20FT (LIQUEFIED CASE)**

Cross Section	Water Level Scenario	Ground Motion Level	Time History	Sliding Surface <sup>3</sup>	K <sub>y</sub> (g)	K <sub>max</sub> (g)	K <sub>y</sub> /K <sub>max</sub>	Slope Deformation (feet)				Probability of Failure <sup>1</sup> (%)	Probability of Failure for Section <sup>2</sup> (%)	Average Probability of Failure for Section (%)	
								Newmark	Makdisi and Seed						
									Best Estimate	Min Estimate	Max Estimate				
Cross Section I (Peat at -20 ft)	Low tide high reservoir	43 years	Landers	A	0.083	0.089	0.93	0.03	0.03	0.03	0.03	0.01	0.19	0.23	
				B	0.070	0.095	0.74	0.03	0.05	0.03	0.07	0.01			
				C	0.042	0.099	0.42	0.20	0.67	0.16	1.18	0.02			
				D	0.027	0.099	0.27	0.54	1.79	0.56	3.02	0.19			
			Whittier Narrows	A	0.083	0.112	0.74	0.03	0.08	0.03	0.13	0.01			
				B	0.070	0.118	0.59	0.11	0.11	0.03	0.20	0.01			
		475 years	Landers	A	0.083	0.218	0.38	0.80	0.82	0.23	1.41	0.53	16.99		14.68
				B	0.070	0.230	0.30	1.35	1.15	0.36	1.94	2.05			
				C	0.042	0.213	0.20	2.38	3.15	1.02	5.28	8.21			
				D	0.027	0.208	0.13	3.30	5.28	1.80	8.76	16.99			
			Whittier Narrows	A	0.083	0.192	0.43	0.62	0.36	0.10	0.62	0.28			
				B	0.070	0.205	0.34	1.03	0.44	0.13	0.75	1.01			
	2500 years	Landers	A	No Convergence				-	-	-	-	95.00	95.00		
			B	No Convergence				-	-	-	-	95.00			
			C	No Convergence				-	-	-	-	95.00			
			D	No Convergence				-	-	-	-	95.00			
		Whittier Narrows	A	No Convergence				-	-	-	-	95.00			
			B	No Convergence				-	-	-	-	95.00			
	High tide low reservoir	43 years	Landers	A	0.055	0.109	0.50	0.22	0.42	0.10	0.75	0.03	0.89	1.11	
				B	0.027	0.112	0.24	0.98	1.79	0.56	3.02	0.89			
				C	0.080	0.103	0.78	0.03	0.08	0.03	0.13	0.01			
				D	0.063	0.101	0.62	0.03	0.19	0.04	0.33	0.01			
			Whittier Narrows	A	0.055	0.125	0.44	0.35	0.34	0.10	0.59	0.07			
				B	0.027	0.128	0.21	1.14	0.94	0.26	1.61	1.32			
475 years		Landers	A	No Convergence				-	-	-	-	95.00	95.00		
			B	No Convergence				-	-	-	-	95.00			
			C	No Convergence				-	-	-	-	95.00			
			D	No Convergence				-	-	-	-	95.00			
		Whittier Narrows	A	No Convergence				-	-	-	-	95.00			
			B	No Convergence				-	-	-	-	95.00			
2500 years	Landers	A	No Convergence				-	-	-	-	95.00	95.00			
		B	No Convergence				-	-	-	-	95.00				
		C	No Convergence				-	-	-	-	95.00				
		D	No Convergence				-	-	-	-	95.00				
	Whittier Narrows	A	No Convergence				-	-	-	-	95.00				
		B	No Convergence				-	-	-	-	95.00				

Note: 1 - For no convergence cases, probabilities of failure were estimated based on slope deformations of 8 feet  
 2 - Failure probability of section was taken as the maximum of the 4 sliding surfaces  
 3 - Sliding surfaces A and B are on the reservoir side and C and D are on the slough side

**TABLE 6 - SUMMARY OF CALCULATED SLOPE DEFORMATIONS AND FAILURE PROBABILITIES FOR CROSS SECTION II WITH BENCH ALTERNATIVE, PEAT AT -40FT (LIQUEFIED CASE)**

Cross Section	Water Level Scenario	Ground Motion Level	Time History	Sliding Surface <sup>3</sup>	K <sub>y</sub> (g)	K <sub>max</sub> (g)	K <sub>y</sub> /K <sub>max</sub>	Slope Deformation (feet)				Probability of Failure <sup>1</sup> (%)	Probability of Failure for Section <sup>2</sup> (%)	Average Probability of Failure for Section (%)
								Newmark	Makdisi and Seed					
									Best Estimate	Min Estimate	Max Estimate			
Cross Section II (Peat at -40 ft)	Low tide high reservoir	43 years	Landers	A	0.060	0.109	0.55	0.09	0.34	0.08	0.59	0.01	1.57	2.14
				B	0.058	0.108	0.54	0.10	0.38	0.10	0.66	0.01		
				C	0.027	0.084	0.32	0.33	1.51	0.40	2.62	0.06		
				D	0.009	0.077	0.12	1.22	6.07	2.30	9.84	1.57		
		Whittier Narrows	A	0.060	0.102	0.59	0.16	0.15	0.03	0.26	0.02	2.71		
			B	0.058	0.103	0.56	0.14	0.16	0.03	0.28	0.01			
			C	0.027	0.089	0.30	0.45	0.58	0.13	1.03	0.13			
			D	0.009	0.080	0.11	1.51	1.35	0.39	2.30	2.71			
		475 years	Landers	A	0.060	0.217	0.28	1.56	1.71	0.46	2.95	2.94	81.66	
				B	0.058	0.214	0.27	1.41	1.72	0.47	2.97	2.28		
				C	0.027	0.183	0.15	3.51	4.35	1.48	7.22	19.34		
				D	0.009	0.156	0.06	9.03	10.17	3.94	16.40	81.66		
	Whittier Narrows	A	0.060	0.197	0.30	2.24	0.54	0.10	0.98	7.15	55.39			
		B	0.058	0.194	0.30	2.04	0.57	0.11	1.02	5.71				
		C	0.027	0.168	0.16	3.47	0.97	0.30	1.64	18.89				
		D	0.009	0.148	0.06	6.44	1.97	0.66	3.28	55.39				
	2500 years	Landers	A	No Convergence				-	-	-	-	95.00	95.00	
			B	No Convergence				-	-	-	-	95.00		
			C	No Convergence				-	-	-	-	95.00		
			D	No Convergence				-	-	-	-	95.00		
	Whittier Narrows	A	No Convergence				-	-	-	-	95.00	95.00		
		B	No Convergence				-	-	-	-	95.00			
		C	No Convergence				-	-	-	-	95.00			
		D	No Convergence				-	-	-	-	95.00			
High tide low reservoir	43 years	Landers	A	0.040	0.116	0.34	0.32	1.16	0.35	1.97	0.06	0.91	1.50	
			B	0.020	0.116	0.17	0.99	3.94	1.31	6.56	0.91			
			C	0.052	0.082	0.63	0.06	0.15	0.03	0.26	0.01			
			D	0.030	0.075	0.40	0.19	0.88	0.11	1.64	0.02			
	Whittier Narrows	A	0.040	0.113	0.35	0.52	0.39	0.12	0.66	0.18	2.08			
		B	0.020	0.114	0.18	1.36	1.15	0.33	1.97	2.08				
		C	0.052	0.079	0.66	0.07	0.10	0.03	0.16	0.01				
		D	0.030	0.073	0.41	0.28	0.34	0.08	0.59	0.04				
	475 years	Landers	A	No Convergence				-	-	-	-	95.00		95.00
			B	No Convergence				-	-	-	-	95.00		
			C	No Convergence				-	-	-	-	95.00		
			D	No Convergence				-	-	-	-	95.00		
Whittier Narrows	A	No Convergence				-	-	-	-	95.00	95.00			
	B	No Convergence				-	-	-	-	95.00				
	C	No Convergence				-	-	-	-	95.00				
	D	No Convergence				-	-	-	-	95.00				
2500 years	Landers	A	No Convergence				-	-	-	-	95.00	95.00		
		B	No Convergence				-	-	-	-	95.00			
		C	No Convergence				-	-	-	-	95.00			
		D	No Convergence				-	-	-	-	95.00			
Whittier Narrows	A	No Convergence				-	-	-	-	95.00	95.00			
	B	No Convergence				-	-	-	-	95.00				
	C	No Convergence				-	-	-	-	95.00				
	D	No Convergence				-	-	-	-	95.00				

Note: 1 - For no convergence cases, probabilities of failure were estimated based on slope deformations of 8 feet  
 2 - Failure probability of section was taken as the maximum of the 4 sliding surfaces  
 3 - Sliding surfaces A and B are on the reservoir side and C and D are on the slough side

**TABLE 7 - SUMMARY OF CALCULATED SLOPE DEFORMATION AND FAILURE PROBABILITIES FOR CROSS SECTION I WITH ROCK BERM, PEAT AT -20FT (NONLIQUEFIED CASE)**

Cross Section	Water Level Scenario	Ground Motion Level	Time History	Sliding Surface	K <sub>y</sub> (g)	K <sub>max</sub> (g)	K <sub>y</sub> /K <sub>max</sub>	Slope Deformation (feet)			Probability of Failure <sup>1</sup> (%)	Probability of Failure for Section <sup>2</sup> (%)	Average Probability of Failure for Section (%)	
								Newmark	Makdisi and Seed					
									Best Estimate	Min Estimate				Max Estimate
Cross Section I (Peat at -20 ft)	Low tide high reservoir	43 years	Landers	Reservoir Slough	0.140	0.097	1.44	0.03	0.03	0.03	0.03	0.01	0.01	
			Whittier Narrows	Reservoir Slough	0.140	0.112	1.25	0.03	0.03	0.03	0.03	0.01		
		475 years	Landers	Reservoir Slough	0.140	0.213	0.66	0.11	0.13	0.03	0.23	0.01	0.01	
			Whittier Narrows	Reservoir Slough	0.250	0.200	1.25	0.03	0.03	0.03	0.03	0.01		
		2500 years	Landers	Reservoir Slough	No Convergence				-	-	-	-	95.00	95.00
			Whittier Narrows	Reservoir Slough	No Convergence				-	-	-	-	95.00	
	High tide low reservoir	43 years	Landers	Reservoir Slough	0.140	0.116	1.21	0.03	0.03	0.03	0.03	0.01	0.01	
			Whittier Narrows	Reservoir Slough	0.270	0.113	2.39	0.03	0.03	0.03	0.03	0.01		
		475 years	Landers	Reservoir Slough	0.140	0.229	0.61	0.27	0.17	0.03	0.30	0.04	0.04	
			Whittier Narrows	Reservoir Slough	0.270	0.214	1.26	0.03	0.03	0.03	0.03	0.01		
		2500 years	Landers	Reservoir Slough	No Convergence				-	-	-	-	95.00	95.00
			Whittier Narrows	Reservoir Slough	No Convergence				-	-	-	-	95.00	

Note: 1 - For no convergence cases, probabilities of failure were estimated based on slope deformations of 8 feet

2 - Failure probability of section was taken as the maximum of the 4 sliding surfaces

**TABLE 8 - SUMMARY OF CALCULATED SLOPE DEFORMATIONS AND FAILURE PROBABILITIES FOR CROSS SECTION II WITH ROCK BERM, PEAT AT -40FT (NONLIQUEFIED CASE)**

Cross Section	Water Level Scenario	Ground Motion Level	Time History	Sliding Surface	K <sub>y</sub> (g)	K <sub>max</sub> (g)	K <sub>y</sub> /K <sub>max</sub>	Slope Deformation (feet)				Probability of Failure <sup>1</sup> (%)	Probability of Failure for Section <sup>2</sup> (%)	Average Probability of Failure for Section (%)
								Newmark	Makdisi and Seed					
									Best Estimate	Min Estimate	Max Estimate			
Cross Section II (Peat at -40 ft)	Low tide high reservoir	43 years	Landers	Reservoir Slough	0.090	0.077	1.17	0.03	0.03	0.03	0.03	0.01	0.01	
			Whittier Narrows	Reservoir Slough	0.110	0.093	1.18	0.03	0.03	0.03	0.03	0.01		
			Whittier Narrows	Reservoir Slough	0.090	0.071	1.27	0.03	0.03	0.03	0.03	0.01		
		475 years	Landers	Reservoir Slough	0.090	0.173	0.52	0.25	0.27	0.05	0.49	0.04	0.08	
			Whittier Narrows	Reservoir Slough	0.110	0.200	0.55	0.33	0.26	0.04	0.47	0.06		
			Whittier Narrows	Reservoir Slough	0.090	0.140	0.64	0.28	0.18	0.05	0.30	0.04		
	2500 years	Landers	Reservoir Slough	No Convergence				-	-	-	-	95.00	95.00	
		Whittier Narrows	Reservoir Slough	No Convergence				-	-	-	-	95.00		
		Whittier Narrows	Reservoir Slough	No Convergence				-	-	-	-	95.00		
	High tide low reservoir	43 years	Landers	Reservoir Slough	0.090	0.090	1.00	0.03	0.05	0.03	0.06	0.01	0.01	
			Whittier Narrows	Reservoir Slough	0.120	0.088	1.36	0.03	0.03	0.03	0.03	0.01		
			Whittier Narrows	Reservoir Slough	0.090	0.089	1.01	0.03	0.05	0.03	0.07	0.01		
		475 years	Landers	Reservoir Slough	No Convergence				-	-	-	-	95.00	95.00
			Whittier Narrows	Reservoir Slough	No Convergence				-	-	-	-	95.00	
Whittier Narrows			Reservoir Slough	No Convergence				-	-	-	-	95.00		
2500 years	Landers	Reservoir Slough	No Convergence				-	-	-	-	95.00	95.00		
	Whittier Narrows	Reservoir Slough	No Convergence				-	-	-	-	95.00			

Note: 1 - For no convergence cases, probabilities of failure were estimated based on slope deformations of 8 feet  
 2 - Failure probability of section was taken as the maximum of the 4 sliding surfaces

**TABLE 9 - SUMMARY OF CALCULATED SLOPE DEFORMATIONS AND FAILURE PROBABILITIES FOR CROSS SECTION I WITH ROCK BERM, PEAT AT -20FT (LIQUEFIED CASE)**

Cross Section	Water Level Scenario	Prob. Of Groundwater Scenario	Ground Motion Level	Prob. Of Ground Motion	Time History	Sliding Surface	K <sub>v</sub> (g)	K <sub>rmax</sub> (g)	K <sub>v</sub> /K <sub>rmax</sub>	Slope Deformation (feet)				Probability of Failure <sup>1</sup> (%)	Probability of Failure for Section <sup>2</sup> (%)	Average Probability of Failure for Section (%)	
										Newmark	Makdisi and Seed						
											Best Estimate	Min Estimate	Max Estimate				
Cross Section I (Peat at -20 ft)	Low tide high reservoir	0.5	43 years	0.7	Landers	Reservoir Slough	0.070	0.095	0.74	0.03	0.05	0.01	0.10	0.01	0.01	0.01	
					Whittier Narrows	Reservoir Slough	0.080	0.099	0.81	0.03	0.03	0.03	0.03	0.01			
					Whittier Narrows	Reservoir Slough	0.070	0.118	0.59	0.11	0.22	0.07	0.43	0.01			
			475 years	0.25	Landers	Reservoir Slough	0.080	0.106	0.75	0.03	0.13	0.03	0.11	0.01	0.01		1.53
					Whittier Narrows	Reservoir Slough	0.070	0.230	0.30	1.35	0.79	0.43	2.49	2.05	2.05		
					Whittier Narrows	Reservoir Slough	0.080	0.208	0.38	0.64	0.38	0.10	0.66	0.30	1.01		1.01
	2500 years	0.05	Landers	Reservoir Slough	No Convergence			-	-	-	-	95.00	95.00	95.00			
			Whittier Narrows	Reservoir Slough	No Convergence			-	-	-	-	95.00	95.00				
			Whittier Narrows	Reservoir Slough	No Convergence			-	-	-	-	95.00	95.00				
	High tide low reservoir	0.5	43 years	0.7	Landers	Reservoir Slough	0.030	0.112	0.27	0.84	1.79	0.56	3.02	0.60	0.80		
					Whittier Narrows	Reservoir Slough	0.120	0.101	1.19	0.03	0.03	0.03	0.03	0.01		0.60	
					Whittier Narrows	Reservoir Slough	0.030	0.128	0.23	1.02	0.74	0.16	1.31	1.00	1.00		
475 years			0.25	Landers	Reservoir Slough	No Convergence			-	-	-	-	95.00	95.00	95.00		
				Whittier Narrows	Reservoir Slough	No Convergence			-	-	-	-	95.00	95.00			
				Whittier Narrows	Reservoir Slough	No Convergence			-	-	-	-	95.00	95.00			
2500 years	0.05	Landers	Reservoir Slough	No Convergence			-	-	-	-	95.00	95.00	95.00				
		Whittier Narrows	Reservoir Slough	No Convergence			-	-	-	-	95.00	95.00					
		Whittier Narrows	Reservoir Slough	No Convergence			-	-	-	-	95.00	95.00					

Note: 1 - For no convergence cases, probabilities of failure were estimated based on slope deformations of 8 feet  
 2 - Failure probability of section was taken as the maximum of the 4 sliding surfaces

**TABLE 10 - SUMMARY OF CALCULATED SLOPE DEFORMATIONS AND FAILURE PROBABILITIES FOR CROSS SECTION II WITH ROCK BERM, PEAT AT -40FT (LIQUEFIED CASE)**

Cross Section	Water Level Scenario	Ground Motion Level	Time History	Sliding Surface	K <sub>y</sub> (g)	K <sub>max</sub> (g)	K <sub>y</sub> /K <sub>max</sub>	Slope Deformation (feet)				Probability of Failure <sup>1</sup> (%)	Probability of Failure for Section <sup>2</sup> (%)	Average Probability of Failure for Section (%)
								Newmark	Makdisi and Seed					
									Best Estimate	Min Estimate	Max Estimate			
Cross Section II (Peat at -40 ft)	Low tide high reservoir	43 years	Landers	Reservoir Slough	0.063 0.042	0.108 0.077	0.58 0.55	0.09 0.11	0.27 0.34	0.08 0.08	0.46 0.60	0.01 0.01	0.01	
			Whittier Narrows	Reservoir Slough	0.063 0.042	0.103 0.080	0.61 0.53	0.14 0.15	0.10 0.13	0.03 0.03	0.16 0.22	0.01 0.02		0.02
			Landers	Reservoir Slough	0.063 0.042	0.214 0.156	0.29 0.27	1.41 1.67	1.57 1.72	0.43 0.47	2.71 2.97	2.27 3.51		3.51
		475 years	Whittier Narrows	Reservoir Slough	0.063 0.042	0.194 0.148	0.32 0.28	2.04 1.97	0.53 0.62	0.09 0.13	0.96 1.11	5.71 5.25	5.71	4.61
			2500 years	Landers	Reservoir Slough	No Convergence			-	-	-	-	95.00 95.00	95.00
		Whittier Narrows		Reservoir Slough	No Convergence			-	-	-	-	95.00 95.00	95.00	
	High tide low reservoir	43 years	Landers	Reservoir Slough	0.037 0.068	0.116 0.075	0.32 0.91	0.33 0.03	1.48 0.03	0.38 0.03	2.58 0.03	0.06 0.01	0.06	0.12
			Whittier Narrows	Reservoir Slough	0.037 0.068	0.114 0.073	0.32 0.93	0.53 0.03	0.53 0.03	0.09 0.03	0.96 0.03	0.19 0.01	0.19	
			475 years	Landers	Reservoir Slough	No Convergence			-	-	-	-	95.00 95.00	
		Whittier Narrows		Reservoir Slough	No Convergence			-	-	-	-	95.00 95.00	95.00	
		2500 years	Landers	Reservoir Slough	No Convergence			-	-	-	-	95.00 95.00	95.00	95.00
			Whittier Narrows	Reservoir Slough	No Convergence			-	-	-	-	95.00 95.00	95.00	

Note: 1 - For no convergence cases, probabilities of failure were estimated based on slope deformations of 8 feet  
 2 - Failure probability of section was taken as the maximum of the 4 sliding surfaces

**Table 10A - Summary of Maximum Calculated Deformations  
475-year Earthquake Event  
(deformations in feet, to nearest 0.1 foot)**

<b>Bottom of Peat at Elevation –20 Feet</b>					
<b>Option</b>	<b>Water Level Scenario</b>	<b>Non-liquefied Case</b>		<b>Liquefied Case</b>	
		<b>Slough-side</b>	<b>Res.-side</b>	<b>Slough-side</b>	<b>Res.-side</b>
Bench	Low tide, high res.	0.7	0.1	3.3	1.4
	High tide, low res.	0.4	0.4	N.C.	N.C.
Rock Berm	Low tide, high res.	<0.1	0.1	0.6	1.4
	High tide, low res.	<0.1	0.4	N.C.	N.C.
<b>Bottom of Peat at Elevation –40 Feet</b>					
Bench	Low tide, high res.	1.6	0.2	9.0	2.2
	High tide, low res.	N.C.	N.C.	N.C.	N.C.
Rock Berm	Low tide, high res.	0.4	0.3	2.0	2.0
	High tide, low res.	N.C.	N.C.	N.C.	N.C.

Notes: Deformations based on Newmark analysis (Tables 3 to 10)  
N.C. = non-convergence; deformations are large (>17 feet)

**Table 11 - Probability of Failure of Cross Section I (Peat at -20 ft) With Bench Alternative**

Cross Section	Water Level Scenario	Probability of Scenario (%)	Ground Motion Level	Probability of Ground Motion (%)	Liquefaction	Probability of Liquefaction (%)	Average Probability of Failure for Section (%)	Probability of Failure in 50 years (%)
Cross Section I (Peat at -20 ft)	Low tide high reservoir	33	43 years	70	Liquefaction	20	0.23	0.011
					Non-Liquefaction	80	0.01	0.002
			475 years	25	Liquefaction	70	14.68	0.848
					Non-Liquefaction	30	0.23	0.006
			2500 years	5	Liquefaction	95	95.00	1.489
					Non-Liquefaction	5	95.00	0.078
	High tide low reservoir	67	43 years	70	Liquefaction	20	1.11	0.104
					Non-Liquefaction	80	0.01	0.004
			475 years	25	Liquefaction	70	95.00	11.139
					Non-Liquefaction	30	0.09	0.005
			2500 years	5	Liquefaction	95	95.00	3.023
					Non-Liquefaction	5	95.00	0.159

**Sum of Failure Probabilities (%)**      16.867

**Table 12 - Probability of Failure of Cross Section II (Peat at -40 ft) With Bench Alternative**

Cross Section	Water Level Scenario	Probability of Scenario (%)	Ground Motion Level	Probability of Ground Motion (%)	Liquefaction	Probability of Liquefaction (%)	Average Probability of Failure for Section (%)	Probability of Failure in 50 years (%)
Cross Section II (Peat at -40 ft)	Low tide high reservoir	33	43 years	70	Liquefaction	20	2.14	0.099
					Non-Liquefaction	80	0.01	0.002
			475 years	25	Liquefaction	70	68.53	3.958
					Non-Liquefaction	30	2.95	0.073
			2500 years	5	Liquefaction	95	95.00	1.489
					Non-Liquefaction	5	95.00	0.078
	High tide low reservoir	67	43 years	70	Liquefaction	20	1.50	0.141
					Non-Liquefaction	80	0.01	0.004
			475 years	25	Liquefaction	70	95.00	11.139
					Non-Liquefaction	30	95.00	4.774
			2500 years	5	Liquefaction	95	95.00	3.023
					Non-Liquefaction	5	95.00	0.159

**Sum of Failure Probabilities (%)**      24.938

**Table 13 - Probability of Failure of Cross Section I (Peat at -20 ft) With Rock Berm Alternative**

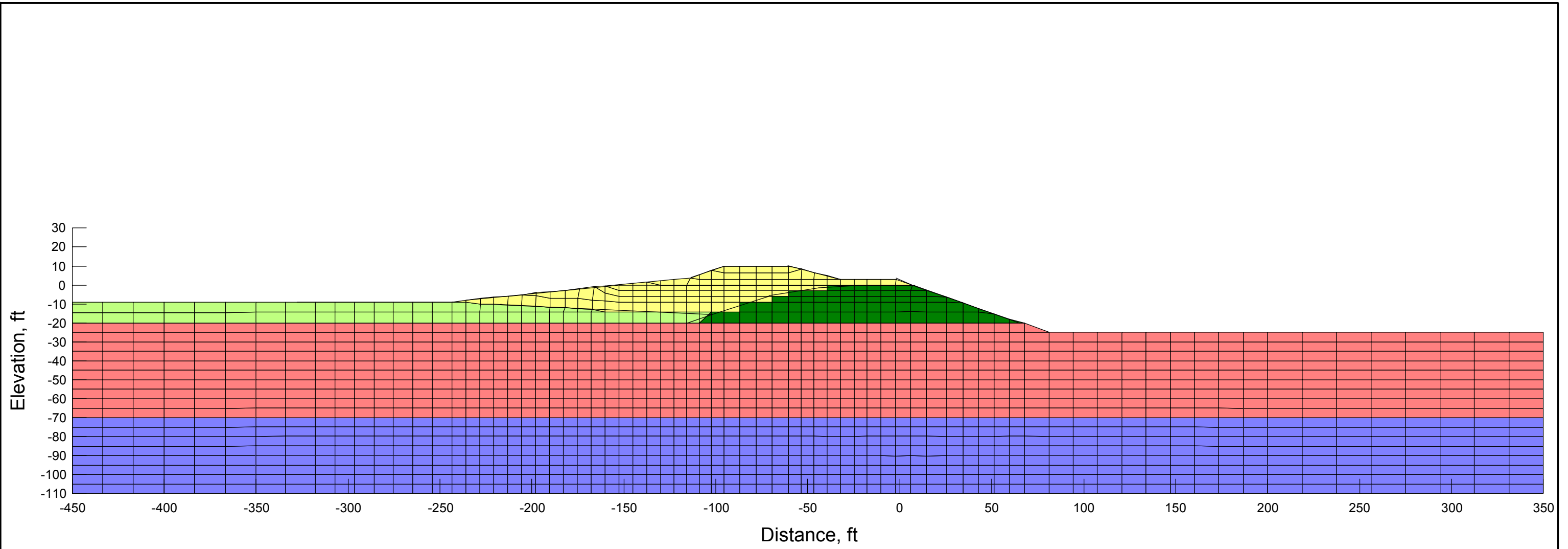
Cross Section	Water Level Scenario	Probability of Scenario (%)	Ground Motion Level	Probability of Ground Motion (%)	Liquefaction	Probability of Liquefaction (%)	Average Probability of Failure for Section (%)	Probability of Failure in 50 years (%)
Cross Section I (Peat at -20 ft)	Low tide high reservoir	33	43 years	70	Liquefaction	20	0.01	0.000
					Non-Liquefaction	80	0.01	0.002
			475 years	25	Liquefaction	70	1.53	0.088
					Non-Liquefaction	30	0.01	0.000
			2500 years	5	Liquefaction	95	95.00	1.489
					Non-Liquefaction	5	95.00	0.078
	High tide low reservoir	67	43 years	70	Liquefaction	20	0.80	0.075
					Non-Liquefaction	80	0.01	0.004
			475 years	25	Liquefaction	70	95.00	11.139
					Non-Liquefaction	30	0.06	0.003
			2500 years	5	Liquefaction	95	95.00	3.023
					Non-Liquefaction	5	95.00	0.159

**Sum of Failure Probabilities (%)**      16.061

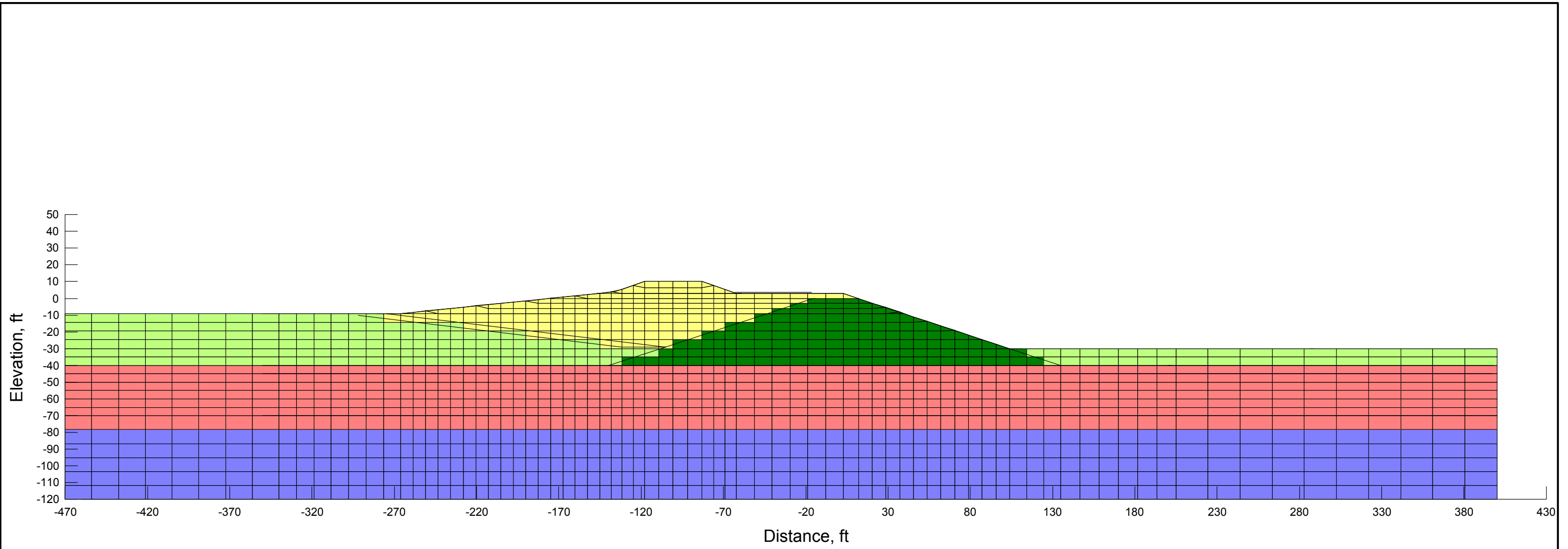
**Table 14 - Probability of Failure of Cross Section II (Peat at -40 ft) With Rock Berm Alternative**

Cross Section	Water Level Scenario	Probability of Scenario (%)	Ground Motion Level	Probability of Ground Motion (%)	Liquefaction	Probability of Liquefaction (%)	Average Probability of Failure for Section (%)	Probability of Failure in 50 years (%)
Cross Section II (Peat at -40 ft)	Low tide high reservoir	33	43 years	70	Liquefaction	20	0.01	0.000
					Non-Liquefaction	80	0.01	0.002
			475 years	25	Liquefaction	70	4.61	0.266
					Non-Liquefaction	30	0.08	0.002
			2500 years	5	Liquefaction	95	95.00	1.489
					Non-Liquefaction	5	95.00	0.078
	High tide low reservoir	67	43 years	70	Liquefaction	20	0.12	0.011
					Non-Liquefaction	80	0.01	0.004
			475 years	25	Liquefaction	70	95.00	11.139
					Non-Liquefaction	30	95.00	4.774
			2500 years	5	Liquefaction	95	95.00	3.023
					Non-Liquefaction	5	95.00	0.159

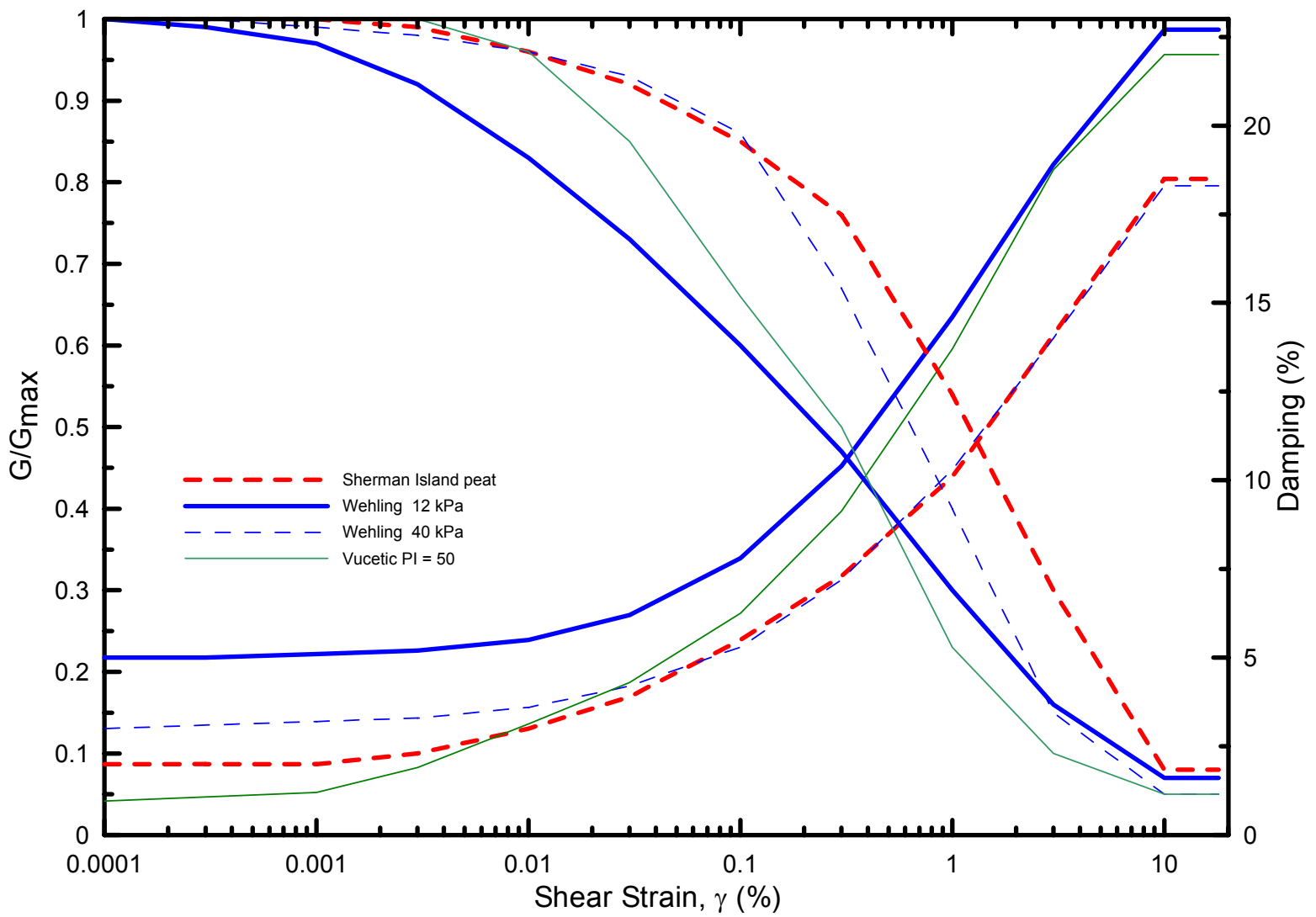
**Sum of Failure Probabilities (%)**      20.948



<b>DELTA WETLANDS PROJECT</b> IN-DELTA STORAGE FEASIBILITY STUDY		FINITE ELEMENT MODEL FOR SEISMIC ANALYSIS CROSS SECTION I ( PEAT AT -20 FT)	Figure 1
	December 2002 Project # 26814105		



<b>IN-DELTA STORAGE PROJECT</b>		FINITE ELEMENT MODEL FOR SEISMIC ANALYSIS CROSS SECTION II ( PEAT AT -40 FT)	Figure 2
<b>URS</b>	December 2002 Project # 26814105		



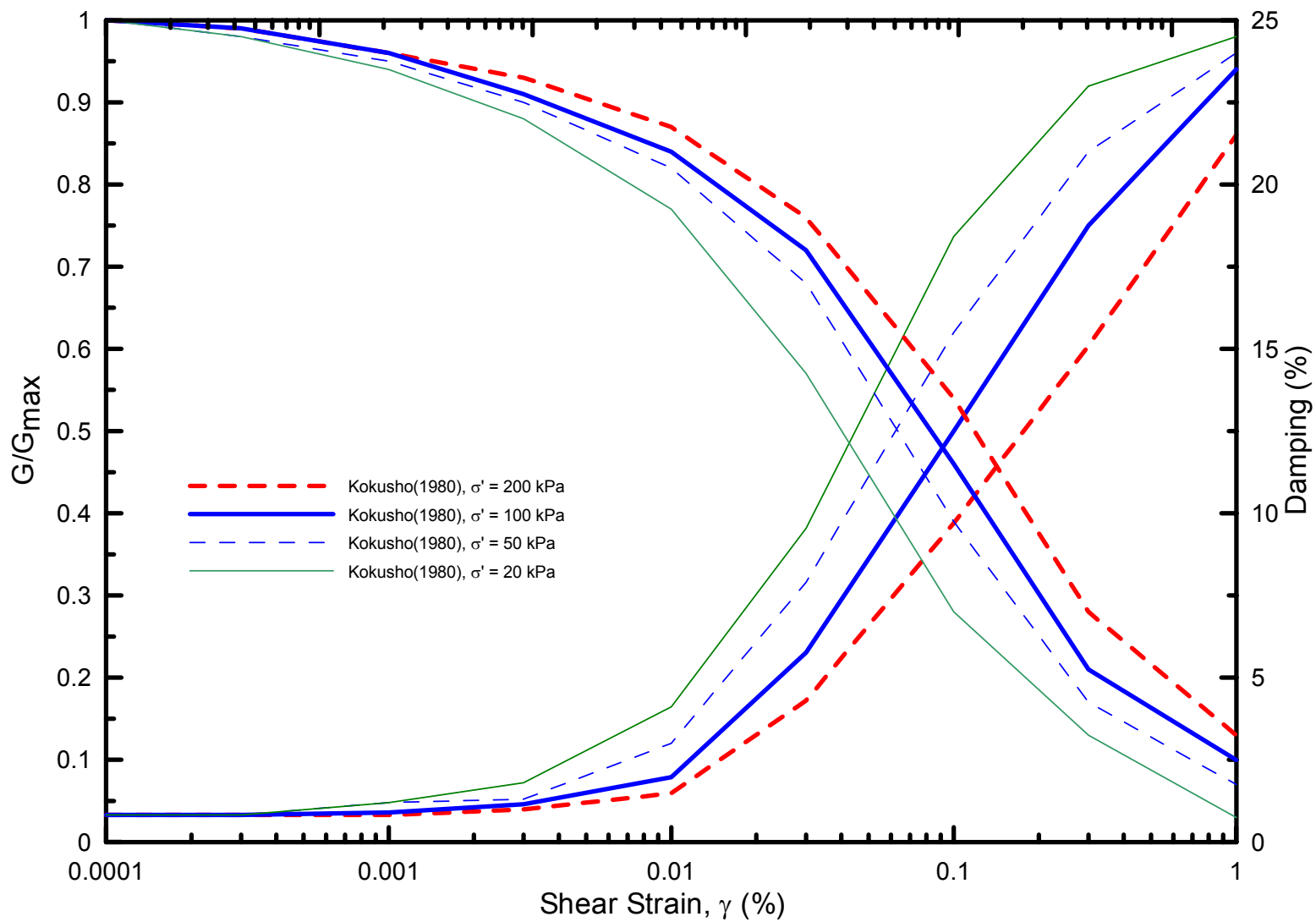
**IN-DELTA STORAGE PROJECT**



December 2002  
Project # 26814105

**MODULUS AND DAMPING CURVES  
FOR CLAY AND PEAT**

Figure 3



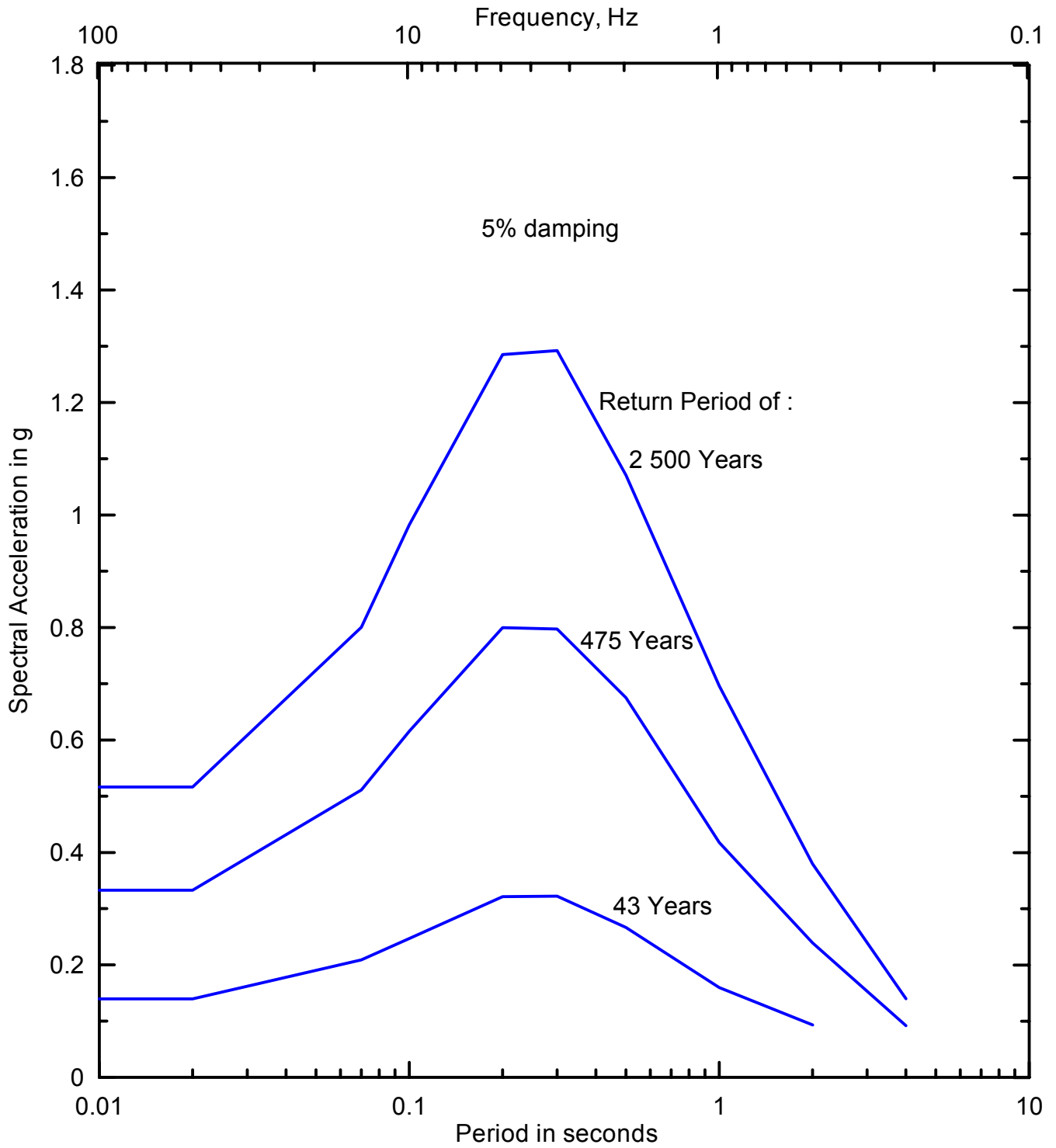
IN-DELTA STORAGE PROJECT

URS

December 2002  
Project # 26814105

MODULUS AND DAMPING CURVES  
FOR SAND

Figure 4



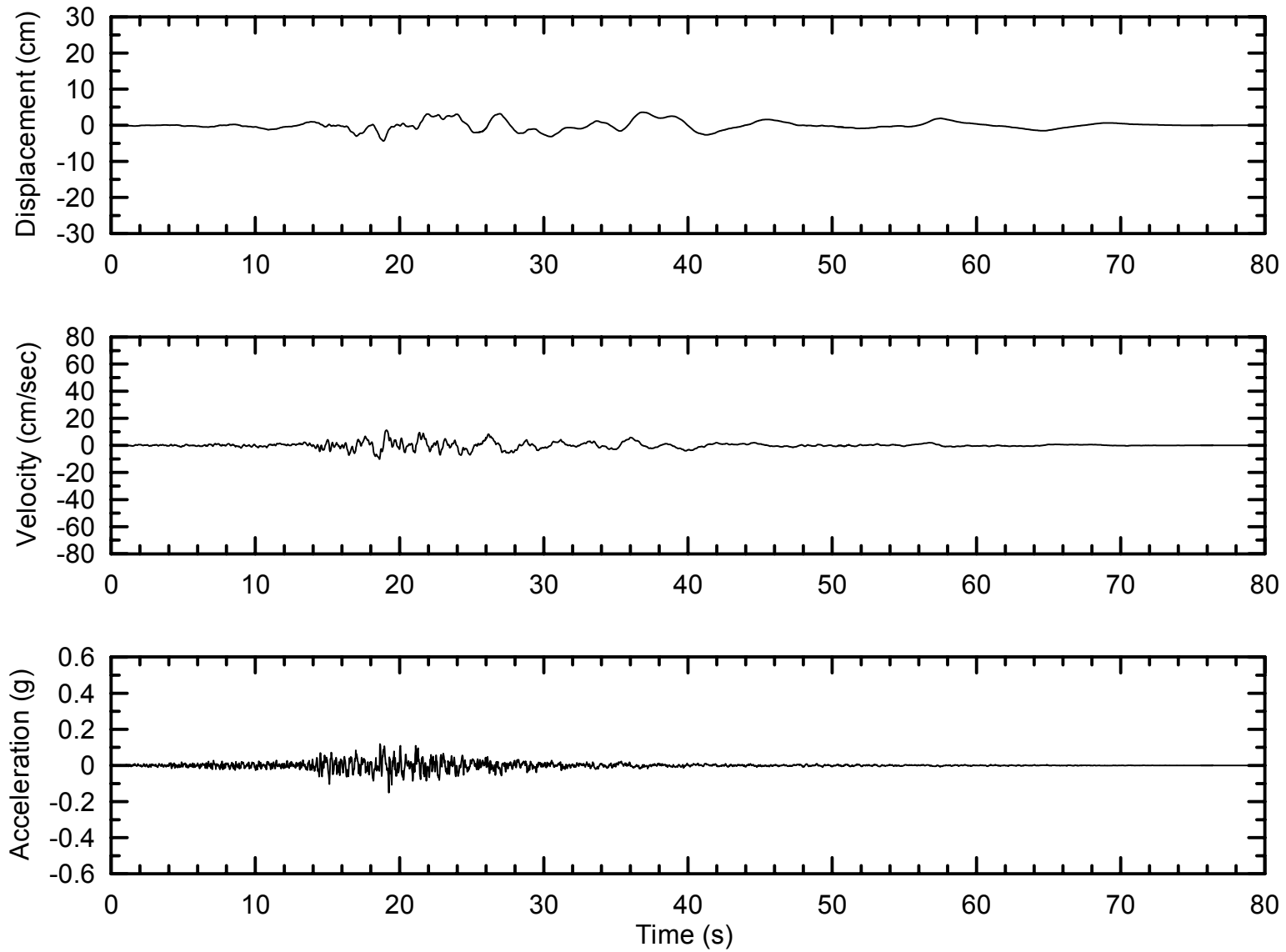
**IN-DELTA STORAGE PROJECT**

**URS**

December 2002  
Project # 26814105

TARGET RESPONSE SPECTRA FOR  
RETURN PERIODS OF 43, 475, 2500 YEARS

Figure 5

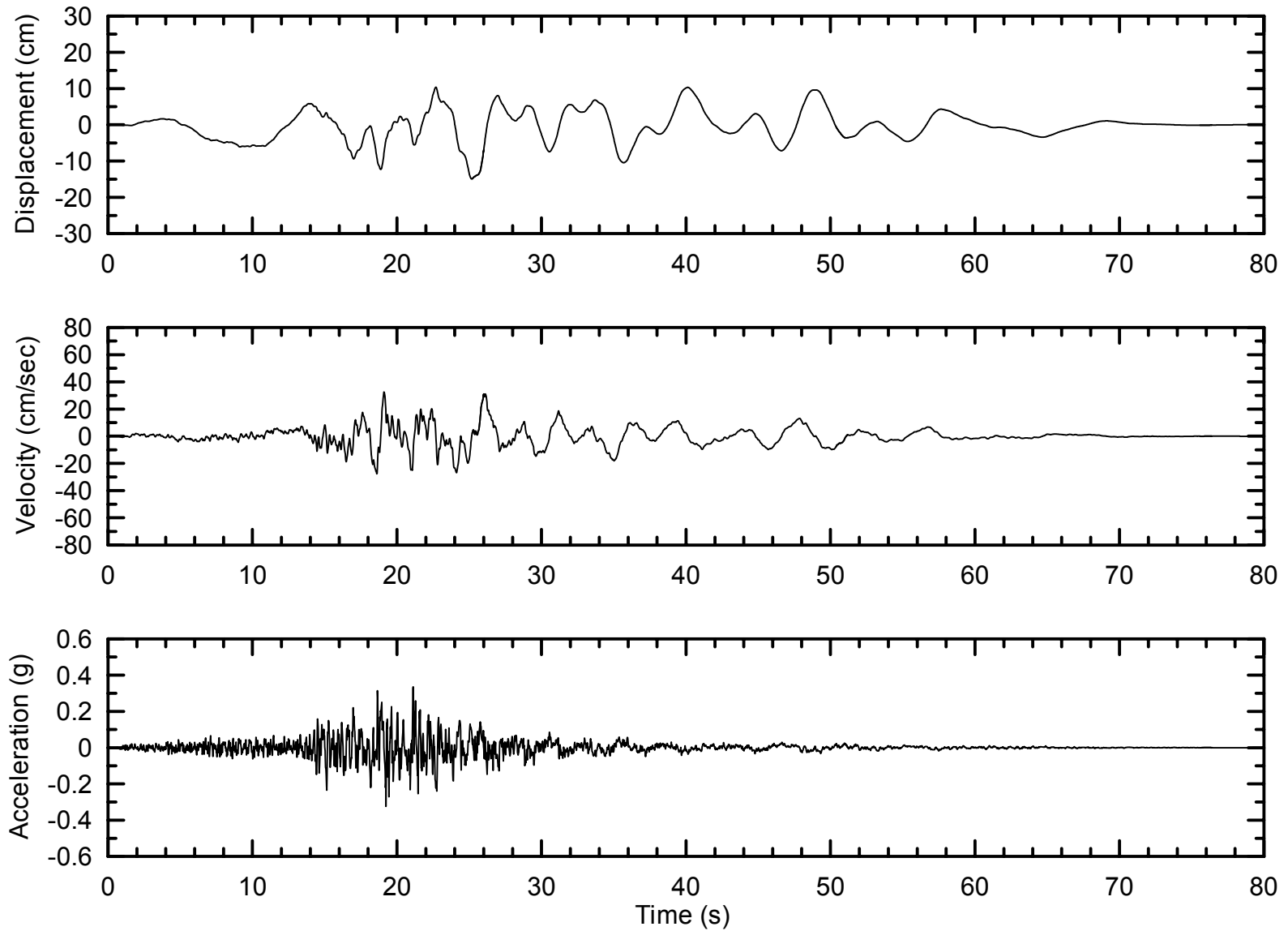


**IN-DELTA STORAGE PROJECT**

**URS** December 2002  
Project # 26814105

MATCHED TIME HISTORY FOR RETURN PERIOD OF 43 YEARS  
FOR 1992 LANDERS EARTHQUAKE  
AT STA.24577, 0 DEG. COMP.

Figure 6



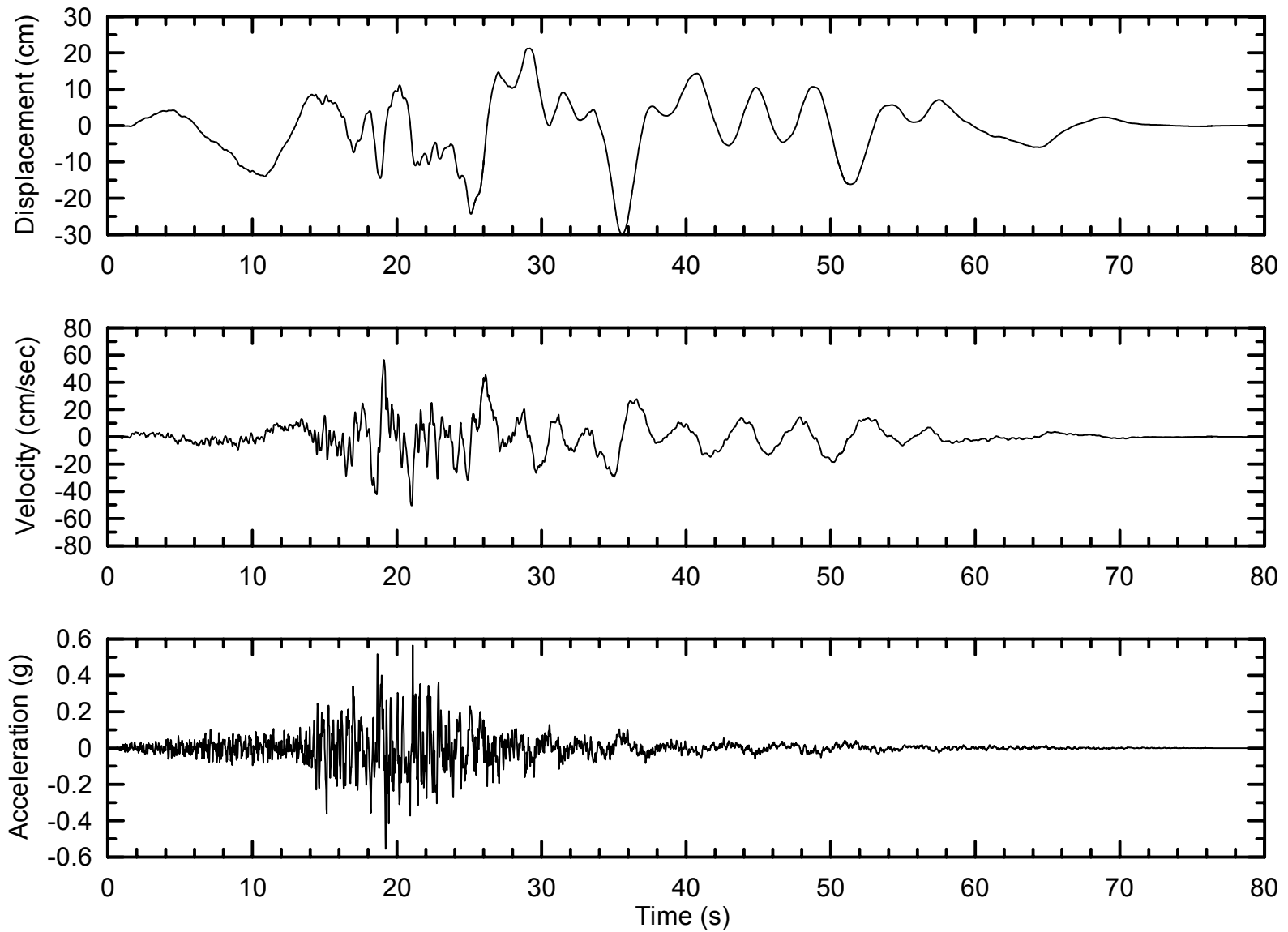
**IN-DELTA STORAGE PROJECT**

**URS**

December 2002  
Project # 26814105

MATCHED TIME HISTORY FOR RETURN PERIOD OF 475 YEARS  
FOR 1992 LANDERS EARTHQUAKE  
AT STA.24577, 0 DEG. COMP.

Figure 7



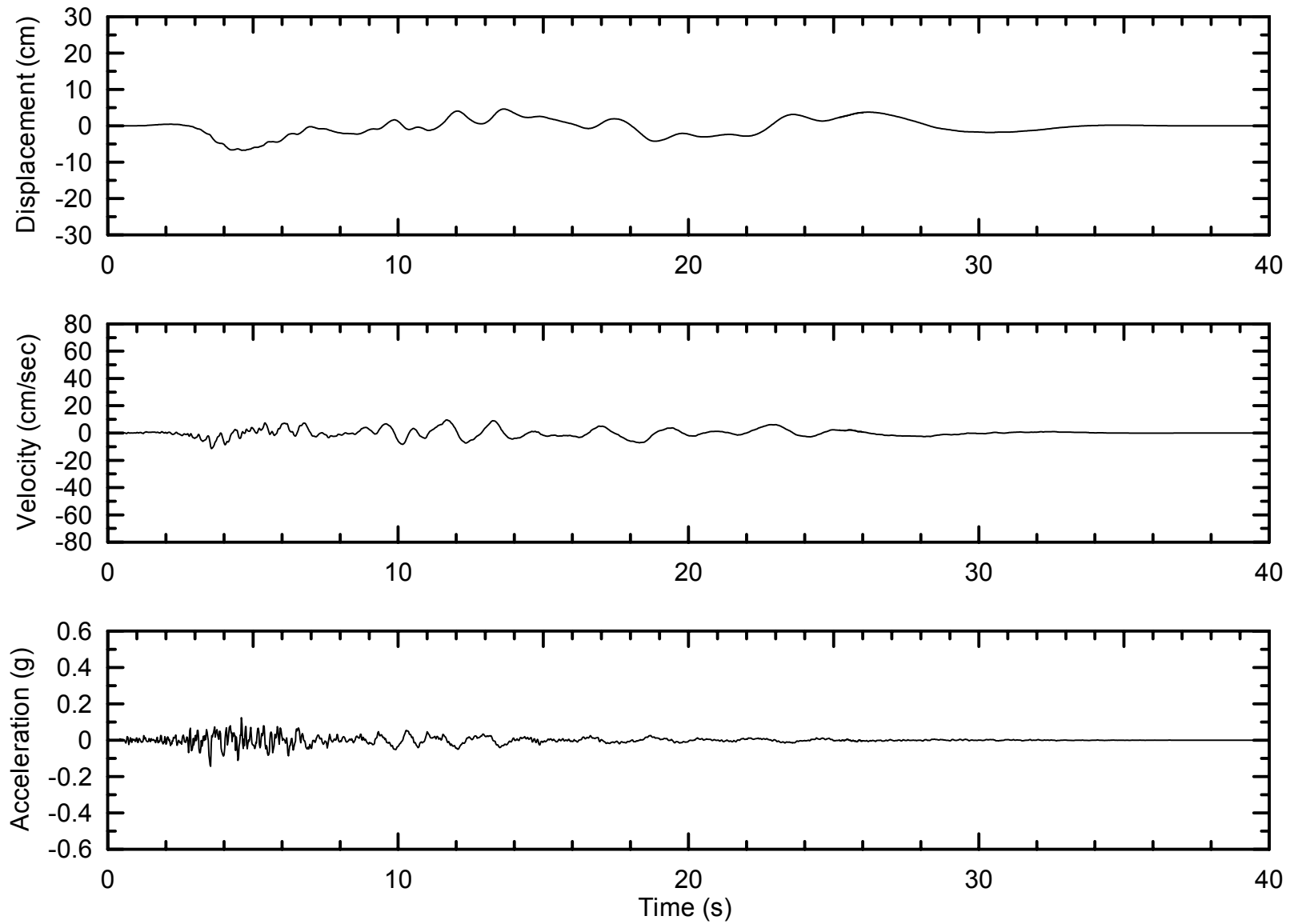
**IN-DELTA STORAGE PROJECT**

**URS**

December 2002  
Project # 26814105

MATCHED TIME HISTORY FOR RETURN PERIOD OF 2500 YEARS  
FOR 1992 LANDERS EARTHQUAKE  
AT STA.24577, 0 DEG. COMP.

Figure 8



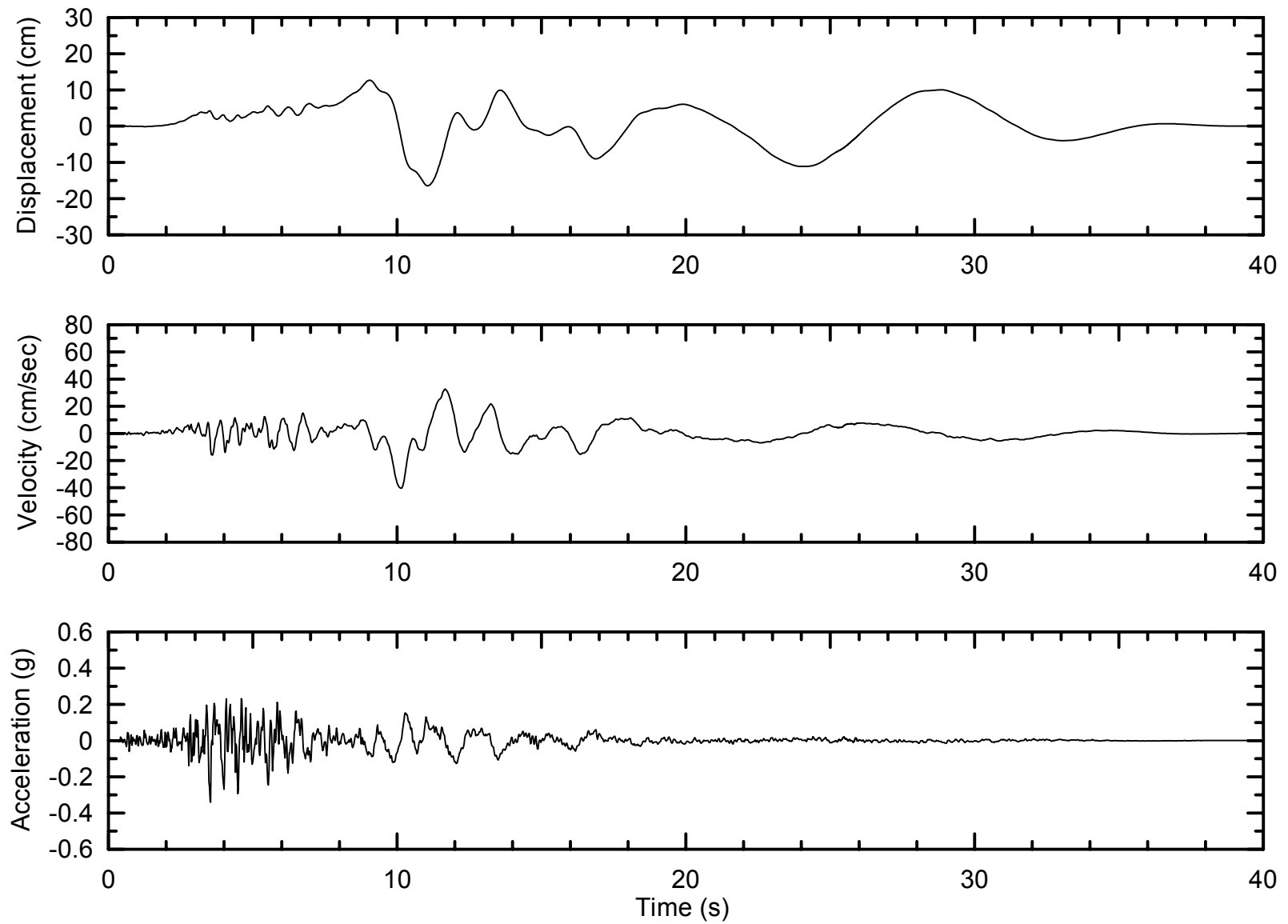
**IN-DELTA STORAGE PROJECT**

**URS**

December 2002  
Project # 26814105

MATCHED TIME HISTORY FOR RETURN PERIOD OF 43 YEARS  
FOR 1987 WHITTIER NARROWS EARTHQUAKE  
AT STA.24402, 90 DEG. COMP.

Figure 9



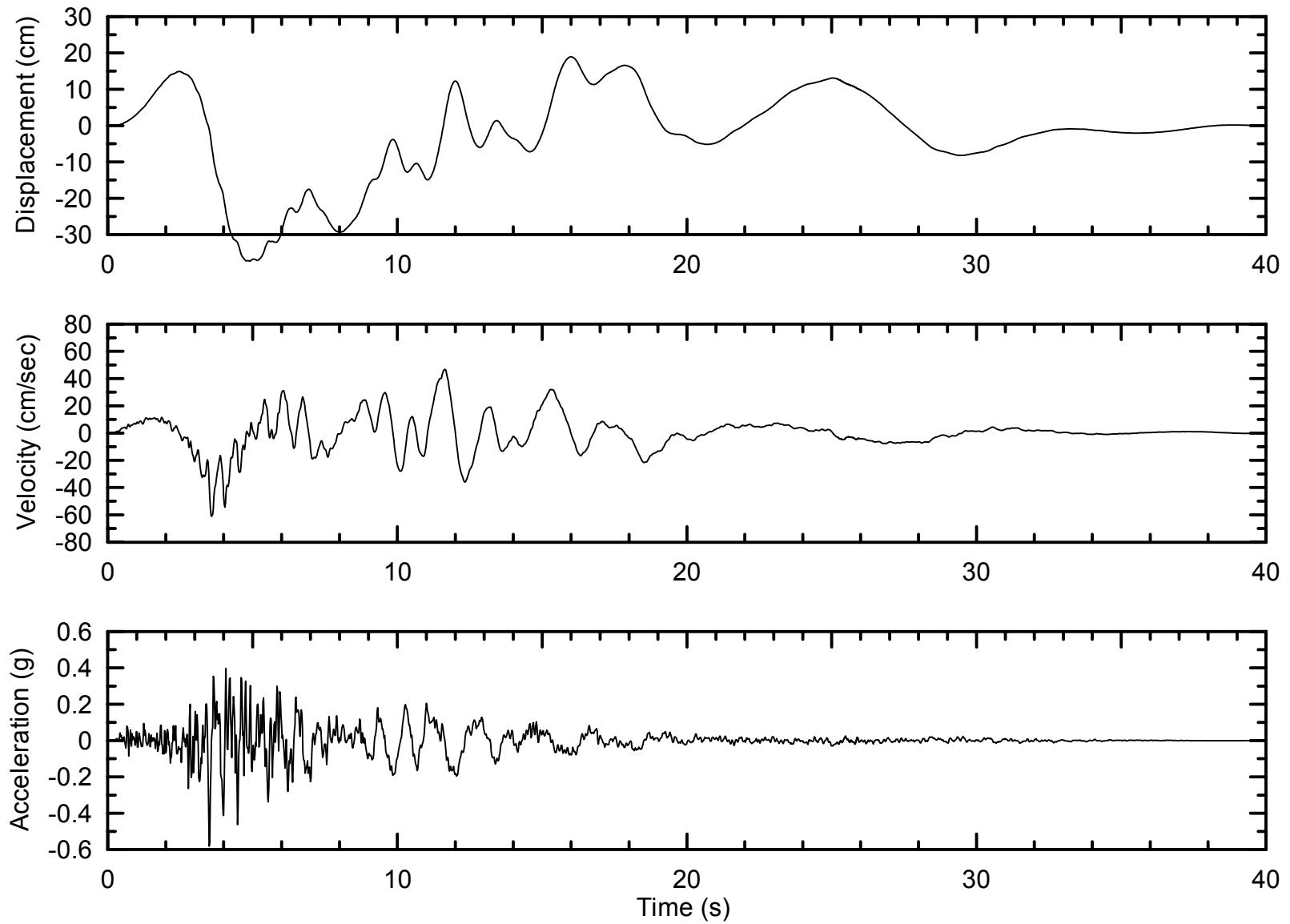
**IN-DELTA STORAGE PROJECT**

**URS**

December 2002  
Project # 26814105

MATCHED TIME HISTORY FOR RETURN PERIOD OF 475 YEARS  
FOR 1987 WHITTIER NARROWS EARTHQUAKE  
AT STA.24402, 90 DEG. COMP.

Figure 10



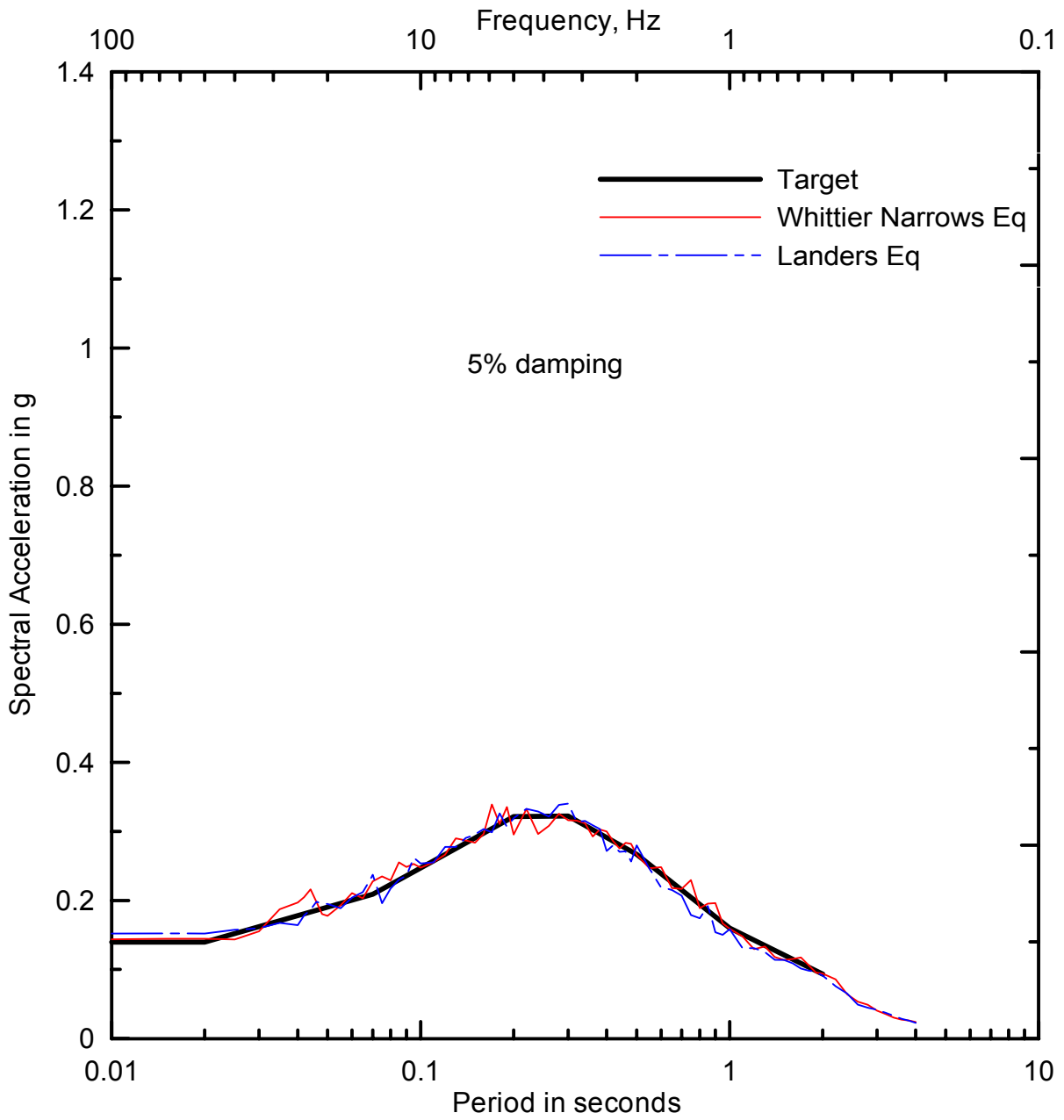
**IN-DELTA STORAGE PROJECT**

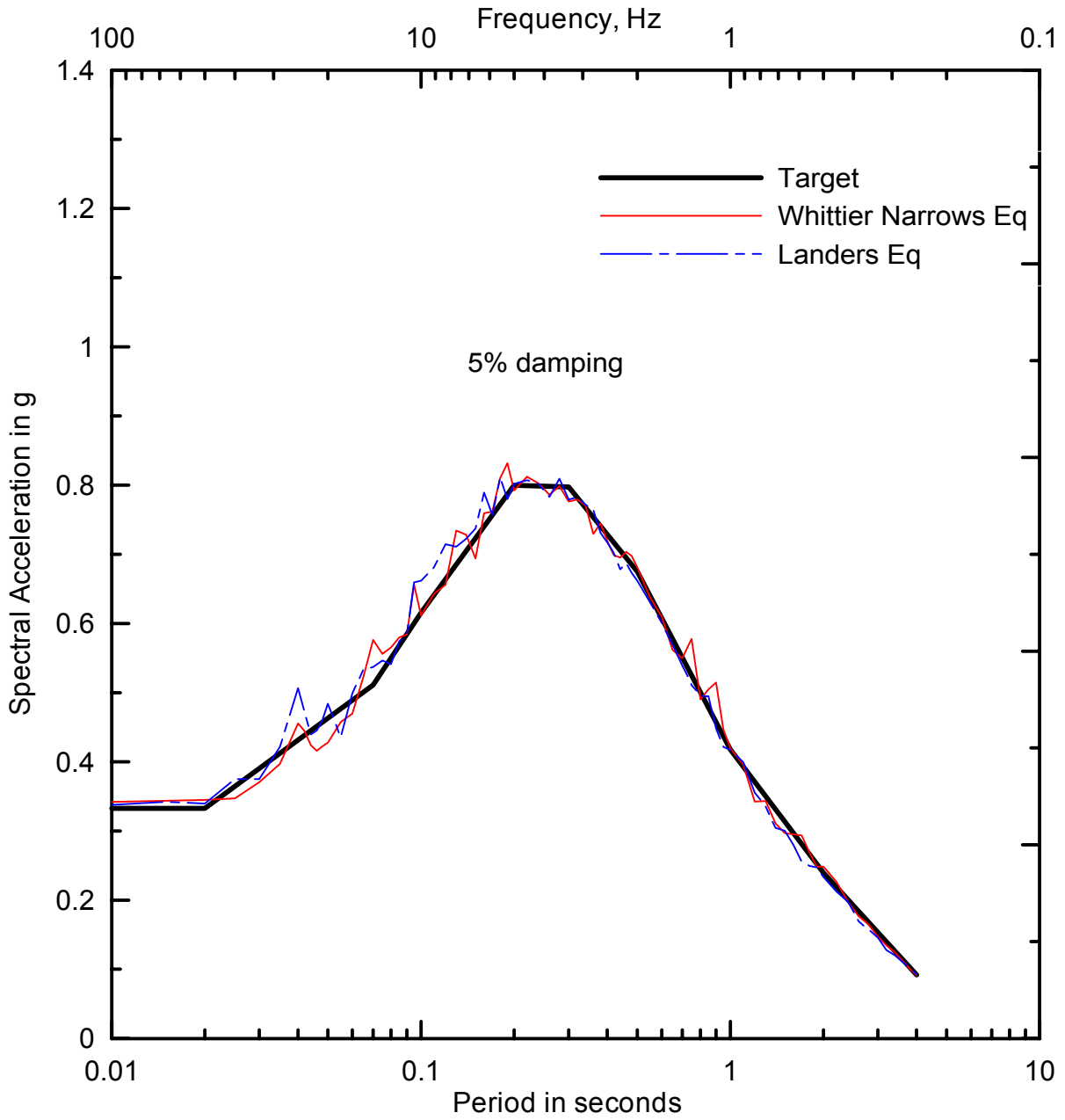
**URS**

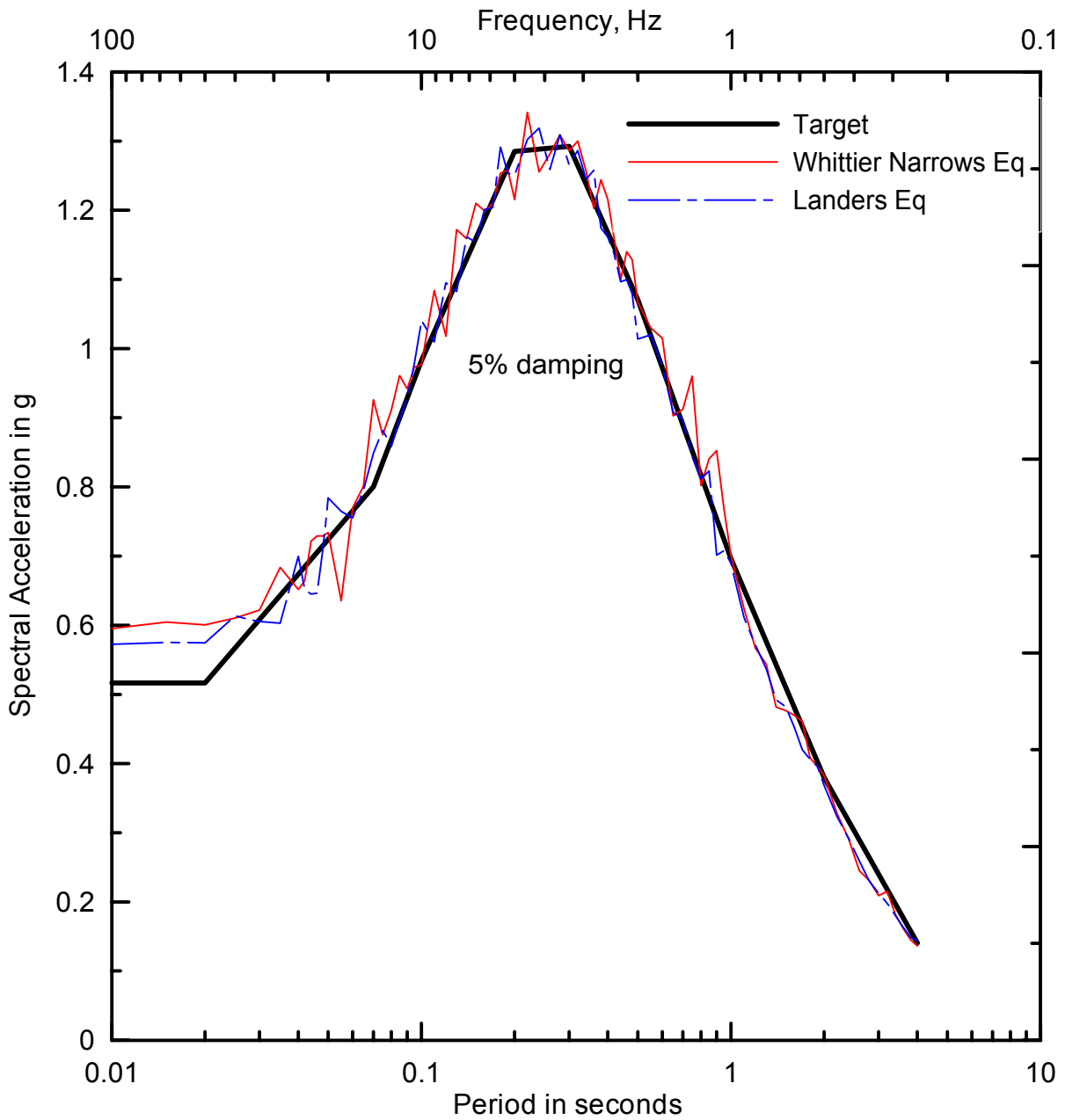
December 2002  
Project # 26814105

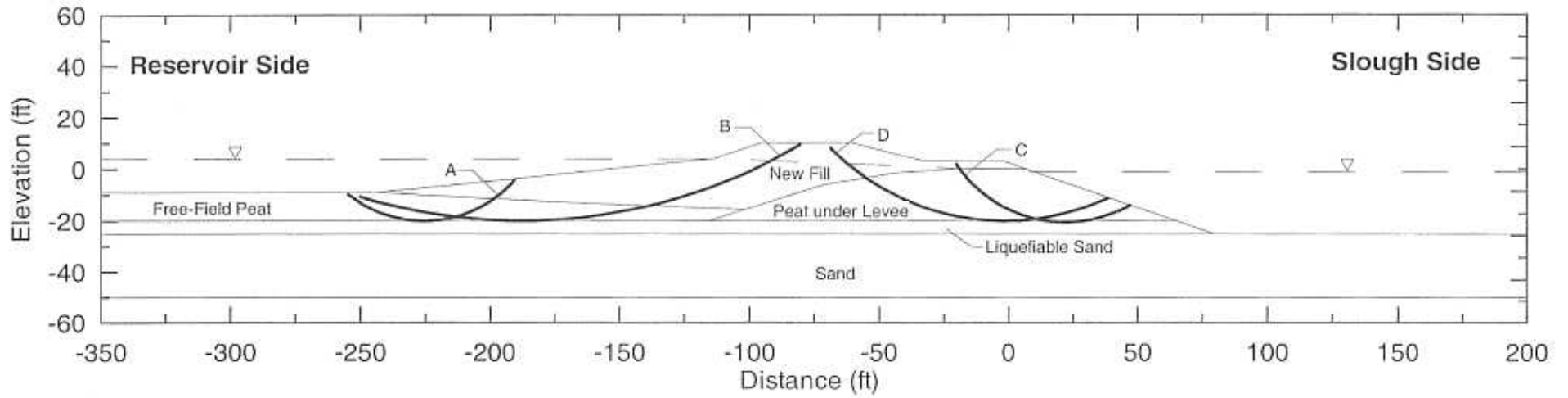
MATCHED TIME HISTORY FOR RETURN PERIOD OF 2500 YEARS  
FOR 1987 WHITTIER NARROWS EARTHQUAKE  
AT STA.24402, 90 DEG. COMP.

Figure 11









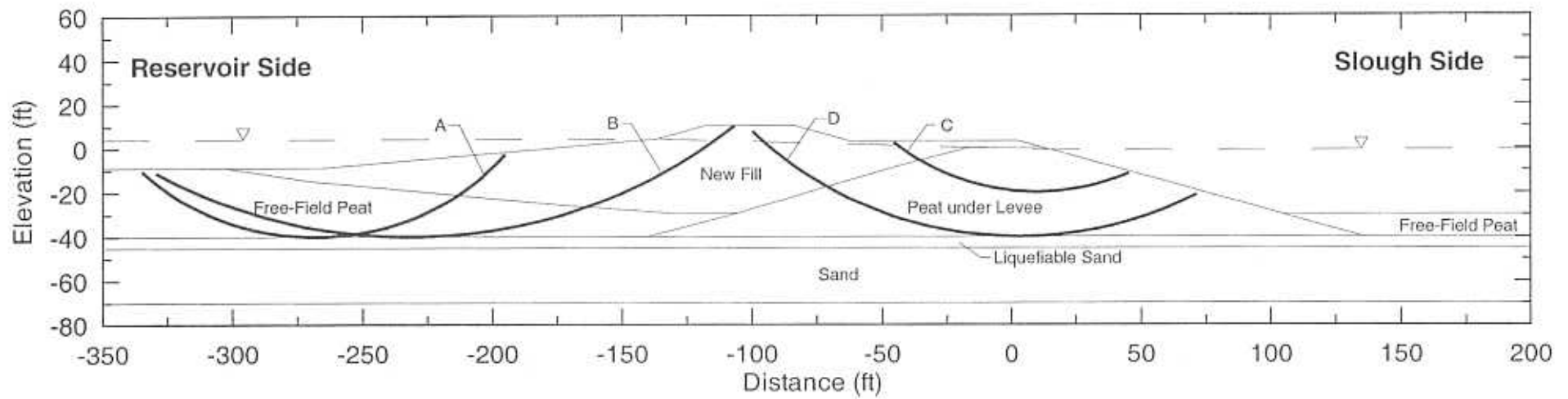
**IN-DELTA STORAGE PROJECT**

**URS**

December 2002  
Project # 26814105

CROSS SECTION I WITH BENCH ALTERNATIVE  
(PEAT AT -20FT)

**Figure 15**



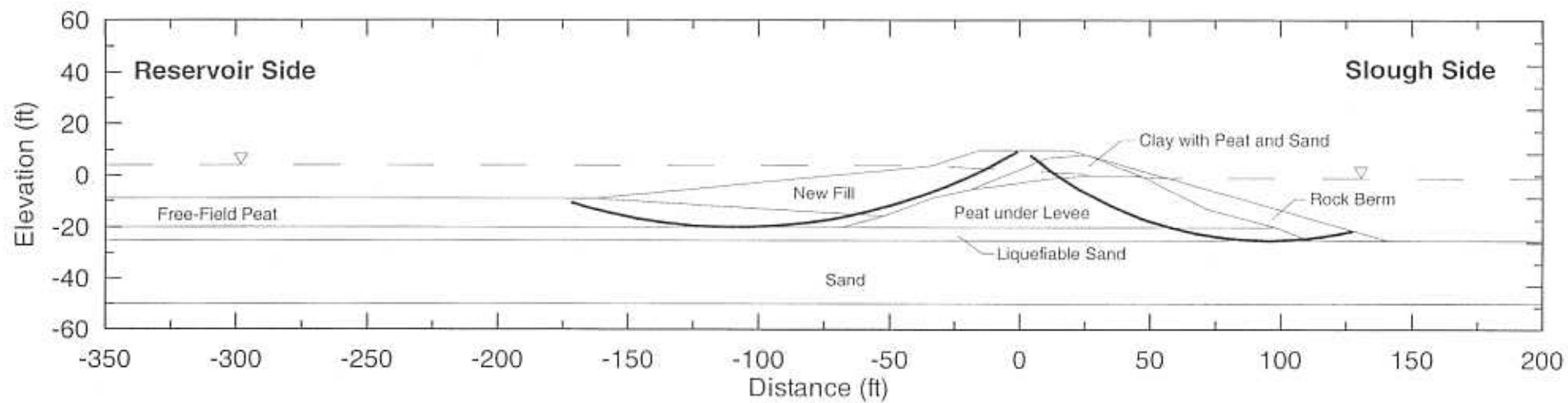
**IN-DELTA STORAGE PROJECT**

**URS**

December 2002  
Project # 26814105

CROSS SECTION II WITH BENCH ALTERNATIVE  
(PEAT AT -40FT)

**Figure 16**



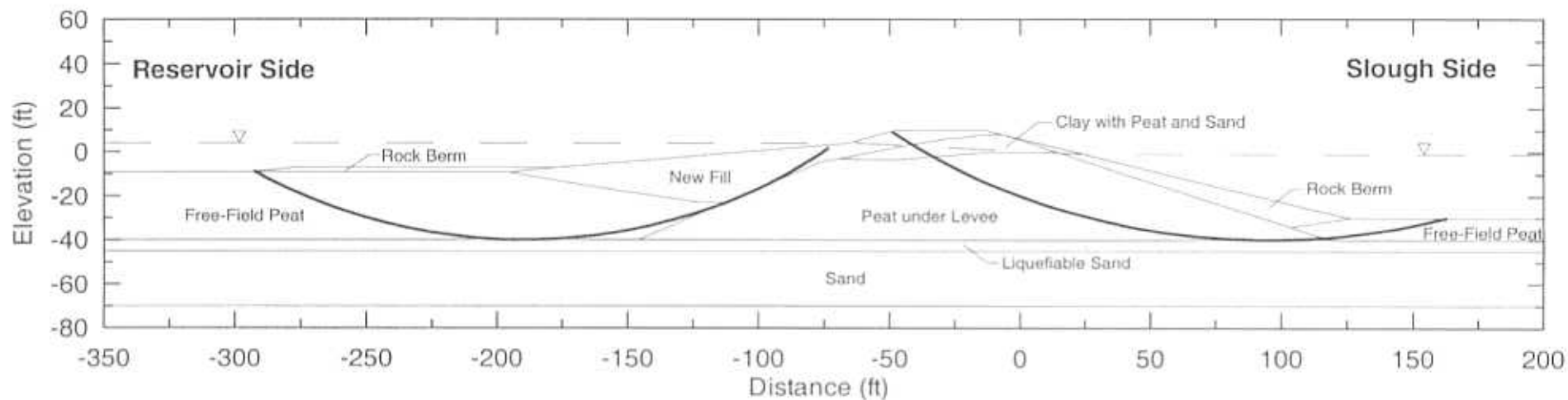
**IN-DELTA STORAGE PROJECT**

**URS**

December 2002  
Project # 26814105

CROSS SECTION I with Rock Berm  
(PEAT AT -20FT)

**Figure 17**



**IN-DELTA STORAGE PROJECT**

**URS**

December 2002  
Project # 26814105

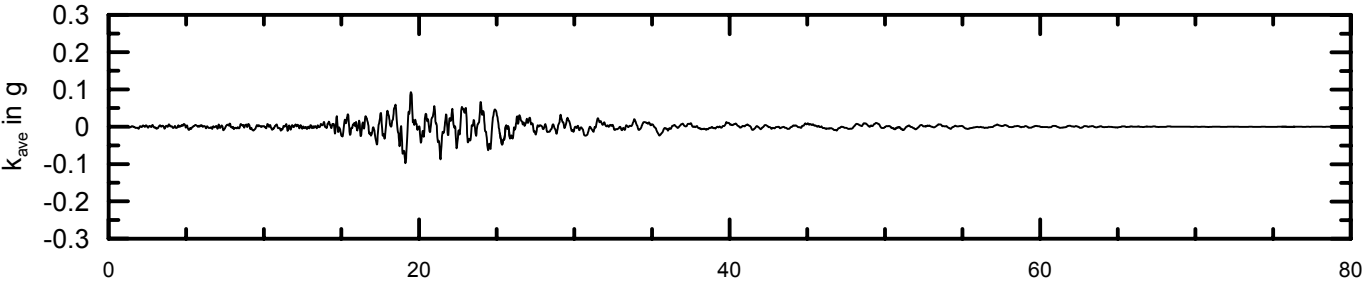
CROSS SECTION II with Rock Berm  
(PEAT AT -40FT)

**Figure 18**

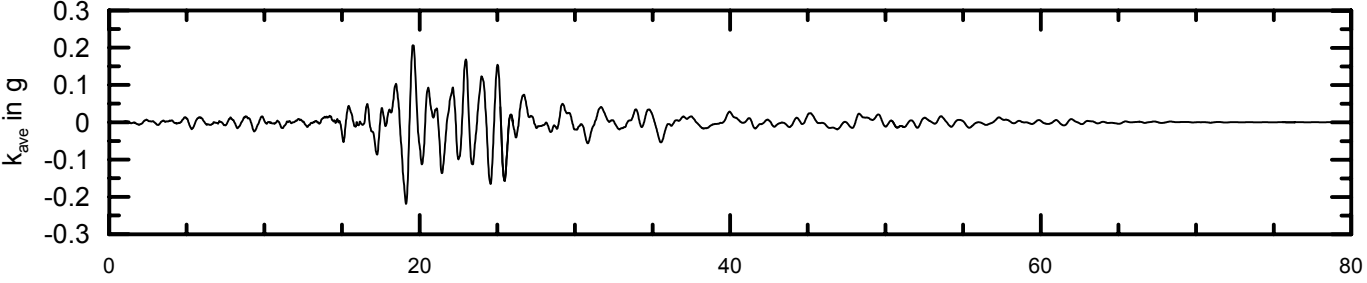
Cross Section I (Peat at - 20ft) - Low Tide High Reservoir  
 475 Years Return Period - Landers Earthquake

Sliding Surface

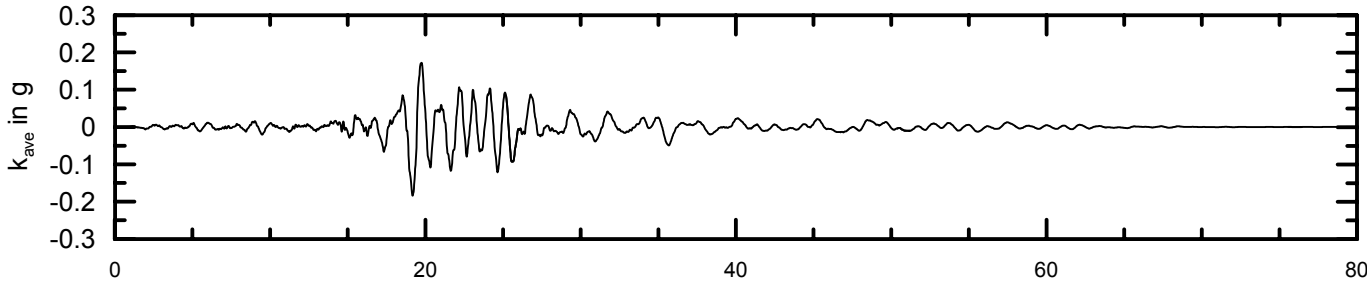
A



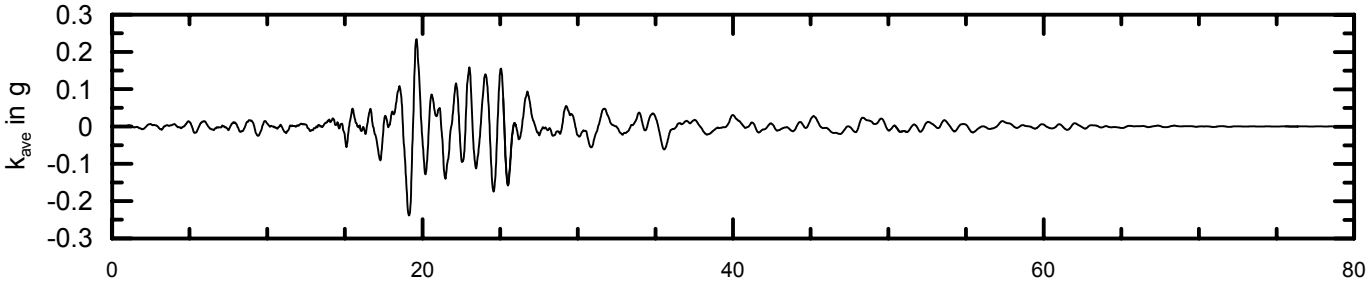
B



C



D



<b>IN-DELTA STORAGE PROJECT</b>	
<b>URS</b>	December 2002 Project # 26814105

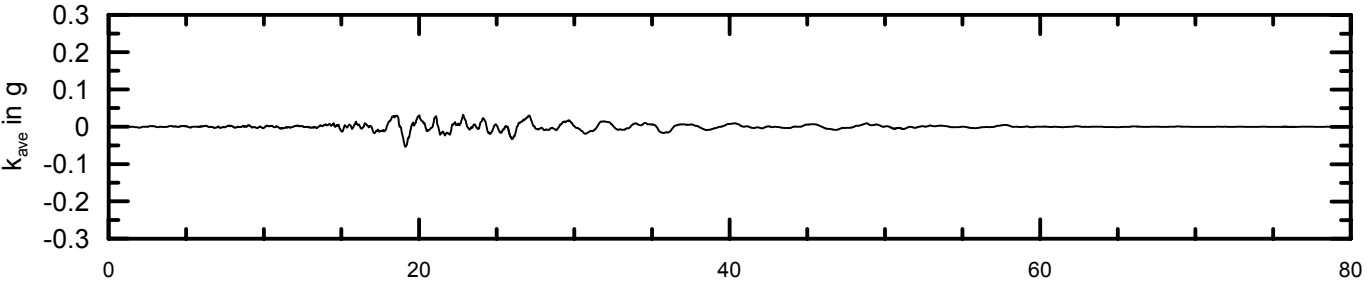
AVERAGE HORIZONTAL ACCELERATION  
 TIME HISTORIES FOR SLIDING MASSES  
 CROSS SECTION I - NONLIQUEFIED CASE  
 FOR LANDERS EARTHQUAKE

Figure 19

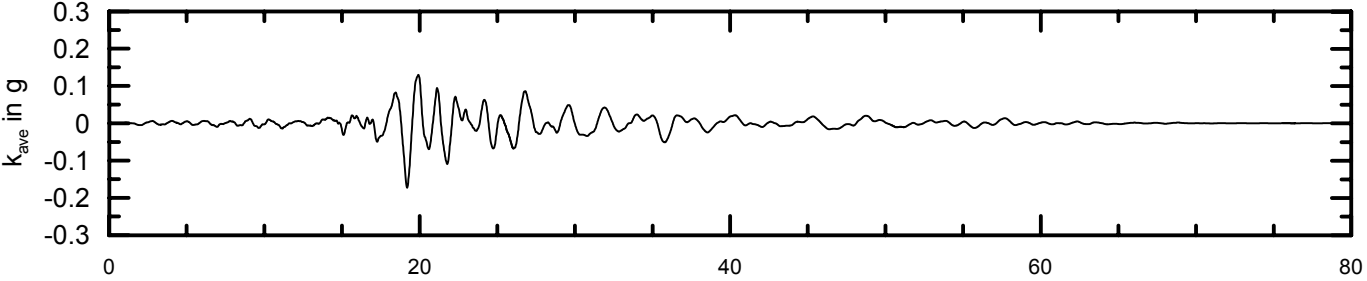
Cross Section II (Peat at -40 ft) -Low Tide High Reservoir  
 475 Years Return Period - Landers Earthquake

Sliding Surface

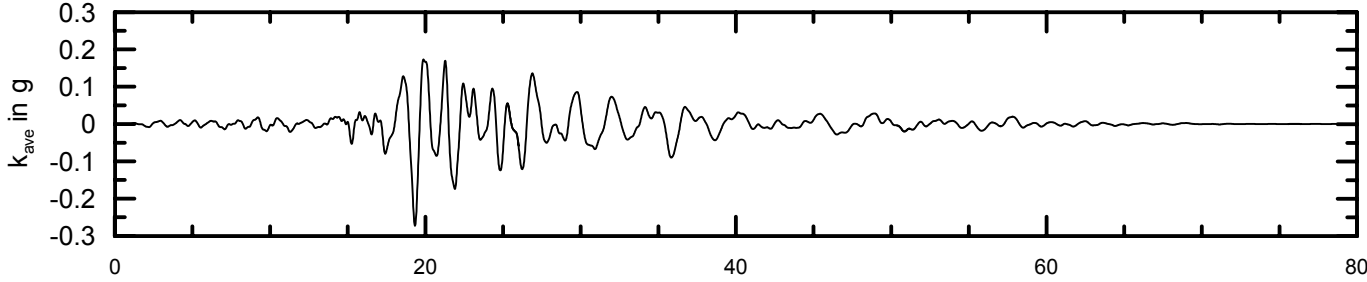
A



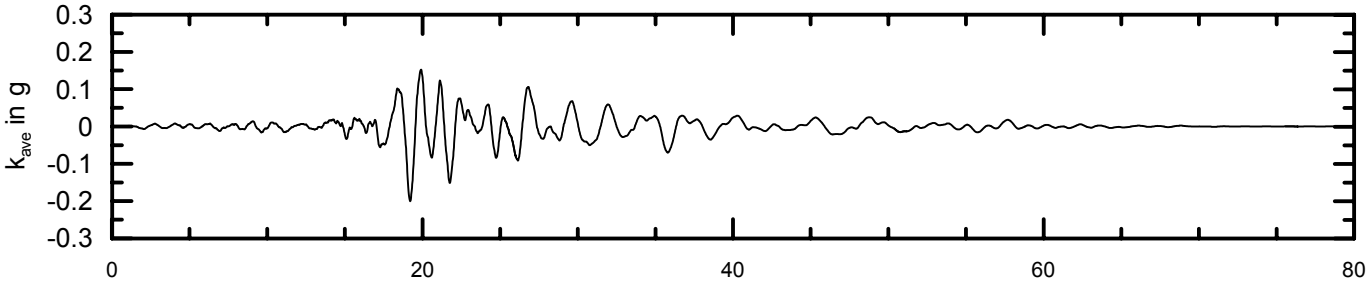
B



C



D



Time in second

**IN-DELTA STORAGE PROJECT**



December 2002  
 Project # 26814105

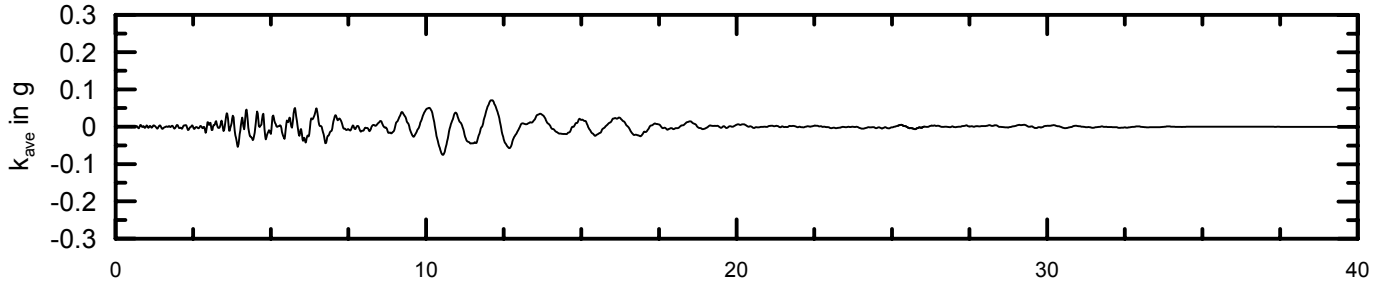
AVERAGE HORIZONTAL ACCELERATION  
 TIME HISTORIES FOR SLIDING MASSES  
 CROSS SECTION II - NONLIQUEFIED CASE  
 FOR LANDERS EARTHQUAKE

Figure 20

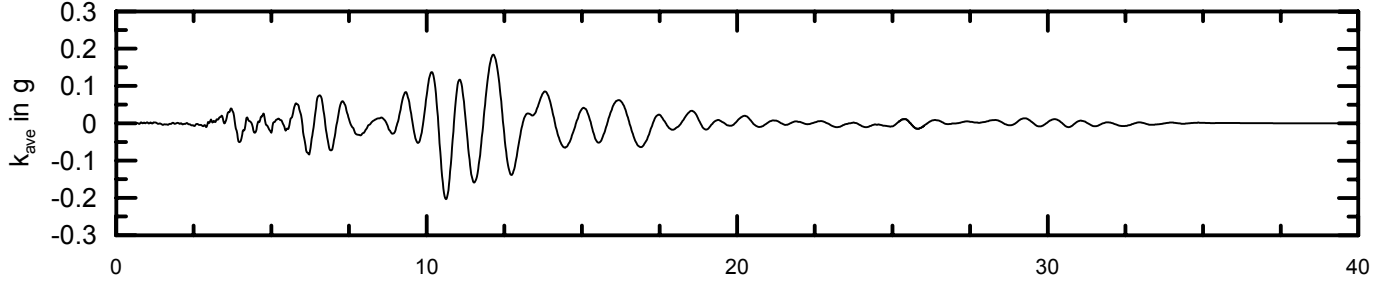
Cross Section I (Peat at - 20ft) - Low Tide High Reservoir  
 475 Years Return Period - Whittier Narrows Earthquake

Sliding Surface

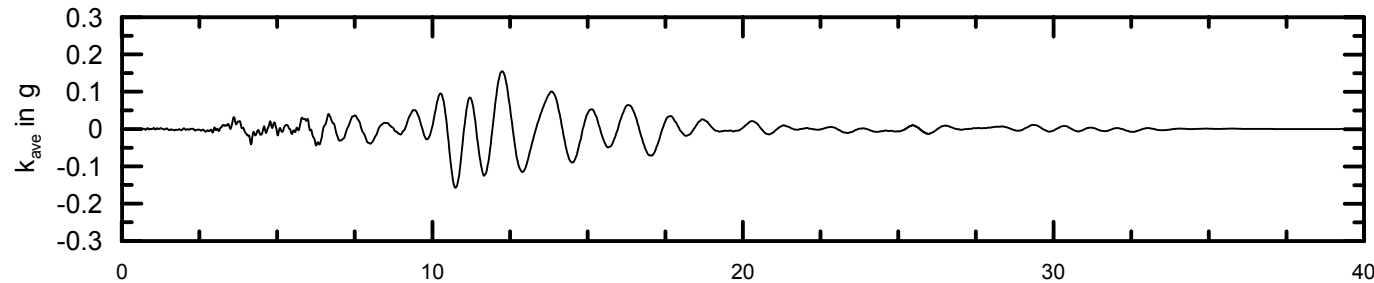
A



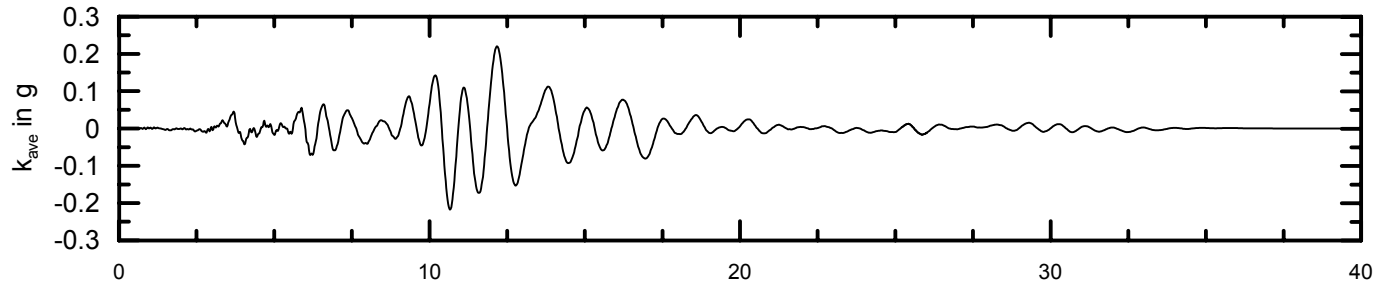
B



C



D



<b>IN-DELTA STORAGE PROJECT</b>	
<b>URS</b>	December 2002 Project # 26814105

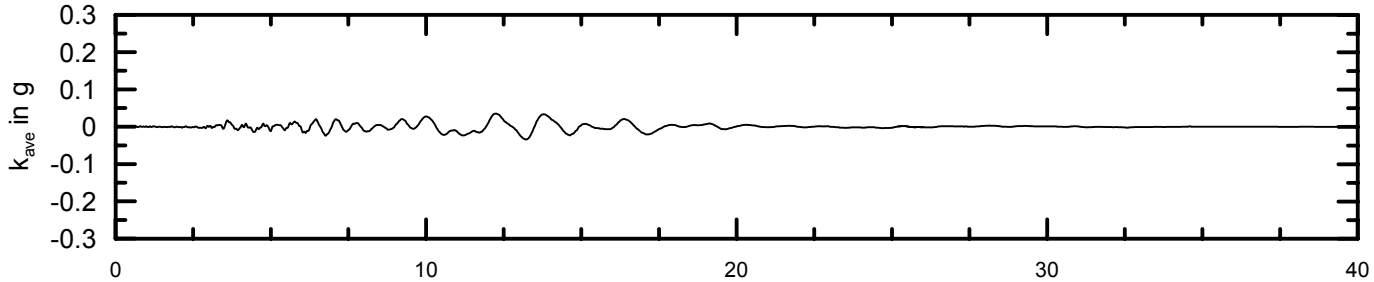
AVERAGE HORIZONTAL ACCELERATION  
 TIME HISTORIES FOR SLIDING MASSES  
 CROSS SECTION I - NONLIQUEFIED CASE  
 FOR WHITTIER NARROWS EARTHQUAKE

Figure 21

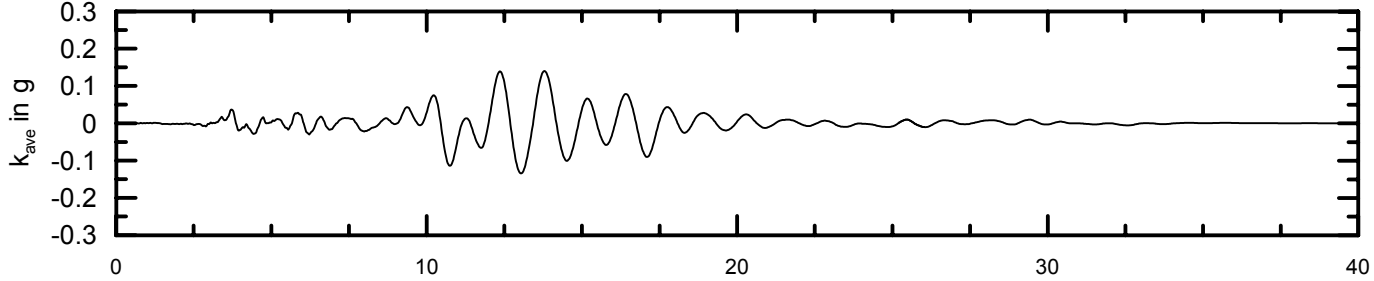
Cross Section II (Peat at -40 ft) -Low Tide High Reservoir  
 475 Years Return Period - Whittier Narrows Earthquake

Sliding Surface

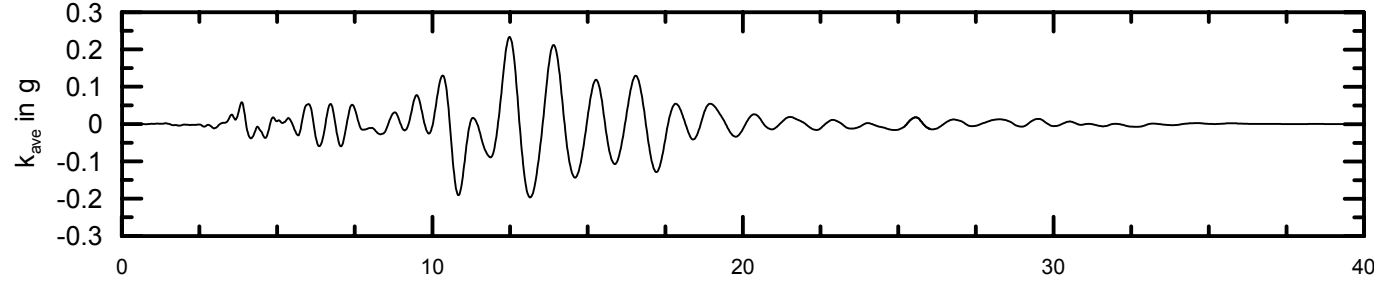
A



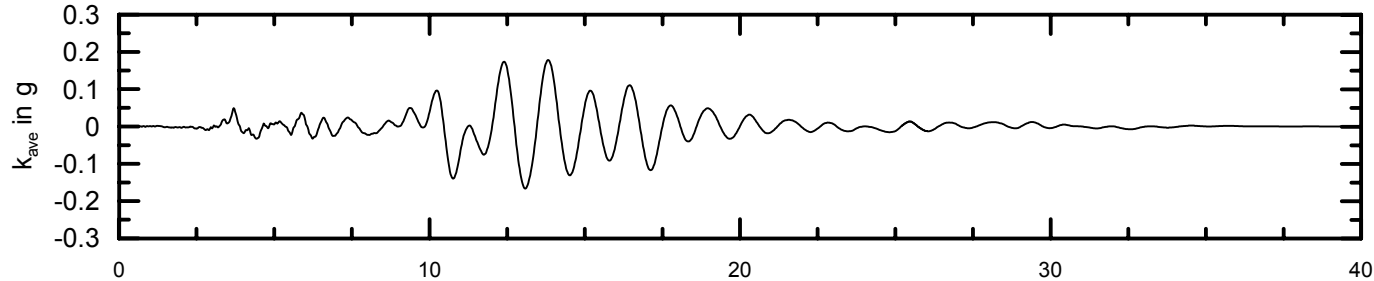
B



C



D



<b>IN-DELTA STORAGE PROJECT</b>	
<b>URS</b>	December 2002 Project # 26814105

AVERAGE HORIZONTAL ACCELERATION  
 TIME HISTORIES FOR SLIDING MASSES  
 CROSS SECTION II - NONLIQUEFIED CASE  
 FOR WHITTIER NARROWS EARTHQUAKE

Figure 22

**Attachment 1**  
**Earthquake Ground Motion Assessment**

**EARTHQUAKE GROUND MOTION ASSESSMENT**  
**In-Delta Water Storage Risk Assessment**  
**Delta Wetland, California**

**INTRODUCTION**

This technical memorandum presents the results of a study conducted by URS to assess potential future earthquake ground motions at the In-Delta water storage facility located near San Francisco Bay region, California. The water storage facility will be constructed by converting two existing islands (Bacon Island and Webb Track) into water storage islands. Perimeter embankments will be built to impound the reservoir water. This study was conducted to address comments on developing site-specific ground motions for the reservoir islands and to allow a more complete seismic hazard characterization at the reservoir islands.

**OBJECTIVE**

The approach taken for this study was to conduct a probabilistic ground-motion analysis to assess the probabilities of exceeding various ground motion intensities at the proposed facility. Specifically, the available geologic and seismologic data, including evaluations previously performed for nearby locations by the Bureau of Reclamation (LaForge et al. (2002) for the Martinez and Contra Loma Dams, Ake, et al. (1999) for the Tracy Fish Test Facility) and Calfed (1998) for the Delta Wetland, were reviewed to evaluate and characterize potential seismic sources and the likelihood of earthquakes of various magnitudes occurring on those sources.

The following sections present the methodology used for the probabilistic seismic hazard analysis, the seismic source characterization, the attenuation relationships used, and the results of analysis.

**PROBABILISTIC GROUND-MOTION ANALYSIS**

**Methodology**

The probabilistic analysis is based on the methodology proposed by Cornell (1968) and includes some of the most recent developments in the model. Assuming that earthquake occurrences are Poisson processes, the probability that a ground motion parameter ‘Z’ (peak and response spectral accelerations) at the site exceeds a specific value ‘z’, in a time period ‘t’, is given by:

$$p(Z > z) = 1 - e^{-\phi(z)t}$$

where  $\phi(z)$  is the annual mean number of seismic events in which the ground motion parameter ‘Z’ at the site exceeds the value ‘z’ (i.e., annual frequency of exceedance).  $\phi(z)$  can be calculated as follows:

$$\varphi(z) = \int_I \int_J \alpha_{m_0} \cdot f(m_i) \cdot p(R = r_j \setminus m_i) \cdot p(Z > z \setminus m_i, r_j)$$

where:

- $\alpha_{m_0}$  = annual mean number of seismic events with magnitudes greater than  $m_0$ ,
- $f(m_i)$  = probability density function for seismic events of magnitude  $m_i$ ,
- $p(R=r_j \setminus m_i)$  = probability that given the occurrence of an earthquake of magnitude  $m_i$ , the source-to-site distance is  $r_j$ ,
- $p(Z > z \setminus m_i, r_j)$  = probability that given the occurrence of an earthquake of magnitude  $m_i$  at the source-to-site distance of  $r_j$ , the ground motion parameter 'Z' at the site exceeds a specific value of  $z$ .

The total annual frequency of exceedance for ground motion parameter 'Z' at the site (i.e., total hazard) is then obtained by summing the hazards from all seismic sources:

$$\varphi_t(z) = \sum_N \varphi_n(z)$$

where N is the number of seismic sources considered in the study.

The uncertainties associated with seismic source parameters (geometry, location and recurrence parameters) were incorporated in the analysis using the logic tree approach, as shown in Figure 2.

### Seismic Source Characterization

Two types of earthquake sources are characterized and used in the analysis. They are: 1) fault sources and areal (random) source zones. Fault sources are modeled as three-dimensional fault surfaces and details of their behavior are incorporated into the source characterization. Areal source zones are regions where earthquakes are assumed to occur randomly within the source boundaries. The detailed discussion of the seismic source characterization is presented in Appendix A. Figure 1 shows the approximate locations of the seismic sources.

Seismic sources are modeled in the hazard analysis in terms of geometry and earthquake recurrence. For fault sources, three recurrence models were used: Characteristic, truncated exponential and maximum magnitude models. They were assigned the following weights: 0.3 for characteristic model, 0.1 for truncated exponential model, and 0.6 for maximum magnitude model. For areal source zones, only the truncated exponential recurrence model was used in the analysis. Figures 3 and 4 present the recurrence rates, as a function of magnitude, calculated for the seismic sources.

### Attenuation Relationships

Earthquake ground motion attenuation relationships used in this study are those developed for deep stiff soil sites by Abrahamson and Silva (1997), Sadigh, et al. (1997),

Boore et al. (1997) and Campbell (1997). These relationships were developed on the basis of statistical analyses of ground motions recorded during past earthquakes having similar tectonic environment with that of western United States. These empirical attenuation relationships were weighted equally.

For Boore et al. (1997) relationships, a shear-wave velocity of 300 m/sec was used. This shear-wave velocity value was selected based on the results of a field measurement conducted at the nearby location (Boulanger et al.,1997).

### **Hazard Results**

The hazards were computed for a point located approximately in the middle of the Bacon Island. Computed seismic hazard curves that relate the amplitudes of peak ground acceleration and spectral accelerations to the annual frequencies of exceedance of those amplitudes are shown in Figure 5 and 6, for peak ground acceleration and 1-0-sec spectral acceleration, respectively. Also plotted on these figures are the contribution curves from the various seismic sources considered in this study. As can be seen from these figures, the hazard at the project site is dominated by the nearby Mt. Diablo Thrust, and to a lesser degree, the Coast Range random zone. The San Andreas, Hayward and Calaveras faults also contribute to the long-period motions, as shown in Figure 4 for the 1-0 sec. Spectral acceleration.

The 5% damped equal-hazard response spectra for the 43-, 100-, 200-, 475-, 1,000-, and 2,500- year return periods were developed using these computed hazard curves, and they are shown in Figures 7. The spectral values at selected periods are listed in Table 1.

**Table 1. Calculated Acceleration Spectral Values at Selected Periods**

Period, sec	5% Acceleration Response Spectral Value, g			
	43-year return period	100-year return period	200-year return period	475-year return period
PGA	0.14	0.20	0.26	0.33
0.075	0.21	0.30	0.39	0.51
0.10	0.25	0.35	0.46	0.62
0.20	0.32	0.46	0.59	0.80
0.30	0.32	0.46	0.59	0.80
0.50	0.27	0.38	0.49	0.68
1.0	0.16	0.24	0.31	0.42
2.0	0.09	0.13	0.17	0.24

### **COMPARISON WITH PREVIOUS STUDY**

The results of the current study were compared with those calculated by Calfed (1998) in Table 2 below. It can be seen that the PGAs calculated using current model are about 15% to 35% higher than those calculated by Calfed (1998).

**Table 2. Comparison with Results of Calfed (1998) Study**

Period	Spectral Acceleration in g							
	43-yr return period		100-yr return period		200-yr return period		475-yr return period	
	Current study	Calfed study	Current study	Calfed study	Current study	Calfed study	Current study	Calfed study
PGA	0.14	0.114	0.20	0.175	0.26	0.19	0.33	0.25

**REFERENCES**

Abrahamson, N.A., and Silva, W.J., 1997, Empirical response spectral attenuation relations for shallow crustal earthquakes: *Seismological Research Letters*, v. 68, no. 1, p. 94-127.

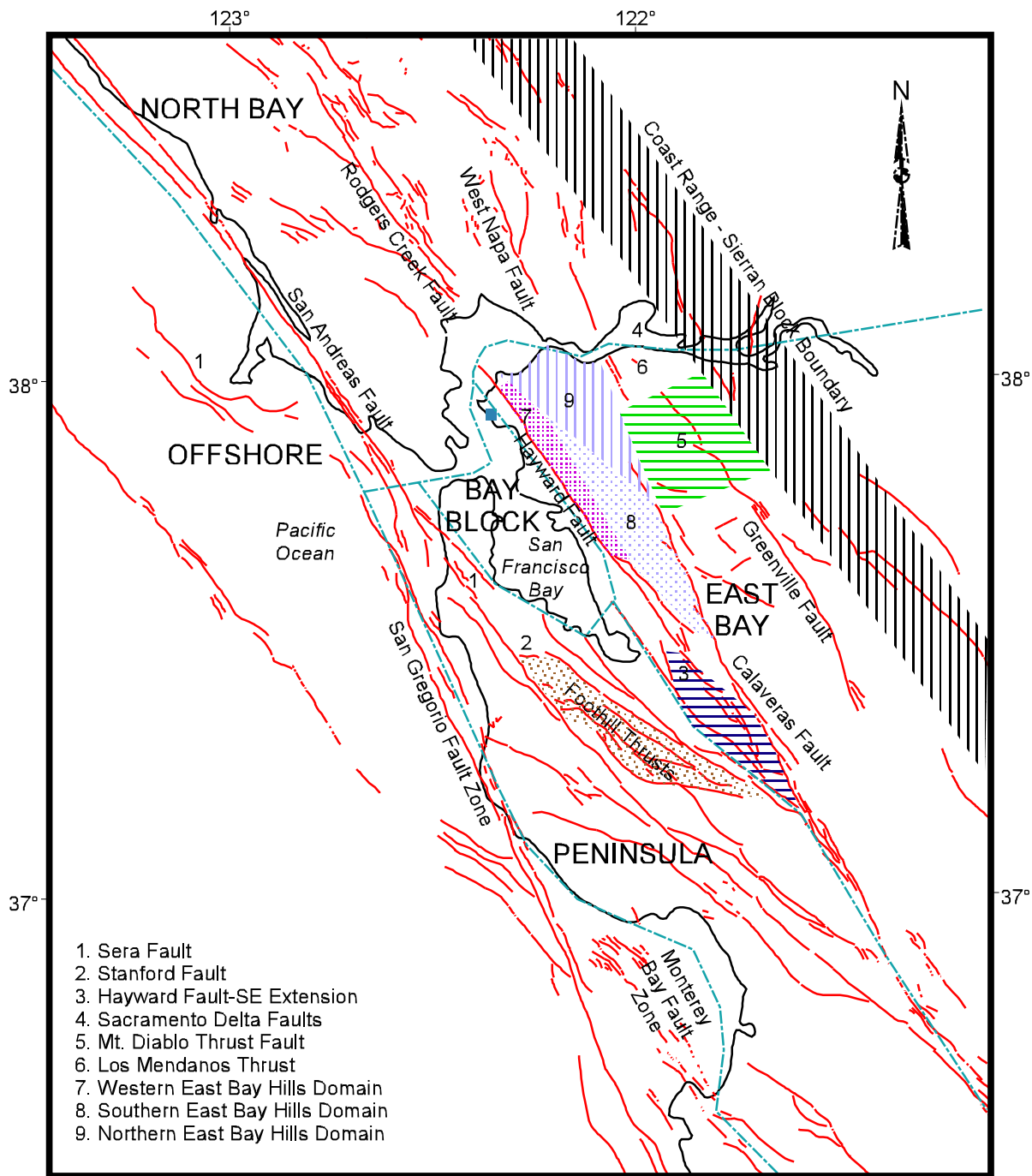
Boulanger, R.W., R. Arulnathan, L. F. Harder, Jr., R.A. Torres, and M.W. Driller, 1997, Dynamic Properties of Sherman Island Peat. Report No. UCD/CGM-97/01, Center for Geotechnical Modeling, Department of Civil and Environmental Engineering, University of California, Davis.

Boore, D.M., Joyner, W.B., and Fumal, T.E., 1997, Equations for estimating horizontal response spectra and peak acceleration from western north American earthquakes: A summary of recent work, *Seismological Research Letters*, Vol. 68, No. 1, January.

Campbell, K.W., 1997, 'Empirical near-source attenuation relationships for horizontal and vertical components of peak ground acceleration, peak ground velocity, and pseudo-absolute acceleration response spectra', *Seismological Research Letters*, Vol. 68, No. 1, January.

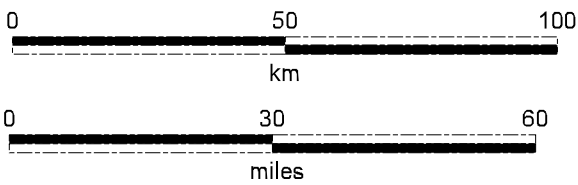
Cornell, C.A., 1968, Engineering seismic risk analysis: *Bulletin of the Seismological Society of America*, v.58, n.5, pp.1583-1606.

Sadigh, K., Chang, C.Y., Egan, J.A., Makdisi, F., and Youngs, R.R., 1997, Attenuation relationships for shallow crustal earthquakes based on California strong motion data, *Seismological Research Letters*, Vol. 68, No. 1, January.



- 1. Sera Fault
- 2. Stanford Fault
- 3. Hayward Fault-SE Extension
- 4. Sacramento Delta Faults
- 5. Mt. Diablo Thrust Fault
- 6. Los Mendanos Thrust
- 7. Western East Bay Hills Domain
- 8. Southern East Bay Hills Domain
- 9. Northern East Bay Hills Domain

 Fault Domain Boundary  
 Fault

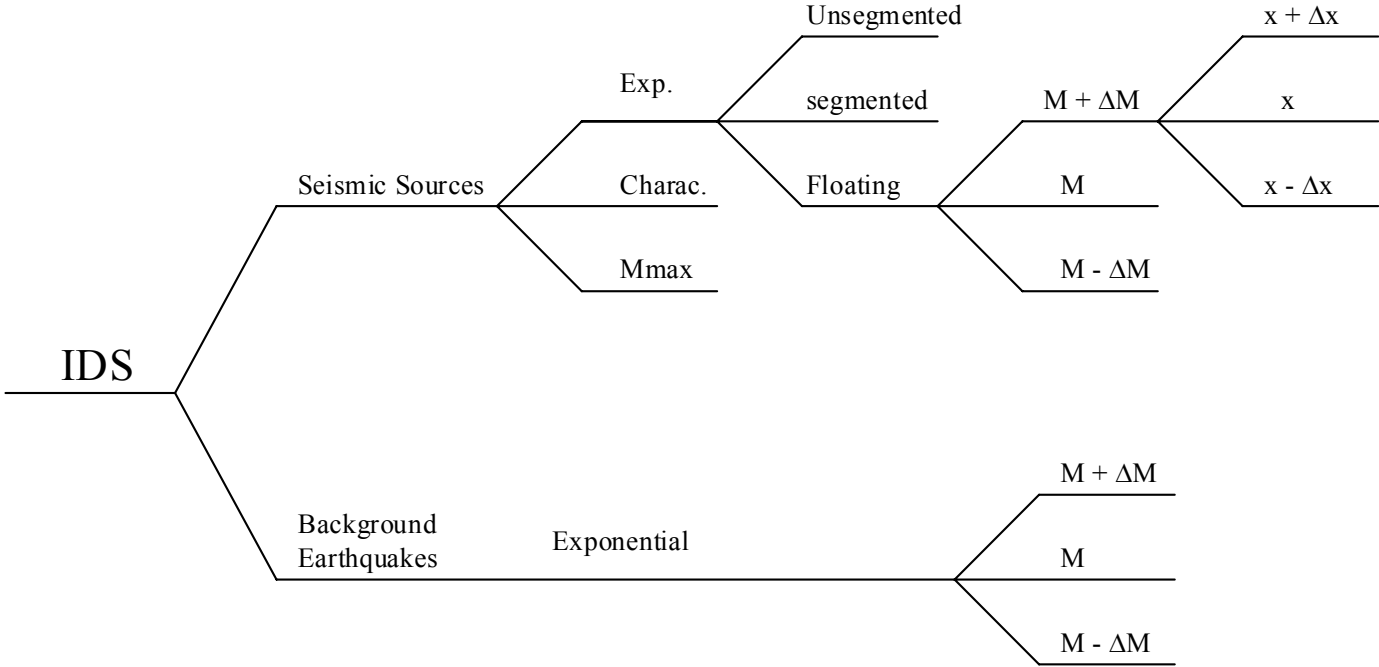


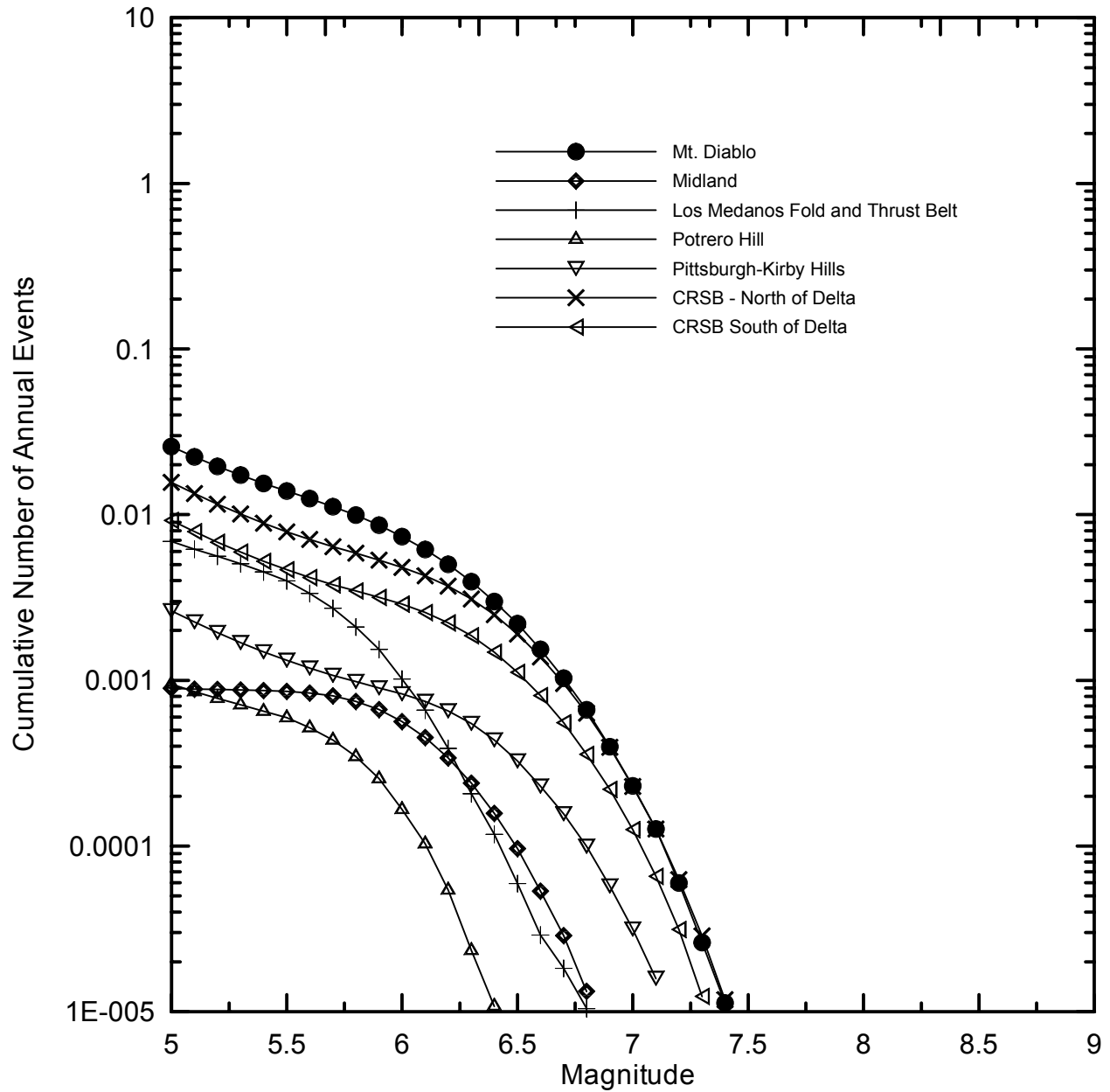
Project No. 26814105  
In-Delta Storage

MAJOR ACTIVE FAULTS

Figure 1

Sources	Recurrence model	Rupture model	Magnitude estimates	Recurrence rates or slip rates
---------	------------------	---------------	---------------------	--------------------------------



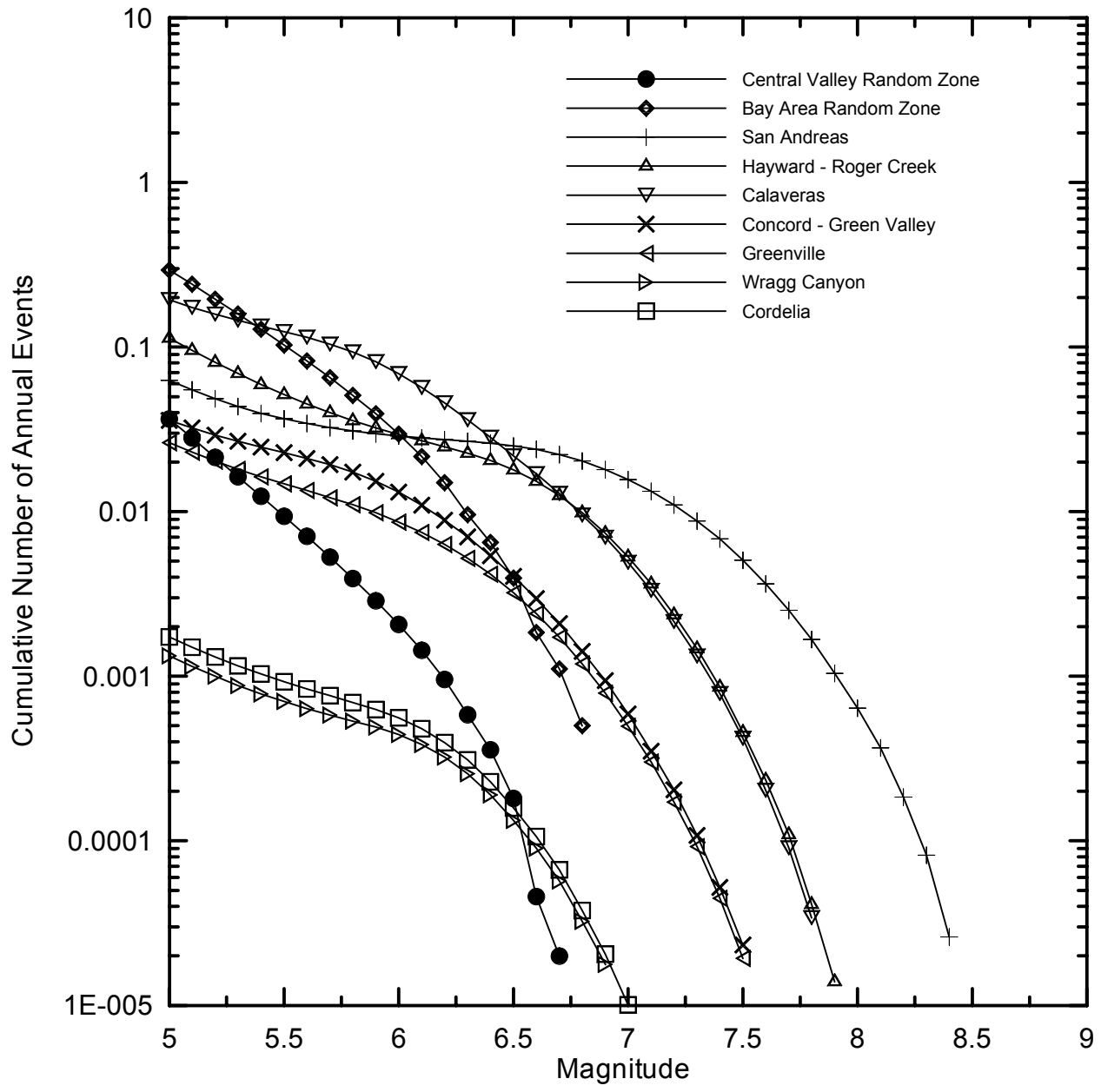


Project # 26814103

**DELTA WETLANDS PROJECT**  
IN-DELTA STORAGE  
FEASIBILITY STUDY

Earthquake Recurrence Relationships  
Calculated for Seismic Sources  
(group #1)

Figure  
3

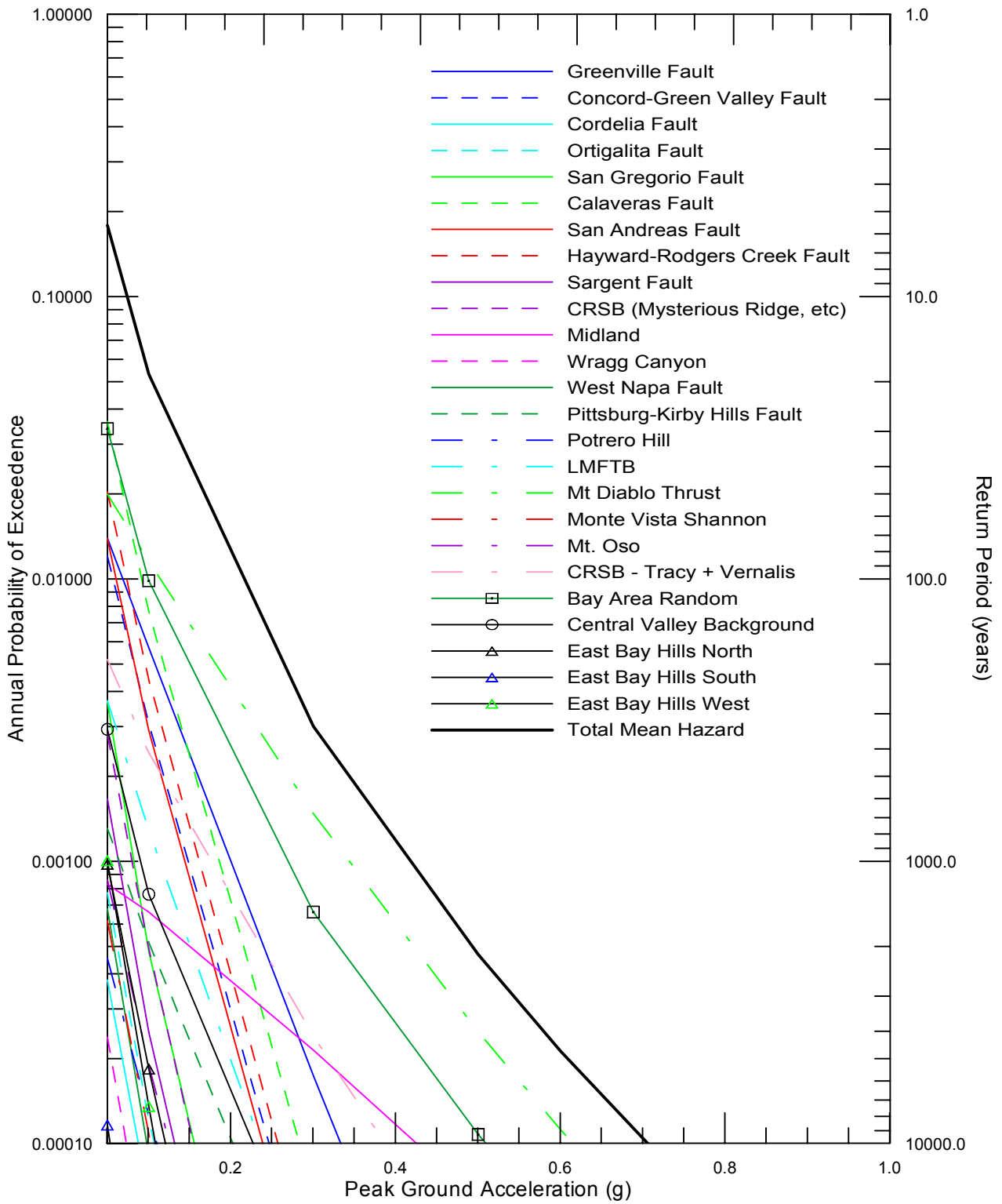


Project # 26814103

**DELTA WETLANDS PROJECT**  
IN-DELTA STORAGE  
FEASIBILITY STUDY

Earthquake Recurrence Relationships  
Calculated for Seismic Sources  
(group #2)

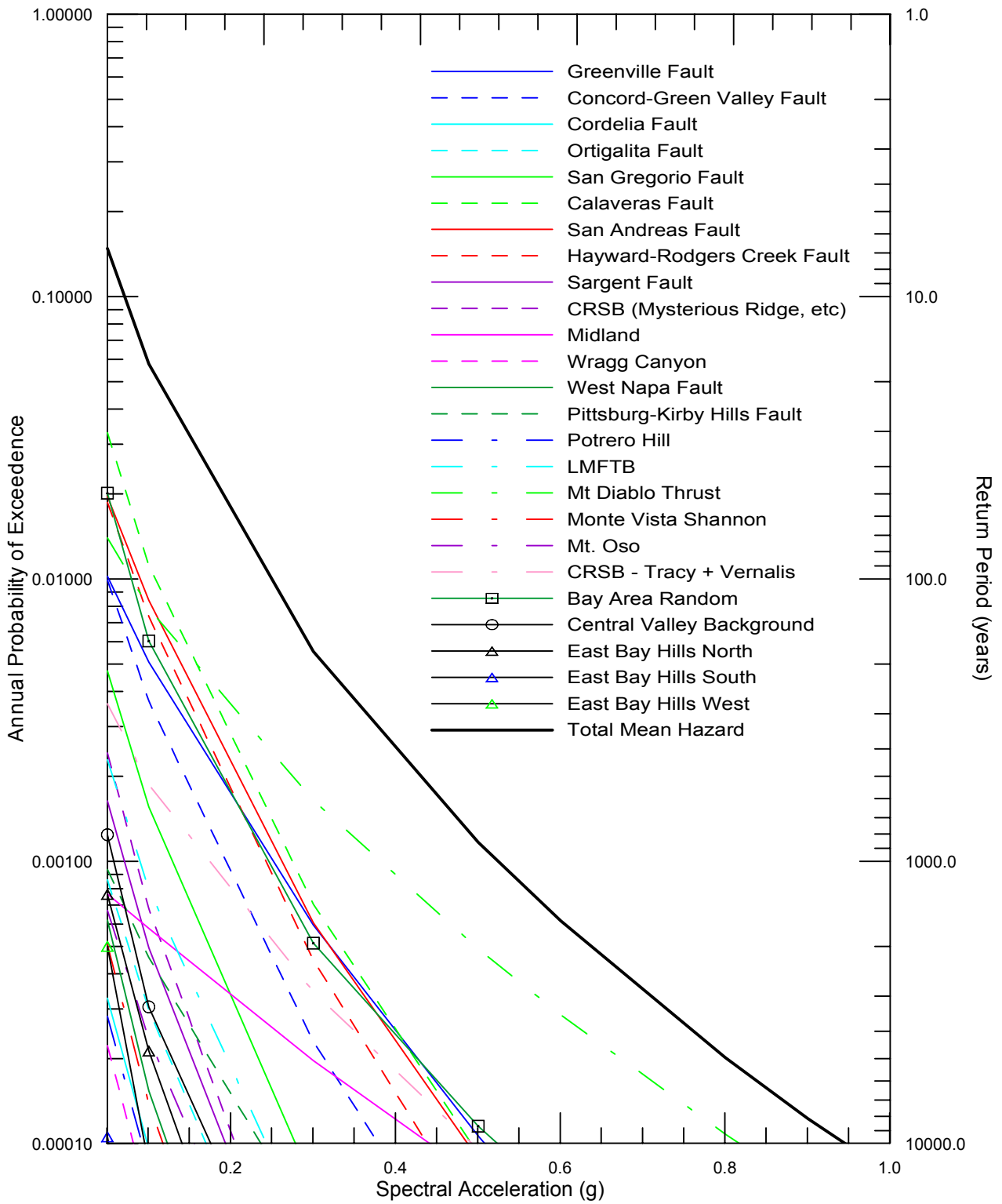
Figure  
4



Project No. 26814105  
 Delta Wetland Project  
 In-Delta Storage  
 Feasibility Study

SEISMIC SOURCE CONTRIBUTIONS TO MEAN  
 PEAK HORIZONTAL ACCELERATION HAZARD

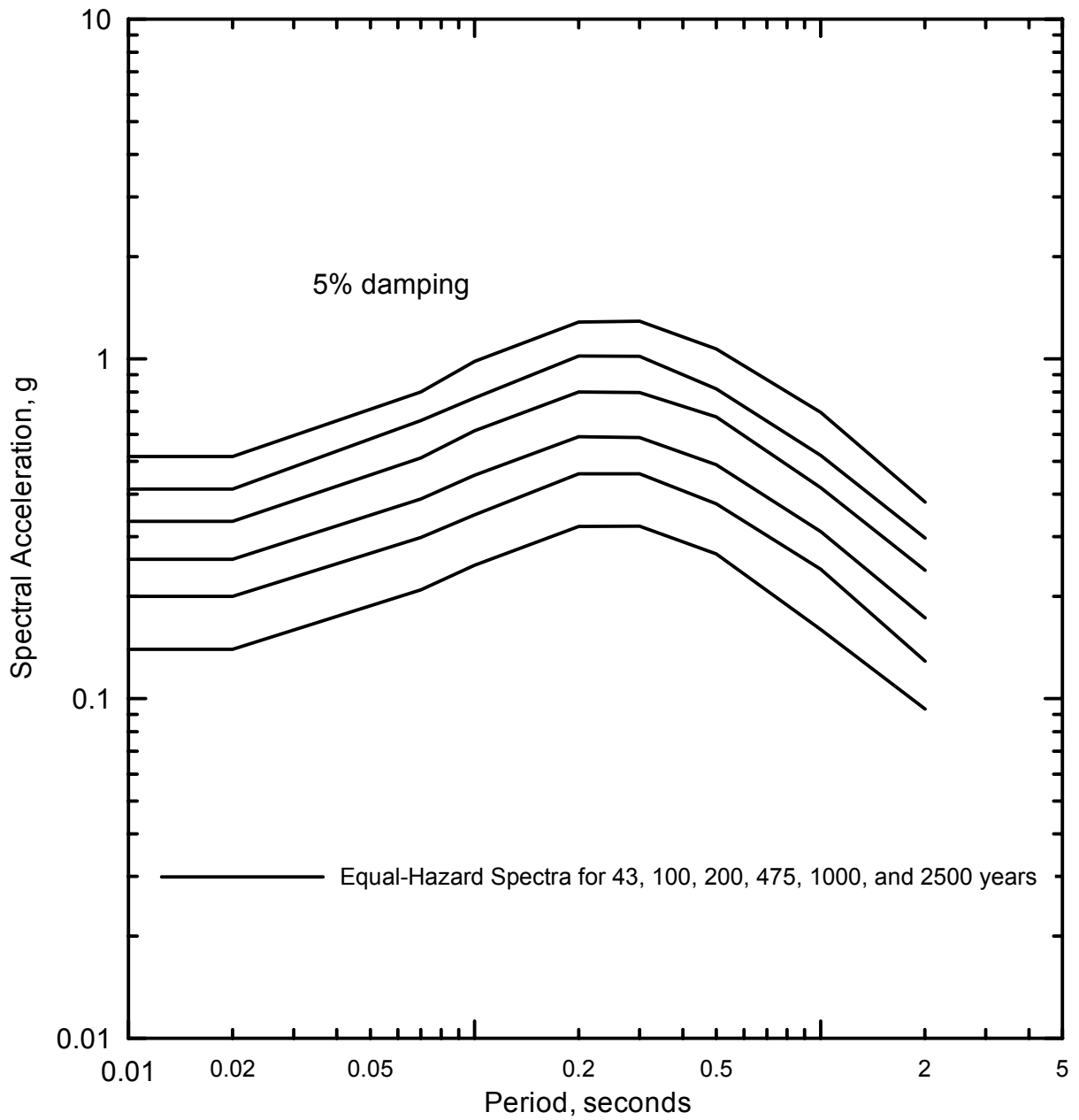
Figure  
 5



Project No. 26814105  
 Delta Wetland Project  
 In-Delta Storage  
 Feasibility Study

SEISMIC SOURCE CONTRIBUTIONS TO MEAN  
 1.0 SEC HORIZONTAL SPECTRAL  
 ACCELERATION HAZARD

Figure  
 6



Project # 26814103

**DELTA WETLANDS PROJECT**  
 IN-DELTA STORAGE  
 FEASIBILITY STUDY

Equal-hazard Acceleration  
 Response Spectra

Figure  
 7

**Appendix A**  
**Seismic Sources**

## **A.1 CHARACTERIZATION OF POTENTIAL SEISMIC SOURCES**

Two types of earthquake sources are characterized in this seismic hazard analysis: (1) fault sources; and (2) areal source zones. Fault sources are modeled as three-dimensional fault surfaces and details of their behavior are incorporated into the source characterization (Section A.2). Areal source zones are regions where earthquakes are assumed to occur randomly (Section A.3). Figures 1 and 2 is the fault map showing the significant and contributing sources used in the In-Delta Storage seismic hazard analysis. Seismic sources are modeled in the hazard analysis in terms of geometry and earthquake recurrence. A source characterization model is presented in Figure 3.

The geometric source parameters for faults include fault location, segmentation model, dip, and thickness of the seismogenic zone. The recurrence parameters include recurrence model, recurrence rate (slip rate or average recurrence interval for the maximum event), slope of the recurrence curve (*b*-value), and maximum magnitude. Clearly the geometry and recurrence are not totally independent. For example, if a fault is modeled with several small segments instead of large segments, the maximum magnitude is lower, and a given slip rate requires many more small earthquakes to accommodate a cumulative seismic moment. For areal source zones, only the areas, maximum magnitude, and recurrence parameters (based on the historical earthquake record) need to be defined.

Uncertainties in the source parameters are included in the hazard model using logic trees. In the logic tree approach, discrete values of the source input parameters have been included along with our estimate of the likelihood that the discrete value represents the actual value. In this probabilistic analysis, generally all input parameters have been represented by three values (Figure 3); the values represent a distribution about the best estimate.

### **A.1.1 Source Geometry**

In the probabilistic analysis, it is assumed that earthquakes of a certain magnitude may occur randomly along the length of a given fault or segment. The distance from an earthquake to the site is dependent on the source geometry, the size and shape of the rupture on the fault plane, and the likelihood of the earthquake occurring at different points along the fault length. The distance to the fault is defined to be consistent with the specific attenuation relationship used to calculate the ground motions. The distance, therefore, is dependent on both the dip and depth of the fault plane, and a separate distance function is calculated for each geometry and each attenuation relationship. The size and shape of the rupture on the fault plane are dependent on the magnitude of the earthquake, with larger events rupturing longer and wider portions of the fault plane.

### **A.1.2 Probability of Activity**

Fault activity is expressed in terms of probability of activity [P(a)]. A fault with a P(a) of 1.0 is definitely active, whereas a fault with a P(a) of 0.0 is completely inactive. Faults that clearly offset or deform Holocene strata are considered to be active and have a P(a) of 1.0. Faults that deform or offset Late Pleistocene strata are considered to be potentially active and have a P(a) of 0.75. As much of the upland regions of the San Francisco Bay region is undergoing contractional reactivation, it is possible that an active fault may not rupture to the Earth's

surface, therefore it may not offset Holocene strata. To account for activity on such ‘blind’ structures, faults which are favorably oriented for reactivation in the current stress regime that have been active during the Pleistocene but do not appear to have been active during the Holocene are assigned a P(a) of 0.5 to 0.75. The Western East Bay Hills thrust fault zone is an example of this type of faulting.

### A.1.3 Maximum Magnitudes

Consistent with current state-of-the-practice, we estimate the maximum magnitudes based on empirical relations between expected rupture dimensions (i.e., fault rupture length and rupture area) and magnitude. Estimates of maximum earthquakes from empirical data such as rupture length and rupture area are limited by uncertainties in the empirical data, range of variation of rupture parameters during different events, and uncertainties in the assessment of rupture parameters for the fault under investigation. Therefore, the final assessment of maximum magnitude is a judgment that incorporates an understanding of specific fault characteristics, the regional tectonic environment, similarity to other faults in the region, and seismicity data (Schwartz *et al.*, 1984).

The most common approach to estimating maximum magnitude is through a comparison of fault rupture length and magnitude. However, considerable uncertainty often exists in the selection of the appropriate rupture length to be used in the analysis (Schwartz *et al.*, 1984). Rupture lengths of past surface-rupture events on a specific fault may provide direct evidence. Where there is evidence for a change in fault behavior or there is a significant change in fault geometry, we have divided the faults into rupture segments.

The empirical relationships for surface rupture length and rupture area used in this maximum magnitude assessment are those developed by Wells and Coppersmith (1994), Working Group on California Earthquake Probabilities (WGCEP; 1999), Somerville *et al.* (1999), Stirling *et al.* (2002), and Hanks and Bakun (2002). In general, the correlation coefficients for the regressions indicate very strong correlation and the standard deviations are approximately 0.30 magnitude unit (Wells and Coppersmith, 1994). The maximum magnitude for each active or potentially active faults in the study region and rupture length are listed in Table 1.

In the probabilistic seismic hazard analysis, the geometry of the seismic sources and recurrence need to be defined. As in some cases, because the fault geometries are not well-constrained, a number of fault rupture scenarios have been considered for each fault (typically three fault dips and three depths for the seismogenic crust, giving rise to nine possible rupture areas). For the majority of faults in the region, the dip is constrained by seismic reflection data and the focal mechanisms of instrumentally-recorded earthquakes.

### A.1.4 Fault Recurrence Models

The recurrence relationships for the faults are modeled using the exponentially truncated Gutenberg-Richter, characteristic earthquake, and the maximum magnitude recurrence models. These models are weighted to represent our judgment on their applicability to the sources. For the areal source zones, only an exponential recurrence relationship is assumed appropriate.

We have used the general approach of Molnar (1979) and Anderson (1979) to arrive at the recurrence for the exponentially truncated model. The number of events exceeding a given magnitude,  $N(m)$ , for the truncated exponential relationship is

$$N(m) = \mathbf{a}(m^o) \frac{10^{-b(m-m^o)} - 10^{-b(m^u-m^o)}}{1 - 10^{-b(m^u-m^o)}} \quad (4)$$

where  $\mathbf{a}(m^o)$  is the annual frequency of occurrence of earthquake greater than the minimum magnitude,  $m^o$ ;  $b$  is the Gutenberg-Richter parameter defining the slope of the recurrence curve; and  $m^u$  is the upper-bound magnitude event that can occur on the source. A  $m^o$  of moment magnitude (**M**) 5 was used for the hazard calculations because smaller events are not considered likely to produce ground motions with sufficient energy to damage well designed structures.

The model that the faults rupture with a "characteristic" magnitude on specific segments has been included. This model is described by Aki (1983) and Schwartz and Coppersmith (1984). We have used the numerical model of Youngs and Coppersmith (1985) for the characteristic model. For the characteristic model, the number of events exceeding a given magnitude is the sum of the characteristic events and the non-characteristic events. The characteristic events are distributed uniformly over  $\pm 0.3$  magnitude unit around the characteristic magnitude and the remainder of the moment rate is distributed exponentially using the above equation with a maximum magnitude one unit lower than the characteristic magnitude (Youngs and Coppersmith, 1985).

The maximum magnitude model can be regarded as an extreme version of the characteristic model. We adopted the model proposed by Wesnousky (1986). In the maximum magnitude model, there is no exponential portion of the recurrence curve, i.e., no events can occur between the minimum magnitude of **M** 5.0 and the distribution about the maximum magnitude.

The recurrence rates for the fault sources are defined by either the slip rate or the average return time for the maximum or characteristic event and the recurrence  $b$ -value. The slip rate is used to calculate the moment rate on the fault using the following equation defining the seismic moment:

$$M_o = \mu A D \quad (5)$$

where  $M_o$  is the seismic moment,  $\mu$  is the shear modulus,  $A$  is the area of the rupture plane, and  $D$  is the slip on the plane. Dividing both sides of the equation by time results in the moment rate as a function of slip rate:

$$\dot{M}_o = \mu A S \quad (6)$$

where  $\dot{M}_o$  is the moment rate and  $S$  is the slip rate.  $M_o$  has been related to **M**, by Hanks and Kanamori (1979):

$$\mathbf{M} = 2/3 \log M_o - 10.7 \quad (7)$$

Using this relationship and the relative frequency of different magnitude events from the recurrence model, the slip rate can be used to estimate the absolute frequency of different magnitude events.

The average return time for the characteristic or maximum magnitude event defines the high magnitude (low likelihood) end of the recurrence curve. When combined with the relative

frequency of different magnitude events from the recurrence model, the recurrence curve is established.

Based on our review of published and unpublished data, and on regional geological and seismological studies, the active and potentially active seismogenic faults listed on Table 1 are considered to be seismic sources significant to the potential In-Delta Storage sites in terms of strong ground shaking. For the purpose of investigating crustal fault activity, the site region encompasses an area within a radius of about 100 km of these sites. Beyond this distance, the potential contribution of crustal faults to ground motions at the site becomes negligible.

### **A.1.5 Fault Recurrence Rates**

A lack of reliable paleoseismic data means that the recurrence rates for many of the faults within the Bay area are either poorly understood or unknown. Fault activity is therefore expressed as an average annual slip rate (in mm/yr) rather than as an interseismic period. Slip rate is calculated by dividing the amount of offset, approximated from the displacement of geomorphic features or erosion surfaces of geologic units, by the inferred age of these features or units. Since the amount of offset during individual events is not known, slip rates cannot be converted into return periods for faulting events. The uncertainty in the slip rates and the other input parameters are accommodated in the probabilistic hazard through the use of logic trees.

## **A.2 SIGNIFICANT SEISMIC SOURCES IN THE SAN FRANCISCO BAY REGION**

Based on our review, active crustal faults or fault zones in the site region have been identified and characterized (Table 1; Figures 1 and 2). The structures include late Quaternary faults in the vicinity of the Delta as well as more distant faults capable of producing large magnitude earthquakes and significant ground shaking. These faults are described as “active” or “potentially active” as defined below. Only faults displaying late Quaternary movement are described in this section.

A fault is considered to be “active” and is considered to be a potential source of future earthquakes if there is compelling evidence for repeated displacement during the Holocene (last 10,000 years), and/or if historical seismicity has been associated with the structure. A fault is considered “potentially active” and is considered a potential source of future earthquakes if there is compelling evidence for displacement during the late Pleistocene and the age of the most recent event is unknown, or if it is likely that seismicity is associated with the fault.

Within the immediate Delta area, a number of potentially active faults have been identified. The characteristics of each fault system are described in more detail in the following sections. Each seismic source has been characterized using the latest geologic, geophysical, and paleoseismic data (both published and unpublished) and the currently accepted models of fault behavior developed by various U.S. Geological Survey Working Groups (WGCEP, 1999; Working Group on Northern California Earthquake Potential, 1996).

### A.2.1 San Gregorio Fault Zone

This northwest-striking fault is the principal active fault west of the San Andreas fault in the coastal region of central California. The fault extends from just offshore of Point Sur, northward to Bolinas Lagoon, where it merges with the North Coast segment of the San Andreas. The majority of the fault is located offshore, with only two short sections, at Seal Cove and Moss Beach, occurring on land. Because of the limited onshore extent of the fault, the fault is relatively poorly understood. Jennings (1994) shows the fault as two distinct segments, separated by a prominent step in Monterey Bay. Simpson *et al.* (1997) carried out one of the few paleoseismic investigations along the fault. They demonstrated late Holocene right-lateral movement on the Seal Cove section of the fault. The most recent surface faulting event on the fault occurred sometime after A.D. 1270 to A.D. 1400, but prior to 1775. A penultimate event occurred between A.D. 680 and A.D. 1400 (Simpson *et al.*, 1997).

Based on geological and paleoseismic data, the San Gregorio fault is divided into two segments: a northern segment extending from Bolinas Lagoon to Monterey Bay and a southern segment from Monterey Bay to just north of Point Sur. The fault is modeled as either unsegmented, where the entire fault ruptures, generating an earthquake of **M** 7.6, or segmented, where the northern and southern segments rupture independently, generating earthquakes of **M** 7.4 and 7.2, respectively. We also consider a **M** 6.9 ‘floating’ earthquake which can rupture any part of the fault. The northern segment of the San Gregorio fault is located approximately 100 km west of the Delta. Estimates of slip along the San Gregorio fault are highly variable. We adopted a preferred slip rate of 7 mm/yr for the unsegmented and northern segment models, with lower and upper bound estimates of 4 mm/yr and 10mm/yr, respectively. The slip rate for the southern segment is 6 mm/yr ( $\pm$  4 mm/yr).

### A.2.2 San Andreas Fault Zone

The dominant active fault structure in this region is the San Andreas fault. The fault extends from the Gulf of California, Mexico, to Point Delgada on the Mendocino Coast in northern California, a total distance of 1,200 km. The San Andreas fault accommodates the majority of the motion between the Pacific and North American plates. This fault is the largest active fault in California and is responsible for the largest known earthquake in Northern California, the 1906 **M** 7.9 San Francisco earthquake (Wallace 1990). Movement on the San Andreas fault is right-lateral strike-slip, with a total offset of some 560 km (Irwin 1990). In northern California, the San Andreas fault is clearly delineated, striking northwest, approximately parallel to the vector of plate motion between the Pacific and North American plates. Over most of its length, the San Andreas fault is a relatively simple, linear fault trace. Immediately south of the Bay, however, the fault splits into a number of branch faults or splays, including the Calaveras and Hayward faults (each is discussed below). In the Bay Area, the main trace of the San Andreas fault forms a linear depression along the Peninsula, occupied by the Crystal Springs and San Andreas Lake reservoirs. Geomorphic evidence for Holocene faulting includes fault scarps in Holocene deposits, right-laterally offset streams, shutter ridges, and closed linear depressions (Wallace, 1990). The 1906 earthquake resulted from rupture of the fault from San Juan Bautista north to Point Delgada, a distance of approximately 475 km. The average amount of slip on the fault during this earthquake was 5.1 m in the area to the north of the Golden Gate and 2.5 m in

the Santa Cruz Mountains (Working Group on Northern California Earthquake Potential [WGNCEP], 1996).

Based on differences in geomorphic expression, fault geometry, paleoseismic chronology, slip rate, seismicity, and historic fault ruptures, the San Andreas fault is divided into a number of fault segments. Each of these segments is capable of rupturing either independently or in conjunction with adjacent segments. In the Bay Area, these segments include the Santa Cruz Mountains, the Peninsula, and the North Coast segments. These fault segments have calculated maximum earthquakes of **M** 7.2, 7.3, and 7.7, respectively. The North Coast segment may also be subdivided into two shorter segments with a boundary at Point Arena. These northern and southern North Coast segments are capable of generating earthquakes of **M** 7.5 and 7.7, respectively. The North Coast segment, or an adjacent fault branch, was the source of the August 18, 1999 **M** 5.0 earthquake located near Bolinas.

South of the Golden Gate, the fault slip rate is  $17 - 3/+ 7$  mm/yr (Hall *et al.*, 1999). North of the Golden Gate, the slip rate increases to  $24 \pm 5$  mm/yr (Niemi and Hall, 1992). The Working Group on California Earthquake Probabilities (1999) assigns a recurrence interval of 361 years to a **M** 8.0 1906-type event on the San Andreas fault, with a 21 percent probability of a **M** 6.7 or larger earthquake on the San Andreas in northern California in the time period 2000 to 2030. Recent investigations by Niemi *et al.* (2002) indicate that the repeat time for large earthquakes on the North Coast segment may be less than 250 years.

### A.2.3 Foothill Thrust Belt

The southwestern margin of the Santa Clara Valley is bounded by the rugged, young southern Santa Cruz Mountains. Late Cenozoic uplift of the mountains has occurred, in part, along a series of northwest-striking reverse faults, known as either the Loma Prieta domain (Aydin and Page, 1984) or Foothills thrust belt (Bürgmann *et al.*, 1994), bordering the northeastern margin of the range front. Bounded by the main trace of the San Andreas fault to the west, this sequence of southwest-dipping thrusts, associated with a restraining left bend in the San Andreas fault, has been responsible for the uplift of the Santa Cruz Mountains (Bürgmann *et al.*, 1994). These faults offset the Pliocene and Pleistocene Santa Clara Formation, and locally offset and deform overlying Quaternary sediments and geomorphic surfaces within the range-front communities of Palo Alto, Los Altos Hills, Cupertino, Saratoga, and Los Gatos, located along the southwestern margin of the Santa Clara Valley (Hitchcock and Kelson 1999; Hitchcock *et al.* 1994). The up-dip projection of the blind Loma Prieta fault, which is interpreted to have been the source of the 1989 **M** 6.9 Loma Prieta earthquake (Bürgmann *et al.*, 1994), coincides with the Foothills thrust belt.

Historical records indicate that a **M** 6.5 earthquake in 1865 may have occurred on a fault east of the San Andreas fault, possibly along the northeastern flank of the Santa Cruz Mountains (Topozada and Borchardt, 1998; Tuttle and Sykes, 1992a; Tuttle and Sykes, 1992b). Based on the magnitude of aseismic deformation of the northeastern Santa Cruz Mountains following the 1989 Loma Prieta earthquake, it is possible that a large component of the total slip on the Foothills thrust belt occurs aseismically in association with slip on the nearby San Andreas fault (Hitchcock and Kelson 1999). It is also possible that one or more segments of the system may

rupture in a single event, producing a moderate- to large-magnitude earthquake (Zoback *et al.*, 1999).

The Berrocal fault is located along the range front between Saratoga and Los Gatos, and extends for 55 km within the range block. Southeast of Los Gatos, the Berrocal fault merges with, or intersects, the Sargent fault. To the northwest, the fault either dies out or merges with the Monte Vista fault. The Berrocal fault is also linked to the San Andreas fault by the north-striking Lexington fault along Los Gatos Creek. Scattered seismicity along and to the southwest of the mapped fault trace may be related to either the Berrocal fault, or a related northeast-vergent blind thrust fault. Significant compressional surface deformation was observed along the Berrocal fault in the Los Gatos and Saratoga areas during the Loma Prieta earthquake (Langenheim *et al.*, 1997).

The 54-km-long Monte Vista fault is one of the primary range-front faults and probably the most extensively studied fault in the Foothills thrust belt. The exposed fault strikes northwest and places Franciscan, Miocene, Santa Clara Formation, and Pleistocene alluvium over Pleistocene and older strata. To the south, the fault merges with the Shannon fault, while at its northern end it intersects the San Andreas, via the Hermit fault, between Woodside and Redwood City. Limited exploratory trenching indicates that the Monte Vista fault has had late Quaternary and possibly Holocene displacement. Recent geomorphic mapping by Hitchcock *et al.* (1994) shows that late Pleistocene fluvial terraces flanking Stevens Creek are deformed. The style of late Quaternary deformation affecting these terrace surfaces is consistent with reverse faulting on the Monte Vista fault. Hitchcock and Kelson (1999) estimated an average late Pleistocene slip rate of  $0.17 \pm 0.09$  mm/yr for the Monte Vista fault.

The Shannon fault, which extends from near Saratoga, south to Coyote Creek near New Almaden, consists of several *en echelon*, southwest-dipping, thrust or reverse fault strands and several subsidiary northeast-dipping normal fault strands. Geomorphic investigations provide evidence of probable late Pleistocene deformation associated with these southwest-dipping, northeast-vergent reverse fault strands (Hitchcock *et al.*, 1994). Trench exposures at the Senator mine west of New Almaden show that the southern segment of the Shannon fault deforms Miocene rock and cuts a paleosol with an estimated age less than 20,000 years (R. McLaughlin, U.S. Geological Survey, *pers. comm.*, to C. Hitchcock, WLA, 1993). As with the Berrocal, Sargent, and Monte Vista faults, compressional surface deformation was locally concentrated along the Shannon fault, in the Los Gatos and Campbell areas, during the Loma Prieta earthquake.

The Cascade fault traverses the coalescent alluvial-fan complex underlying the Santa Clara Valley approximately 2 to 6 km northeast of the Santa Cruz Mountains range front. Hitchcock *et al.* (1994) show a strong correlation between the mapped trace of the Cascade fault and fault-related geomorphic features, including vegetation lineaments, closed depressions, linear drainages, stream profile convexities, and high-sinuosity stream reaches. These features are developed in late Pleistocene and possibly Holocene deposits; thus, they provide evidence for late Pleistocene (and possibly Holocene) displacement along the Cascade fault. Between Los Altos Hills and Los Gatos, most of the major streams show longitudinal-profile convexities where they cross the mapped trace of the Cascade fault. In general, the crests of the convexities coincide with the zone of lineaments. These relations indicate late Pleistocene uplift along this section of the Cascade fault (Hitchcock *et al.*, 1994). Although this provides little or no information on the sense of slip and the amount and direction of fault dip, it is likely that the

Cascade fault is a southwest-dipping, northeast-vergent reverse fault similar to, but perhaps having a shallower dip in the near surface than the Monte Vista, Berrocal, and Shannon faults.

The faults of the Foothill thrust belt are considered active and capable of generating large-magnitude earthquakes. The Thrust Fault Subgroup of the WGCEP (1999) considered these faults capable of generating earthquakes of **M** 6.2 to 7. Fault slip rates are considered to be in the range 0.2 to 0.8 mm/yr, with 0.5 mm/yr being the preferred estimate. Estimates for the maximum earthquake within this source zone range from **M** 6¼ to 7.

### A.2.4 Sargent fault

The 56-km-long Sargent fault zone is a northwest-striking, northeast-verging, reverse-oblique fault zone that intersects the San Andreas fault to the north near Lake Elsman, and the Calaveras fault to the south beneath the southern Santa Clara Valley near Hollister. The fault exhibits a prominent component of right-lateral slip, as shown by geomorphic offsets and fault plane slickensides exposed near Loma Prieta (Bryant *et al.*, 1981). Prescott and Burford (1976) measured  $3 \pm 1$  mm/yr creep along the southern third of the Sargent fault. Like several of the faults in the Foothills thrust belt, the Sargent fault experienced triggered slip during the 1989 **M** 6.9 Loma Prieta earthquake (Aydin *et al.*, 1992). From a trenching investigation along the southern part of the fault, Nolan *et al.* (1995) calculated a preliminary slip rate of only 0.6 mm/yr, and a recurrence interval of 1,200 years for the southernmost part of the fault; however, these estimates are based on poorly constrained data. Based on its proximity to the San Andreas fault, the WGNCEP (1996) did not consider the northern two-thirds of the Sargent fault to be an independent seismic source. This fault is modeled as a single rupture segment with a slip rate of  $3.0 \pm 1.5$  mm/yr. The maximum magnitude for the Sargent fault is estimated to be **M** 7.1.

### A.2.5 Hayward Fault

The Hayward fault extends for 100 km from the area of Mount Misery, east of San Jose, to Point Pinole on San Pablo Bay. At Point Pinole, the Hayward fault runs into San Pablo Bay. The northern continuation of this fault system is the Rodgers Creek fault. The two faults are separated by a 5-km-wide right step beneath San Pablo Bay (the Rodgers Creek fault is discussed below). Systematic right-lateral geomorphic offsets and creep offset of cultural features have been well documented along the entire length of the fault (Lienkaemper, 1992). The last major earthquake on the Hayward fault, in October 1868, occurred along the southern segment of the fault. This **M** 6.8 event caused toppling of buildings in Hayward and other localities within about 5 km of the fault. The surface rupture associated with this earthquake is thought to have extended for approximately 30 km, from Warm Springs to San Leandro, with a maximum reported displacement of 1 m. The Hayward fault is considered the most likely source of the next major earthquake in the Bay Area (WGCEP, 1999). As well as undergoing displacement earthquake ruptures, the Hayward fault also moves by aseismic creep. Measurements along the fault over the last two decades show that the creep rate is 5 to 9 mm/yr (Lienkaemper and Galehouse, 1997).

Recent research of historical documents has led to the conclusion that an earthquake in 1836, previously thought to have occurred on the northern Hayward fault, occurred elsewhere

(Topozada and Borchardt, 1998), thereby increasing the time since the last earthquake on this segment of the fault. Recent paleoseismic trenching along the northern Hayward fault indicates that the last surface rupturing earthquake along this part of the fault was sometime between 1626 and 1724 (Lienkaemper *et al.*, 1997). This study also indicated at least four surface-rupturing earthquakes in the last 2,250 years. The WGCEP (1999) assigns maximum earthquakes of **M** 6.6 and 6.9, and recurrence intervals of 387 and 371 years, for the northern and southern segments of the Hayward fault, respectively. Rupture of the entire fault zone would generate an earthquake of **M** 7.1. Using more recent rupture area – magnitude relationships, we assign **M** 6.9, 7.1, and 7.3 to rupture of the northern and southern segments, and entire Hayward fault, respectively. We also incorporate a third Hayward fault segment – the southeast extension – that has an estimated maximum earthquake of **M** 6.5. This part of the fault only has a slip rate of  $3 \pm 2$  mm/yr. The WGCEP (1999) considers the Hayward-Rodgers Creek fault system the most likely source of the next **M** 6.7 or larger earthquake in the Bay Area, with a 32 percent probability of occurring in the time period 2000 to 2030. Our model also incorporates a scenario where the Hayward fault ruptures along with the Rodgers Creek fault. Rupture of the entire length of both faults would generate a maximum earthquake of **M** 7.6. Rupture of the Rodgers Creek fault and the northern segment of the Hayward fault would generate a maximum event of **M** 7.4.

### A.2.6 Hayward Southeast Extension

The northeastern margin of Santa Clara Valley, including Evergreen Valley, is marked by a northeast-dipping sequence of thrusts that are part of the East Bay Hills structural domain (Aydin and Page, 1984) or Graymer's (1995) Fremont subzone of the southern Hayward fault. This sequence of southwest-verging, reverse faults is located in the restraining left-step between the Calaveras and Hayward faults. The faults include the Piercy, Coyote Creek, Silver Creek, Evergreen, Quimby, Berryessa, Crosley, and Warm Springs faults. Like the Foothill thrust belt on the western side of Santa Clara Valley, this series of reverse and reverse-oblique faults marks the margin of a region of rapid late Cenozoic uplift. The Crosley, Berryessa, and Warm Springs faults have been interpreted as structures that may transfer slip from the southern Hayward fault to the Calaveras fault (Graymer *et al.*, 1995). Jones *et al.* (1994) show these faults as a steeply dipping zone of thrusts that roots in the Calaveras fault at an approximately 6.2 mile (10 km) depth. Outcrop mapping, however, suggests that many of these faults are moderate to relatively low-angle features that may root into the Calaveras fault at shallower depths. The thrust fault traces are slightly oblique, rotated about 10° to 15° counterclockwise, to the main strike-slip faults.

Although seismicity in this area is diffuse, relocation of microearthquake epicenters indicates that contemporary seismicity may be associated with faults that dip moderately to the east (Woodward-Clyde Consultants, 1994). Earthquake focal mechanisms also indicate northwest-striking reverse faulting. No large, historical earthquakes have been conclusively attributed to the thrust faults along the eastern Santa Clara Valley margin (Oppenheimer *et al.*, 1990). Jaumé and Sykes (1996) suggest that the July 1, 1911, **M** 6.2 earthquake may have occurred on a thrust fault parallel to the Calaveras fault; however, macroseismic intensity data indicate that this event is more likely to have occurred on the Calaveras fault (Bakun, 1999; Topozada, 1984). The recent activity of many of these faults is inconclusive, and in some cases it is unclear whether the mapped trace is of tectonic or landslide origin. The range front along the northeastern side of Santa Clara Valley is modified by many large-scale slope failures.

The Evergreen fault is typical of faults in this area. This fault is an east-dipping reverse or reverse-oblique fault striking northwest across the piedmont of Evergreen Valley, east of San Jose. A recent trenching investigation at this site showed that the Evergreen fault is a moderate to low-angle (less than 45°) thrust fault, displacing Knoxville shale, up to the east, against gravels of the Santa Clara Formation (Fenton *et al.*, 1995). The fault plane was observed to cut up through the gravels and paleosol horizons estimated to be late Pleistocene in age. Overlying gravels were also observed to have been warped. The trench exposures were interpreted as indicating that the Evergreen fault had experienced coseismic rupture during the late Pleistocene, but that this rupture had not propagated to the surface. Rather, it had just resulted in warping of the ground surface. Slickensides on the fault surface indicated that fault slip was not purely reverse, but incorporated a small component of lateral movement.

The WGNCEP (1996) assigns a maximum earthquake of **M** 6.4 with a recurrence interval of 220 years for the Hayward Southeast Extension.

### **A.2.7 Rodgers Creek Fault**

As indicated previously, the Hayward fault runs into San Pablo Bay at Point Pinole. The northern continuation of this fault system is the Rodgers Creek fault. The two faults are separated by a 5-km-wide right step beneath San Pablo Bay. The Rodgers Creek fault is 44 km long and has a similar geomorphic expression to the Hayward. At its northern end, the Rodgers Creek fault is separated from the Healdsburg fault by a 3-km-wide right step, and separated from the Maacama fault by a 10-km-wide right step (Wagner and Bortugno, 1982). Holocene activity along the Rodgers Creek is indicated by a series of fault scarps in Holocene deposits, side-hill benches, right-laterally offset streams, and closed linear depressions. Paleoseismic investigations by Schwartz *et al.* (1992) revealed three events in 925 to 1,000 years. This gives a preferred recurrence of 230 years for a maximum earthquake of **M** 7.2. The calculated slip rate for the Rodgers Creek fault is  $9 \pm 2$  mm/yr.

### **A.2.8 Calaveras Fault**

This fault is a main component of the San Andreas system, branching off the main San Andreas fault south of Hollister, and extending northwards for approximately 120 km to die out in the area of Danville. The predominant sense of motion on the Calaveras fault is right-lateral, strike-slip. A smaller component of vertical displacement is evident in some areas along the fault trace. The Calaveras fault can be divided into two distinct sections, northern and southern, with the boundary located at Calaveras Reservoir. Oppenheimer and Lindh (1992) suggest that rupture of the entire 40-km-long northern Calaveras fault is possible and could generate a **M** 7 earthquake. The Calaveras fault has generated a number of moderate-size earthquakes in historic time, including (1) the 1861 Richter local magnitude ( $M_L$ ) 5.9 event, (2) the 1886  $M_L$  5.4 event, (3) the 1897  $M_L$  6.2 event, (4) a probable  $M_L$  6.5 event in 1911, (5) the 1988  $M_L$  5.1 Alum Rock event, (6) the 1979  $M_L$  5.9 Coyote Lake event, and (7) the 1984  $M_L$  6.2 Morgan Hill event.

To the south of Calaveras Reservoir, microseismicity clearly delineates the active trace of the fault. Little microseismicity is associated with the northern section of the fault, and only the 1861 earthquake can be attributed to this portion of the fault. This event is reported to have caused 8.1 miles (13 km) of surface rupture, extending from San Ramon to Dublin (Toppozada *et al.*, 1981). The lack of a well-defined fault and the diffuse nature of seismicity at the northern

end of the San Ramon Valley suggest that the Calaveras fault may die out just to the south of Walnut Creek, with strain being transferred across the East Bay Hills and onto the Hayward fault (Aydin 1982). The northern section of the fault may, therefore, be less active than the southern section. The long-term slip rate and contemporary creep rate for the southern Calaveras fault are approximately  $15 \pm 3$  mm/yr (WGCEP, 1999), while the northern Calaveras fault has a creep rate of approximately 6 mm/yr (Prescott and Lisowski 1983) and a long-term geologic slip rate of  $6 \pm 1$  mm/yr (Simpson *et al.* 1999). The WGCEP (1999) suggests a recurrence interval of 359 years for a maximum earthquake of **M** 7.0 on the northern Calaveras fault. The recurrence interval for a maximum event of **M** 6.7 on the southern Calaveras fault is approximately 546 years.

Several rupture scenarios, including a floating **M** 6¼ are considered for this fault (Table 1). The WGCEP (1999) assigned a **M** 7.1 and 7.3 for rupture of the south-central and central Calaveras fault segments, respectively. However, recent paleoseismic investigations on the central Calaveras fault indicate that there have been no large, surface rupturing earthquakes along this reach of the fault in the last 2,700 years (Kelson and Baldwin, 2002).

### **A.2.9 Concord-Green Valley Fault**

The Concord fault, and its continuation on the northern side of Suisun Bay, the Green Valley fault, is a northwest-striking right-lateral strike-slip fault of the San Andreas system. The Concord fault extends for 18 km along the eastern margin of Ygnacio Valley, from the northern slopes of Mount Diablo to Suisun Bay. North of the Bay, the Green Valley fault extends northwards for a distance of approximately 43 km. The northern end of the Green Valley fault is defined by a change in fault strike and a gap in microseismicity (WGCEP 1999). The WGCEP (1999) also included the Cordelia fault within the Concord-Green Valley fault system.

Both the Concord and Green Valley faults exhibit aseismic creep. Galehouse (1992) measured a creep rate of 3 to 6 mm/yr. Relatively few paleoseismic data exist for either fault. Wills *et al.* (1994) showed 30 to 60 m of right-lateral offset has occurred across the Concord fault during the Holocene (the last 10,000 years). Snyder *et al.* (1994) estimate a slip rate range of 2.6 to 10.8 mm/yr. The WGCEP (1999) has assigned a slip rate of  $4 \pm 2$  mm/yr for the Concord and  $5 \pm 2$  mm/yr for the Green Valley fault. Baldwin *et al.* (2001) calculates a slip rate of 3.8 to 4.8 mm/yr for both the Concord and southern Green Valley faults. Based on differences in geomorphic expression, fault geometry, paleoseismic chronology, slip rate, and seismicity, the Concord-Green Valley fault is divided into three fault segments: the Concord fault, the southern Green Valley, and northern Green Valley faults. The segment boundary between the Concord and Green Valley faults is taken to be the middle of Suisun Bay. The boundary between the southern and northern Green Valley segments is located at the northern end of Green Valley, north of Cordelia. Rupture of the Concord and Green Valley faults, independently of each other, would generate maximum earthquakes of **M** 6.5 and 7.0, respectively. The Green Valley fault may also rupture as independent north and south segments, generating maximum earthquakes of **M** 6.7. A rupture along the entire length of both faults would generate a maximum earthquake of **M** 7.1.

### **A.2.10 Cordelia Fault**

This fault is a north-striking right-lateral strike-slip fault that has often been assumed to be part of the Green Valley fault system. Paleoseismic investigations, however, have indicated that the

Cordelia fault has a much lower slip rate than the Green Valley fault and, therefore, may be an independent seismic source (Kieffer *et al.*, 1994). The Cordelia fault extends from south of Cordelia to the western shore of Lake Curry as a series of discontinuous north and north-northwest-striking fault strands. The geomorphic expression of the fault is more subdued than that of the Green Valley fault, being confined to tonal lineaments in Holocene deposits and right-lateral deflections of small drainages (Bryant, 1981). No contemporary seismicity is recorded along the fault (Wong, 1990). Based on differences in geomorphic expression and fault geometry, the Cordelia fault is divided into two fault segments: the northern and southern Cordelia fault. The boundary between the two fault segments is considered to be the subtle change in fault strike north of Cordelia. This presents three possible rupture models: independent rupture of the north and south segments, and rupture of the entire fault. These scenarios would generate maximum earthquakes of **M** 6.5, 6.2, and 6.6, respectively. Fault activity is expressed in terms of slip rate, as determined by recent paleoseismic investigations (Kieffer *et al.*, 1994). The preferred slip rate is 0.6 mm/yr, with a minimum of 0.05 mm/yr and a maximum of 1.0 mm/yr.

#### **A.2.11 Coast Range-Sierran Block Boundary (CRSB)**

The CRSB is a complex zone of thrust faulting that marks the boundary between the Coast Range block and the Sierran basement rocks that are concealed beneath the Great Valley sedimentary rocks of the Sacramento and San Joaquin valleys. The basal detachment within the CRSB is a low-angle, west-dipping thrust accommodating eastward thrusting of the Coast Range block over the Sierran block. Above this detachment is a complex array of west-dipping thrusts and east-dipping back-thrusts. The CRSB extends for over 500 km, from near Red Bluff in the northern Sacramento Valley to Wheeler Ridge in the southern San Joaquin Valley (Wakabayashi and Smith, 1994; Wong *et al.*, 1988).

The CRSB was the probable source of the two **M** 6¼ to 6½ 1892 Vacaville-Winters earthquakes and the 1983 **M** 6.5 Coalinga earthquake (Wong *et al.*, 1988). Although the faults themselves do not rupture to the surface, the CRSB is marked along much of its length by an alignment of fault-propagation folds such as the Rumsey Hills. This relatively simple geomorphic expression is interrupted by the Delta where the CRSB takes a right-step between the Montezuma Hills to the north and the Los Medanos Hills to the south (Wakabayashi and Smith, 1994). This complexity is most likely the result of the interaction of right-lateral strike-slip faulting and left-stepping restraining bends on these faults that belong to the San Andreas fault system (Unruh *et al.*, 1997; Wakabayashi and Smith, 1994).

Based on differences in geomorphic expression and fault geometry, Wakabayashi and Smith (1994) divided the CRSB into a number of segments. Working Group on Northern California Earthquake Potential (1996) has since modified this segmentation model, using the rupture geometry of the 1983 Coalinga earthquake as a “characteristic” event. Recent investigations by Unruh and Hector (1999) and O’Connell *et al.* (2001) have further refined the segmentation of the CRSB in the region surrounding the Delta. These faults are discussed in the following sections. The CRSB faults are considered as independent seismogenic sources, capable of generating maximum earthquake in the range **M** 6.5 to 7.0. Where no further information is available, fault activity is expressed in terms of slip rate as determined by Wakabayashi and

Smith (1994) and refined by WGNCEP (1996). The preferred geologic slip rate is 1.5 mm/yr, with an error of  $\pm 0.5$  mm/yr.

### ***CRSB North of the Delta***

Recent investigations carried out by U.S. Bureau of Reclamation along the western margin of the Sacramento Valley north of Vacaville have greatly increased the understanding of the fault geometry in the fold and thrust belt of the CRSB (O'Connell and Unruh, 2000; O'Connell *et al.*, 2001). Previous models of faulting in this area had inferred a wedge back-thrust geometry (Unruh *et al.*, 1997). These recent investigations have revealed a fault-propagation fold geometry, with the main active structures being a series of west-dipping blind thrusts separated by lateral tears faults or oblique folds above lateral ramps (O'Connell *et al.*, 2001). Three main fault sources are considered in this area, from north to south, the Mysterious Ridge, Trout Creek, and Gordon Valley blind thrusts. These sources are considered capable of generating earthquakes of **M** 6.5 to 6.9. The structural complexity of this zone of faulting and the considerable structural elevation differences among these segments indicates that multi-segment rupture is unlikely.

### ***Sacramento Delta Faults***

Recent investigations in the Delta region have revealed a number of Quaternary active thrust faults beneath a series of right-stepping *en echelon* anticlines to the north of Mount Diablo (Unruh and Hector, 1999; Weber-Band, 1998). These faults include the Roe Island thrust, Potrero Hills thrust fault, Pittsburg-Kirby Hills fault, and the Midland fault.

Previous models for seismic sources in the Delta region have assumed a through-going buried or blind thrust fault representing the local continuation of the CRSB (Wakabayashi and Smith, 1994) through the central part of the Delta. The lack of Coalinga-type anticlines through the Delta region indicates that blind thrusts of the CRSB, if present, must have a lower slip rate than the "type" structures of the CRSB to the south. Unruh and Lettis (1998) proposed an alternative kinematic model for the deformation in this region that does not involve a through-going CRSB thrust structure; instead, they have a series of smaller, less active thrust faults.

The Roe Island thrust underlies the asymmetric Roe Island anticline in Suisun Bay. This fold and the underlying thrust fault are well documented from gas exploration wells and seismic reflection data (Unruh and Hector, 1999). The northeast-dipping thrust fault is considered capable of generating a maximum earthquake of **M** 5.5 to **M** 6.0 (Unruh and Hector, 1999). Slip-rate estimates range from 0.3 to 0.7 mm/yr, with a preferred value of 0.5 mm/yr.

The Los Medanos thrust is interpreted by Unruh and Hector (1999) to underlie the asymmetric, southwest-tilted Los Medanos and Concord anticlines. Based on an estimate of potential fault rupture area from the length of the overlying folds and the down-dip width from structural cross sections, Unruh *et al.* (1997) estimated a maximum earthquake magnitude of **M** 6 for the Los Medanos thrust fault. However, due to uncertainties on the fault geometry and the interaction of the fault with neighboring faults, namely the Roe Island thrust to the northwest and the Pittsburg-Kirby Hills fault to the east, the maximum event for the Los Medanos thrust ranges from **M** 5<sup>3</sup>/<sub>4</sub> to **M** 6<sup>1</sup>/<sub>4</sub>. Estimates for the slip rate on the Los Medanos thrust range from 0.3 to 0.7 mm/yr.

Although they have slightly different geometries, the Los Medanos and Rose Island thrusts may merge at a common decollement horizon, thus there is a possibility that they may rupture simultaneously, generating a maximum earthquake of **M** 6.6.

The Potrero Hills thrust fault underlies the north-tilted Potrero Hills anticline, located just south of Fairfield. Unruh and Hector (1999) consider this fault capable of generating a maximum earthquake of **M** 6. Estimates of fault slip-rate range from 0.1 to 0.6 mm/yr, with 0.3 mm/yr representing the best estimate for the long-term slip rate.

The Pittsburg-Kirby Hills fault (PKHF) is a right-lateral tear fault that bounds the eastern margin of a series of folds and thrusts in the Grizzly Bay-Van Sickle Island area (Unruh *et al.*, 1997). The PKHF is highlighted by a linear alignment of microseismicity, which is unusual in that it occurs at depths of 20 to 25 km (Wong *et al.*, 1988). Weber-Band (1998) argued that the PKHF is an east-dipping reverse fault, however, focal mechanisms indicate that the movement on the fault is almost pure right-lateral strike-slip. The 1889 **M** 6 Antioch earthquake may possibly have occurred on the PKHF (Unruh and Lettis, 1998). Empirical relationships among fault length, fault rupture area, and earthquake magnitude indicate that the maximum earthquake for the PKHF is **M** 6.7. Estimates for the slip rate of the PKHF range from 0.3 to 0.7 mm/yr.

The Midland fault is a west-dipping fault located along the eastern margin of the Montezuma Hills. This fault accommodated subsidence of the Sacramento basin during early Tertiary time. From detailed analysis of seismic reflection data, late Cenozoic reactivation of the Midland fault to accommodate reverse slip and horizontal crustal shortening has been documented (Weber-Band, 1998). This reverse reactivation of the Midland fault has resulted in uplift of the eastern Montezuma Hills. From the offset of known Cenozoic reflectors, the Midland fault is estimated to have a slip rate of 0.1 to 0.6 mm/yr. The preferred estimate is 0.15 mm/yr (Jeff Unruh, William Lettis and Associates, Inc., *pers. comm.*, 1999). The maximum earthquake for the Midland fault is **M** 6.3 ± 0.3.

### **CRSB South of the Delta**

Previous models for segmentation of the CRSB south of the Sacramento River inferred a continuous zone of faulting along the eastern side of the Diablo Range (Wakabayashi and Smith, 1994; WGNCEP, 1996). More recent studies have shown that the regional fault geometry is more complex. Instead of one, continuous through-going fault zone, there is in fact a broad zone of *en echelon* folds and thrusts, including the Mount Diablo blind thrust, between the Sacramento River delta and the Livermore Valley. The CRSB *sensu stricto* begins again along the eastern range front of the Altamont Hills. Two segments of this southern part of the CRSB are of importance to ground shaking hazard to the In-Delta storage project. These are the range front west of Tracy (herein called the ‘Tracy segment’) and the range front west of Vernalis (the ‘Vernalis’ segment). The geometry of these structures is not known, but from analogy with other sections of the CRSB, it is assumed that these are west-dipping blind thrusts located beneath east-facing monoclinical warps (a fault-propagation fold geometry). Assuming a 15° dip and a ‘Coalinga-type’ geometry (fault extending from 4 km to 10 km depth), the Tracy and Vernalis blind thrusts are considered capable of generating maximum earthquake of **M** 6.8 and 6.6, respectively. Rupture of both segments would generate a maximum earthquake of **M** 7.0. The

slip rate for these faults is between 0.29 and 2.3 mm/yr, with a preferred estimate of 0.42 mm/yr based on vertical separation rates calculated by Sowers *et al.* (2000).

#### **A.2.12 Mount Diablo 'Blind' Thrust**

This thrust fault is a northeast-dipping, southwest propagating thrust fault beneath the Mount Diablo anticline. Unruh and Sawyer (1995) proposed that slip on the northern Greenville fault appears to die out northward because the fault steps to the northwest (left) across Mount Diablo to join with the right-lateral Concord fault. This model argues that the Mount Diablo anticline is a contractional left-stepover between the Greenville and Concord faults. Unruh and Sawyer (1995) specifically proposed that Mount Diablo is an asymmetric, southwest-vergent fault-propagation fold underlain by a northeast-dipping blind thrust fault that links the northern Greenville fault to the Concord fault.

Long-term average Quaternary shortening rates across the Mount Diablo region, estimated from construction of balanced cross sections, are  $3.4 \pm 0.9$  mm/yr (Unruh and Sawyer, 1997). Considering the likely fault geometry, an average slip rate for the Mount Diablo thrust would be approximately  $4.1 \pm 1.4$  mm/yr. The likely geometry of this blind thrust fault indicates that it is capable of generating a maximum earthquake of **M** 6.9. Along-strike complexities indicate that the Mount Diablo thrust may be segmented, with the segments being separated by northeast-striking tear faults. If this is the case, then the maximum earthquake for each segment would be **M** 6.2 to 6.6. Based on an average coseismic slip during the maximum event and the calculated slip rate, Unruh and Sawyer (1997) proposed an average recurrence of approximately 230 to 740 years for the Mount Diablo thrust.

#### **A.2.13 Greenville Fault**

This fault is a north-northwest- to northwest-striking strike-slip fault of the San Andreas system in the northern Diablo Range. The fault extends from Bear Valley to just north of Livermore Valley. Evidence for right-lateral displacement on the Greenville fault includes right-laterally offset drainages and sidehill benches, and right-lateral surface offsets observed along traces of the fault following the January 1980 Livermore earthquake sequence (Hart, 1981). Seismicity associated with the fault is characterized by a subvertical alignment of epicenters extending to depths of approximately 17 km at the latitude of Livermore Valley (Hill *et al.*, 1990). Focal mechanisms indicate primarily right-lateral strike-slip motion on northwest-striking nodal planes (Oppenheimer and Macgregor-Scott, 1992). The Greenville fault generally is assumed to continue north of Livermore Valley as the Marsh Creek-Clayton system; however, the well-defined surface trace of the fault dies out or diminishes markedly several km north of Livermore Valley, and the Marsh Creek-Clayton fault system is considerably less active than the northern Greenville fault east of Livermore. The restraining step over model of Unruh and Sawyer (1997) indicates that slip from the Greenville fault is transferred to the Concord fault, and therefore the Clayton-Marsh Creek fault is either inactive or not part of the Greenville fault system.

Available data on the late Quaternary slip rate of the Greenville fault are sparse and have significant uncertainties. Based on correlation of terraces south of Livermore Valley offset by the Greenville fault, Wright *et al.* (1982) documented approximately 90 m of Pleistocene

displacement. The deformed terraces were estimated by Wright *et al.* (1982) to be 125,000 to 180,000 years old, based on soil profile development, thus implying a slip rate of 0.5 to 0.7 mm/yr. Paleoseismic trench investigations across one of the strands of the northern Greenville fault documented evidence for Holocene surface-rupturing events, using an assumed 1:3 ratio of vertical to horizontal separation. Wright *et al.* (1982) estimated a horizontal slip rate of approximately 0.1 to 0.3 mm/yr. The WGNCEP (1996) assigned a maximum earthquake of **M** 6.9 and a minimum slip rate of 2 mm/yr to the Greenville fault. The recurrence interval is estimated to be on the order of 550 years. Recent investigations by Sawyer and Unruh (1998, 2002) indicate a 70-km length for the active Greenville fault. Preliminary Holocene slip rate estimates from a site at the northern end of the Livermore Valley are  $4.1 \pm 1.8$  mm/yr (Sawyer and Unruh, 2002).

#### **A.2.14 Ortigalita Fault**

The Ortigalita fault is a 66-km-long, north-northwest-striking, right-lateral strike-slip fault located in the southern Diablo Range. The fault extends from Panoche to southeast of Mount Stakes. The fault consists of two distinct geometric sections, separated by a 5-km-wide right-step across San Luis Reservoir. Much of the fault is delineated by persistent microseismicity. The fault is marked by geomorphic indicators of recent strike-slip faulting, including deflected drainages, shutter ridges, sidehill benches, and vegetation lineaments (Anderson *et al.*, 1982, 2001). Paleoseismic trenching investigations have estimated a slip rate of 0.5 to 2.5 mm/yr for the fault north of San Luis Reservoir. South of the reservoir, the slip rate is considerably less, approximately 0.2 to 1.0 mm/yr (Anderson *et al.*, 2001). The maximum earthquake for rupture of the entire Ortigalita fault is **M** 7.4. Independent rupture of the northern segment would generate a maximum earthquake **M** 7.0 while the southern segment would generate a maximum earthquake of **M** 7.2. The geometric complexity of the southern part of the Ortigalita, generally forming 17 to 27 km long fault strands, would more likely rupture as smaller earthquakes, of **M** 6.5 to 6.7.

#### **A.2.15 Mt. Oso Anticline**

The Mount Oso anticline is located in the left-step between the Ortigalita and Greenville faults. The location of this fold, in what is considered a restraining step between two active right-lateral strike-slip faults, indicates that it may be undergoing active contractional deformation. In addition, the southwest-vergent geometry of this fold suggests that it may be underlain by a northwest-dipping blind thrust, similar to that beneath Mount Diablo (Jeff Unruh, Wm. Lettis & Associates, Inc., *pers. comm.*, 2002). The geometry and activity of this structure is the subject of speculation. Without further information, we assign this zone a probability of activity of 0.5. Conservatively, we assume that the entire zone beneath Mt. Oso between the Greenville and Ortigalita faults is underlain by a blind thrust dipping at 20°. We also assume that the fault is capable of generating a maximum earthquake similar to the Mount Diablo blind thrust.

#### **A.2.16 East Bay Thrust Domains**

The East Bay Hills are a region of youthful, elevated topography between the Hayward and Calaveras faults. Late Cenozoic crustal shortening across this region is shown by folded

Miocene and Pliocene rocks, and the presence of discrete thrust faults that repeat parts of the Neogene stratigraphy. Geomatrix Consultants (1998) have documented evidence for late Pleistocene and possibly Holocene surface faulting on secondary structures related to the Franklin fault near Walnut Creek. Wakabayashi and Sawyer (1998) have also obtained paleoseismic evidence for late Pleistocene to Holocene surface rupture on the Miller Creek fault. Based on the elevated topography, late Cenozoic folding, and paleoseismic evidence for surface-rupturing earthquakes, the Thrust Faults Subgroup of the 1999 WGCEP (Jeff Unruh, unpublished memo, 1998) concluded that active thrust-related seismic sources exist within the East Bay hills. However, given the limited amount of paleoseismic information, rather than characterize individual faults, the Thrust Fault Subgroup defined a series of areal source zones, rather than try to characterize discrete fault sources. These zones are:

- The Western East Bay Hills domain, bounded by the Hayward fault to the west and the Moraga-Miller Creek-Palomares faults to the east. This domain contains the active Miller Creek thrust fault (Wakabayashi and Sawyer, 1998). This elongate zone is considered capable of generating a maximum earthquake of **M** 6. The slip rate, considered to be comparable to measured uplift rates in this area (Kelson and Simpson, 1996), is approximately 1.0 mm/yr.
- The southern East Bay Hills domain is roughly a triangular region bounded to the west by the Western East Bay Hills domain, by the northern Calaveras fault to the east, and by the Bollinger thrust fault to the north and northeast. The maximum length of thrust faults in this domain is about 15 km. This domain is considered capable of generating earthquakes of **M** 6¼ to 6½. Slip rates, calculated from measured uplift rates and assuming slip on thrust faults that dip 30° to 45°, are in the range 0.1 to 1.0 mm/yr, with 0.3 mm/yr representing the best-estimate value.
- The northern East Bay Hills domain is the region that lies north of the Bollinger thrust fault and west of the western domain. This domain contains the Pinole, Southampton, and Franklin faults. Geomatrix Consultants (1998) assigned a maximum earthquake of **M** 6¾ to the Franklin fault. The Thrust Fault Subgroup assigned a maximum earthquake of **M** 6¼ to 6¾ to the northern domain. The slip rate for this domain is 1.0 to 4.0 mm/yr. The higher value assumes that slip from the northern Calaveras fault is transferred through this region (Aydin 1982).

### A.2.17 West Napa Fault

This fault is a north-northwest-striking right-lateral strike-slip fault comprising a series of *en echelon* fault strands along the western side of the Napa Valley, from south of Napa to Yountville, a distance of approximately 25 km. The fault is characterized by well-defined active fault features, including tonal lineaments, fault scarps in Holocene deposits, closed depressions, and right-laterally offset drainages. Very little contemporary seismicity is associated with this fault (Wong, 1990). To date, no independent paleoseismic data exist for the West Napa fault. Current estimates of 1 mm/yr for the slip rate and 700 years for the recurrence interval are based upon “regional strain book-keeping” (WGNCEP 1996).

Based on differences in geomorphic expression and fault geometry, the West Napa fault is divided into two segments: a northern segment along the western side of the Napa Valley from

Napa to just north of Yountville and a southern segment from Napa across the Napa Valley towards American Canyon. This presents three possible rupture models: independent rupture of the north and south segments, and rupture of the entire fault. These rupture models are capable of generating maximum earthquakes of **M** 6.6, 6.4, and 6.8 for the north, south, and entire rupture, respectively. Fault activity is defined in terms of the 1.0 mm/yr proxy slip rate determined by the WGNCEP (1996). The minimum and maximum slips rates are 0.5 and 2.0 mm/yr, respectively.

### **A.3 BACKGROUND EARTHQUAKES**

To account for the hazard from background (floating or random) earthquakes in the probabilistic seismic hazard analysis that are not associated with known or mapped faults, regional seismic source zones were used. In most of the western U.S., the maximum magnitude of earthquakes not associated with known faults usually ranges from **M** 6 to 6½. Repeated events larger than these magnitudes generally produce recognizable fault-or-fold related features at the earth's surface (e.g., dePolo, 1994). An example of a background earthquake is the 1986 **M** 5.7 Mt. Lewis earthquake that occurred east of San Jose.

Earthquake recurrence estimates in the region are required to quantify the hazard. The site region was divided into two regional seismic source zones: the Coast Ranges and Central Valley. The recurrence parameters for the Coast Ranges source zone was adopted from the WGCEP (1999) and Dreger (2000). The *b*-values, 0.91 and 0.86, respectively, were assigned equal weights in the hazard analysis. The recurrence values for the Central Valley zone were adopted from URS Corporation (2001). Maximum earthquakes for both zones of **M** 6.5 ± 0.3 were used in the analysis.

### **A.4 REFERENCES**

- Abrahamson, N.A. and Silva, W.J., 1997, Empirical response spectral attenuation relations for shallow crustal earthquakes: *Seismological Research Letters*, v. 68, p. 94-127.
- Aki, K., 1983, Seismological evidence for in support of the existence of "characteristic earthquakes", *Earthquake Notes*, v. 54, p. 60-61.
- Anderson, J.G., 1979, Estimating the seismicity from geological structures for seismic risk studies, *Bulletin of the Seismological Society of America*, v. 69, p. 163-168.
- Anderson, L.W., LaForge, R. and Anders, M.H., 1982, Seismotectonic study of the San Luis Area, Eastern Diablo Range, California for San Luis Dam, O'Neill Dam, Los Banos Detention Dam, and Little Panoche Detention Dam, San Luis Unit, Central Valley Project, U.S. Bureau of Reclamation, Seismotectonic Report 82-2, 89 p.
- Anderson, L.W. and Piety, L.A., 2001, Geologic seismic source characterization of the San Luis-O'Neill area, eastern Diablo Range, California for B.F. Sisk and O'Neill Forebay dams, San Luis Unit, Central Valley Project, California, U.S. Bureau of Reclamation, Seismotectonic Report 2001-2, 76 p.
- Aydin, A., 1982, The East Bay Hills, a compressional domain resulting from interaction between the Calaveras and Hayward-Rodgers Creek faults, *in* Proceedings, Conference on Earthquake

## Appendix A Seismic Sources

---

- Hazards in the Eastern San Francisco Bay Area, Hart, E.W., Hirschfeld, S.E. and Schulz, S.S. (eds.), California Division of Mines and Geology, Special Publication 62, p. 11-22.
- Aydin, A., Johnson, A.M. and Fleming, R.W., 1992, Right-lateral-reverse surface rupture along the San Andreas and Sargent faults associated with the October 17, 1989, Loma Prieta, California, earthquake, *Geology*, v. 20, p. 1,063-1,067.
- Aydin, A. and Page, B.M., 1984, Diverse Pliocene-Quaternary tectonics in a transform environment, San Francisco Bay region, California, *Geological Society of America Bulletin*, v. 95, p. 1,303-1,317.
- Bakun, W.H., 1999, Seismic activity of the San Francisco Bay region, *Bulletin of the Seismological Society of America*, v. 89, p. 764-784.
- Baldwin, J.N., Koehler, R.D. and Barron, A., 2001, Paleoseismic Feasibility Study of the Green Valley Fault, San Francisco Bay Area, California, Final Technical Report for U.S. Geological Survey National Earthquake Hazard Reduction Program Award Number 01 -HQGR-0123.
- Boore, D.M., Joyner, W.B., and Fumal, T.E., 1997, Equations for estimating horizontal response spectra and peak acceleration from western North American earthquakes: A summary of recent work, *Seismological Research Letters*, v. 68, p. 128-153.
- Bryant, W.A., Smith, D.P. and Hart, E.W., 1981, Sargent, San Andreas and Calaveras fault zone - evidence for recency in the Watsonville East, Chittenden and San Felipe quadrangles, California, California Division of Mines and Geology, Open-File Report 81-7, 3 map sheets, 1:24,000 scale.
- Bürgmann, R., Arrowsmith, R. and Dumitru, T., 1994, Rise and fall of the southern Santa Cruz Mountains, California, from fission tracks, geomorphology, and geodesy, *Journal of Geophysical Research*, v. 99B, p. 20,181-20,202.
- Campbell, K.C., 1999, Hybrid empirical model for estimating strong ground motion in regions of limited strong motion recordings, *Proceedings of the OECD-NEA Workshop on the Engineering Characterization of Seismic Input*, Brookhaven National Laboratory, November 15-17.
- Cornell, C. A., 1968, Engineering seismic risk analysis, *Bulletin of the Seismological Society of America*, v. 58, p. 1583-1606.
- dePolo, C.M., 1994, The maximum background earthquake for the Basin and Range Province, western North America, *Bulletin of the Seismological Society of America*, v. 84, p. 466-472.
- Fenton, C.H., Wong, I.G. and Sawyer, J.E., 1995, Geological and seismological investigations of the Evergreen fault, southeastern San Francisco Bay Area, California, *Bulletin of the American Association of Petroleum Geologists*, v. 79, p. 584.
- Galehouse, J., 1992, Creep rates and creep characteristics of eastern San Francisco Bay Area faults: 1979-1992, *in* *Proceedings of the Second Conference on Earthquake Hazards in the Eastern San Francisco Bay Area*, Borchardt, G., Hirschfeld, S.E., Lienkaemper, J.J., McClellan, P., Williams, P.L. and Wong, I.G. (eds.), California Department of Conservation, Division of Mines and Geology, p. 45-53.

## Appendix A Seismic Sources

---

- Geomatrix Consultants, 1998, Final Report, Walnut Creek Water Treatment Plant Expansion Seismic Study - Phase II, Report prepared for East Bay Municipal Utility District, Seismic Improvement Program, 1330 Broadway, Suite 800, Oakland, California 94612 57 p.
- Graymer, R., 1995, Geology of the southeast San Francisco Bay Area hills, California, *in* Recent Geologic Studies in the San Francisco Bay Area, Sanginés, E.M., Andersen, D.W. and Buising, A.B. (eds.), Pacific Section, Society of Economic and Petroleum Geologists v. 76, p. 115-124.
- Graymer, R.W., Jones, D.L. and Brabb, E.E., 1995, Geologic Map of the Hayward fault zone, Contra Costa, Alameda, and Santa Clara Counties, California: A digital database, U.S. Geological Survey, Open-File Report, 1:50,000.
- Hall, N.T., Wright, R.H. and Clahan, K.B., 1999, Paleoseismic studies of the San Francisco Peninsula segment of the San Andreas fault zone near Woodside, California, *Journal of Geophysical Research*, v. 104, p. 23,215-23,236.
- Hanks, T.C. and Bakun, W.H., 2002, A bilinear source-scaling model for  $M$ -log  $A$  observations of continental earthquakes, *Bulletin of the Seismological Society of America*, v. 92, p. 1,841-1,846.
- Hanks, T.C. and Kanamori, H., 1979, A moment magnitude scale, *Journal of Geophysical Research*, v. 84, p. 2,348-2,349.
- Hart, E.W., 1981, Greenville fault, California Division of Mines and Geology, Fault Evaluation Report 117, 27 p.
- Hill, D.P., Eaton, J.P. and Jones, L.M., 1990, Seismicity, 1980-86, *in* The San Andreas fault system, Wallace, R.E. (ed.) U.S Geological Survey Professional Paper 1515, p. 115-151.
- Hitchcock, C.S. and Kelson, K.I., 1999, Growth of late Quaternary folds in southwest Santa Clara Valley, San Francisco Bay Area, California: Implications of triggered slip for seismic hazard and earthquake recurrence, *Geology*, v. 27, p. 387-390.
- Hitchcock, C.S., Kelson, K.I. and Thompson, S.C., 1994, Geomorphic investigations of deformation along the northeastern margin of the Santa Cruz Mountains, William Lettis & Associates, Inc., Final Technical Report, U.S. Geological Survey National Earthquake Hazards Reduction Program Award No. 1434-92-G-2220, 33 p.
- Irwin, W.P., 1990, Geology and plate tectonic development, *in* The San Andreas Fault System, California, Wallace, R.E. (ed.) U.S. Geological Survey Professional Paper 1515, p. 61-80.
- Jaumé, S.C. and Sykes, L.R., 1996, Evolution of moderate seismicity in the San Francisco Bay region, 1850 to 1993: seismicity changes related to the occurrence of large and great earthquakes, *Journal of Geophysical Research*, v. 101, p. 765-789.
- Jennings, C.W., 1994, Fault activity map of California and adjacent areas with locations and ages of recent volcanic eruptions, California Division of Mines and Geology, 1:750,000.
- Jones, D.L., Graymer, R., Wang, C., McEvelly, T.V. and Lomax, A., 1994, Neogene transpressive evolution of the California Coast Ranges, *Tectonics*, v. 13, p. 561-574.
- Kelson, K.I. and Baldwin, J.N., 2002, Paleoseismology of the central Calaveras fault, Furtado Ranch site, Gilroy, California, Annual Summary Report prepared for U.S. Geological Survey

## Appendix A Seismic Sources

- National Earthquake Hazards Reduction Program Award 01-HQ-GR-0124 (<http://erp-web.er.usgs.gov/reports/annsum/vol43/nc/g0124.pdf>), 5 p.
- Kelson, K.I. and Simpson, G.D., 1996, Late Quaternary deformation of the southern East Bay Hills, Alameda County, CA, *in* Toward Assessing the Seismic Risk Associated With Blind Faults, San Francisco Bay Region, Jayko, A.S. and Lewis, S.D. (eds.), U.S. Geological Survey Open-File Report 96-267, p. 110-118.
- Kieffer, D.S., Lessin, E.E., Fisher, G.R., Clahan, K.B., Wright, R.H. and Wesling, J.R., 1994, Paleoseismic investigation of the Cordelia fault, Fairfield, Solano County, California, Abstracts with Program Geological Society of America, v. 26, p. A-207.
- LaForge, R. and Ake, J., 1999, Probabilistic seismic hazard analysis for Mormon Island Auxiliary Dam, Folsom Project, Central Valley Project, California, U.S. Bureau of Reclamation, Seismotectonic Report 94-3, 109 p.
- Lienkaemper, J.J., 1992, Map of recently active traces of the Hayward fault, Alameda and Contra Costa counties, California, U.S. Geological Survey, Miscellaneous Field Studies Map MF-2196, 1:24,000.
- Lienkaemper, J.J. and Galehouse, J.S., 1997, Revised long-term creep rates on the Hayward fault, Alameda and Contra Costa Counties, California, U.S. Geological Survey, Open-File Report 97-690, 18 p.
- Lienkaemper, J.J., Kelson, K.I., Lettis, W.R., Schwartz, D.P., Southon, J. and Williams, P.L., 1997, The northern Hayward fault, CA: Preliminary timing of paleoearthquakes, EOS, Transactions of the American Geophysical Union, Supplement, v. 78, p. F439.
- Lindh, A.G., 1983, Preliminary assessment of long-term probabilities for large earthquakes along selected fault segments of the San Andreas fault system in California, US Geological Survey Open-File Report 83-63, 14.p.
- McGuire, R.K., 1974, Seismic structural response risk analysis incorporating peak response regressions on earthquake magnitude and distance, Massachusetts Institute of Technology Department of Civil Engineering/Research Report R74-51.
- McGuire, R.K., 1978, FRISK: Computer program for seismic risk analysis using faults as earthquake sources, U.S. Geological Survey Open-File Report 78-1007.
- Niemi, T.M., 2002, Determination of high resolution paleoearthquake chronology for the northern San Andreas fault at the Vedanta Marsh site, Marin County, CA, Annual Summary Report prepared for U.S. Geological Survey National Earthquake Hazards Reduction Program Award 01-HQ-GR-0194, <http://erp-web.er.usgs.gov/reports/annsum/vol43/nc/01HQGR0194.htm>.
- Niemi, T. and Hall, N.T., 1992, Late Holocene slip rate and recurrence of great earthquakes on the San Andreas fault in northern California, *Geology*, v. 20, p. 195-198.
- Nolan, J.M., Zinn, E.N. and Weber, G.E., 1995, Paleoseismic study of the southern Sargent fault, Santa Clara and San Benito Counties, California, U.S. Geological Survey, NEHRP Final technical Report Award No. 1434-94-G-2466, 23 p.
- O'Connell, D.R.H. and Unruh, J.R., 2000, Updated seismotectonic evaluation of faults within 10 km of Monticello Dam, Solano Project, California, U.S. Bureau of Reclamation, Seismotectonic Report 99-5, 101 p.

## Appendix A Seismic Sources

---

- O'Connell, D.R.H., Unruh, J.R. and Block, L.V., 2001, Source characterization and ground-motion modeling of the 1892 Vacaville-Winters earthquake sequence, California, *Bulletin of the Seismological Society of America*, v. 91, p. 1,471-1,497.
- Oppenheimer, D.H. and Lindh, A.G., 1992, The potential for earthquake rupture of the northern Calaveras fault, *in* *Proceedings of the Second Conference on Earthquake Hazards in the Eastern San Francisco Bay Area*, Borchardt, G., Hirschfeld, S.E., Lienkaemper, J.J., McClellan, P., Williams, P.L. and Wong, I.G. (eds.), California Department of Conservation, Division of Mines and Geology, p. 233-240.
- Oppenheimer, D.H. and Macgregor-Scott, N., 1992, The seismotectonics of the eastern San Francisco Bay region, *in* *Proceedings of the Second Conference on Earthquake Hazards in the Eastern San Francisco Bay Area*, Borchardt, G., Hirschfeld, S.E., Lienkaemper, J.J., McClellan, P., Williams, P.L. and Wong, I.G. (eds.), California Department of Conservation, Division of Mines and Geology, p. 11-16.
- Oppenheimer, D.H., Bakun, W.H., and Lindh, A.G., 1990, Slip partitioning of the Calaveras fault, California, and prospects for future earthquakes, *Journal of Geophysical Research*, v. 95, p. 8483-8498.
- Page, B.M., 1981, The southern Coast Ranges, *in* *The geotectonic development of California*, Ernst, W.G. (ed.) Prentice-Hall, Englewood Cliffs, New Jersey, p. 329-417.
- Prescott, W.H. and Burford, R.O., 1976, Slip on the Sargent fault, *Bulletin of the Seismological Society of America*, v. 66, p. 1,013-1,016.
- Prescott, W.H. and Lisowski, M., 1983, Strain accumulation along the San Andreas fault system east of San Francisco Bay, California, *Tectonophysics*, v. 97, p. 41-56.
- Sadigh, K., Chang, C.Y., Egan, J.A., Makdisi, F., and Youngs, R.R., 1997, Attenuation relationships for shallow crustal earthquakes based on California strong motion data, *Seismology Research Letters*, v. 68, p. 180-189.
- Sawyer, T.L. and Unruh, J.R., 2002, Paleoseismic investigation of the Holocene slip rate on the Greenville fault, eastern San Francisco Bay area, California, Report prepared for U.S. Geological Survey National Earthquake Hazards Reduction Program Award No. 00HQGR0055, p.
- Schwartz, D.P. and Coppersmith, K.J., 1984, Fault behavior and characteristic earthquakes: examples from the Wasatch and San Andreas fault zones, *Journal of Geophysical Research*, v. 89, p. 5,681-5,698.
- Schwartz, D.P., Coppersmith, K.J. and Swan, F.H., III, 1984, Methods for estimating maximum earthquake magnitudes, *Proceedings of the Eighth World Conference on Earthquake Engineering*, Prentice-Hall, Englewood Cliffs, New Jersey, p. 279-285.
- Schwartz, D.P., Pantosti, D., Hecker, S., Okomura, K., Budding, K.E. and Powers, T., 1992, Late Holocene behavior and seismogenic potential of the Rodgers Creek fault zone, Sonoma County, California, *in* *Proceedings of the Second Conference on Earthquake Hazards in the Eastern San Francisco Bay Area*, Borchardt, G., Hirschfeld, S.E., Lienkaemper, J.J., McClellan, P., Williams, P.L. and Wong, I.G. (eds.), California Department of Conservation, Division of Mines and Geology, p. 393-398.

## Appendix A Seismic Sources

---

- Simpson, G.D., Thompson, S.C., Noller, J.S. and Lettis, W.R., 1997, The northern San Gregorio fault zone: Evidence of the timing of late Holocene earthquakes near Seal Cove, California, *Bulletin of the Seismological Society of America*, v. 87, p. 1,158-1,170.
- Simpson, G.D., Baldwin, J.N., Kelson, K.I. and Lettis, W.R., 1999, Late Holocene slip rate and earthquake history for the northern Calaveras fault at Welch Creek, eastern San Francisco Bay Area, California, *Bulletin of the Seismological Society of America*, v. 89, p. 1,250-1,263.
- Snyder, D.L., Borchardt, G. and Wills, C.J., 1994, Initial paleoseismic study of the Concord fault, California, *EOS, Transactions of the American Geophysical Union, Supplement*, v. 75, p. 684.
- Somerville, P., Irikura, K., Graves, R., Sawada, S., Wald, D., Abrahamson, N., Iwasaki, Y., Kagawa, T., Smith, N. and Kowada, A., 1999, Characterizing crustal earthquake slip models for prediction of strong ground motion, *Seismological Research Letters*, v. 70, p. 59-80.
- Sowers, J.M. and Ludwig, K.R., 2000, Quaternary Deformation along the East Front of the Diablo Range near Tracy, California: Year 2, Annual Summary Report prepared for U.S. Geological Survey National Earthquake Hazard Reduction Program Award # 99-HQ-GR-0101 6 p.
- Stirling, M., Rhoades, D. and Berryman, K., 2002, Comparison of earthquake scaling relations derived from data of the instrumental and preinstrumental era, *Bulletin of the Seismological Society of America*, v. 92, p. 812-830.
- Topozada, T.R., 1984, History of earthquake damage in Santa Clara County and comparison of the 1911 and 1984 earthquakes, *in* The 1984 Morgan Hill, California earthquake, Bennett, J.H. and Sherburne, R.W. (eds.), California Division of Mines and Geology Special Publication No. 68, p. 237-248.
- Topozada, T.R., Bennett, J.H., Hallstrom, C.L., and Youngs, L.G., 1992, 1898 "Mare Island" earthquake at the southern end of the Rodgers Creek fault., *in* G. Borchardt and others (eds.), Proceedings of the Second Conference on Earthquake Hazards in the Eastern San Francisco Bay Area, California Department of Conservation, Division of Mines and Geology Special Publication 113, p. 385-392.
- Topozada, T.R. and Borchardt, G., 1998, Re-evaluation of the 1836 "Hayward fault" and 1838 San Andreas fault earthquakes, *Bulletin of the Seismological Society of America*, v. 88, p. 140-159.
- Topozada, T.R., Real, C., and Parke, D.L. 1981, Preparation of isoseismal maps and summaries of reported effects of the pre-1900 California earthquakes, California Division of Mines and Geology Open-File Report 81-11, 181 p.
- Tuttle, M. and Sykes, L., 1992, Re-evaluation of the 1838, 1865, 1868, and 1890 earthquakes in the San Francisco Bay Area, *in* Proceedings of the Second Conference on Earthquake Hazards in the Eastern San Francisco Bay Area, Borchardt, G., Hirschfeld, S.E., Lienkaemper, J.J., McClellan, P., Williams, P.L. and Wong, I.G. (eds.), California Department of Conservation, Division of Mines and Geology, p. 81-89.
- Tuttle, M.P. and Sykes, L.R., 1992, Re-evaluation of several large historic earthquakes in the vicinity of Loma Prieta and peninsular segments of the San Andreas fault, California, *Bulletin of the Seismological Society of America*, v. 82, p. 1,802-1,820.

## Appendix A Seismic Sources

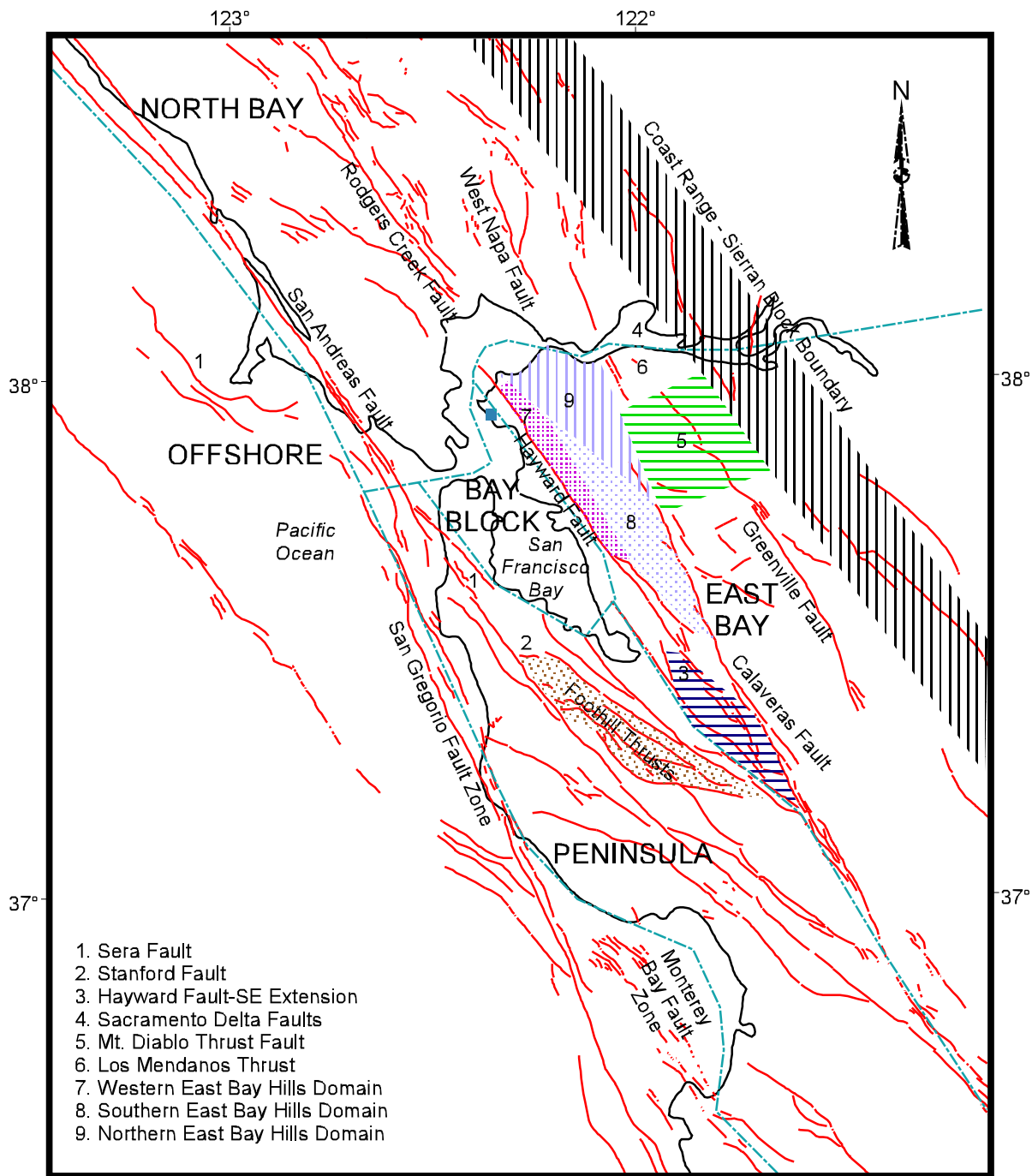
---

- Unruh, J.R. and Hector, S.T., 1999, Subsurface characterization of the Potrero-Ryer Island thrust system, western Sacramento-San Joaquin Delta, northern California, William Lettis and Associates, Inc., Final Technical Report, U.S. Geological Survey, National Earthquake hazards Reduction Program Award No. 1434-HQ-96-GR-02724, 32 p.
- Unruh, J.R. and Lettis, W.R., 1998, Kinematics of transpressional deformation in the eastern San Francisco Bay region, California, *Geology*, v. 26, p. 19-22.
- Unruh, J.R. and Moores, E.M., 1992, Quaternary blind thrusting in the southwestern Sacramento Valley, California, *Tectonics*, v. 11, p. 192-203.
- Unruh, J.R. and Sawyer, T.L., 1995, Late Cenozoic growth of the Mount Diablo fold-and-thrust belt, central Contra Costa County, California, and implications for transpressional deformation of the northern Diablo Range, *Bulletin of the American Association of Petroleum Geologists*, v. 79, p.
- Unruh, J.R. and Sawyer, T.L., 1997, Assessment of blind seismogenic sources, Livermore Valley, eastern San Francisco Bay region, William Lettis and Associates, Inc., Final Report to U.S. Geological Survey National Earthquake Hazards Reduction Program Award No. 1434-95-G-2611, 95 p.
- Unruh, J.R. and Sawyer, T.L., 1998, Paleoseismic investigation of the northern Greenville fault, eastern San Francisco Bay Area, California, William Lettis and Associates, Inc., Final Technical Report, National Earthquake Hazards Reduction Program Award No. 1434-HQ-97-GR-03146, 34 p.
- Unruh, J.R., Hector, S.T., Williams, P.L. and Rector, J.W., 1997, Transpressional tectonics of the western Sacramento-San Joaquin delta, eastern San Francisco Bay region, California, *EOS, Transactions of the American Geophysical Union, Supplement*, v. 78, p. F631.
- Unruh, J.R., Simpson, G.D., Hitchcock, C.S. and Lettis, W.R., 1997, Seismotectonic evaluation Stony Gorge and East park Dams, Orland Project, Monticello Dam, Solano Project, North Coast ranges, California, William Lettis & Associates, Inc., Final Report prepared for U.S. Bureau of Reclamation 145 p.
- URS Corporation, 2001, Deterministic and probabilistic seismic hazard analyses, Folsom Dam, central California, unpublished report prepared for U.S. Army Corps of Engineers.
- Wagner, D.L. and Bortugno, E.J., 1982, Geologic map of the Santa Rosa quadrangle, California Division of Mines and Geology, Regional Geologic Map Series No. 2A, 1:250,000.
- Wakabayashi, J. and Sawyer, T.L., 1998, Paleoseismic investigation of the Miller Creek fault, eastern San Francisco Bay Area, California, Final Technical Report, U.S. Geological Survey National Earthquake Hazards Reduction Program Award No. 1434-HQ-96-GR-02724, 17 p.
- Wakabayashi, J. and Smith, D.L., 1994, Evaluation of recurrence intervals, characteristic earthquakes and slip-rates associated with thrusting along the Coast Range-Central Valley geomorphic boundary, *Bulletin of the Seismological Society of America*, v. 84, p. 1960-1970.
- Wallace, R.E., 1990, The San Andreas Fault System, California, U.S. Geological Survey, Professional Paper 1515, 283 p.
- Weber-Band, J., 1998, Neotectonics of the Sacramento-San Joaquin Delta area, east-central Coast Ranges, California, Unpublished Ph.D., University of California, Berkeley, 216 p.

## Appendix A Seismic Sources

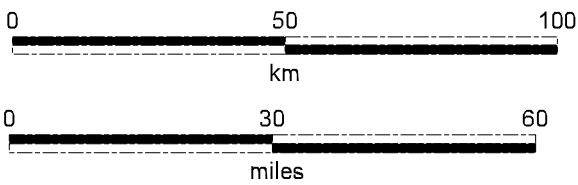
---

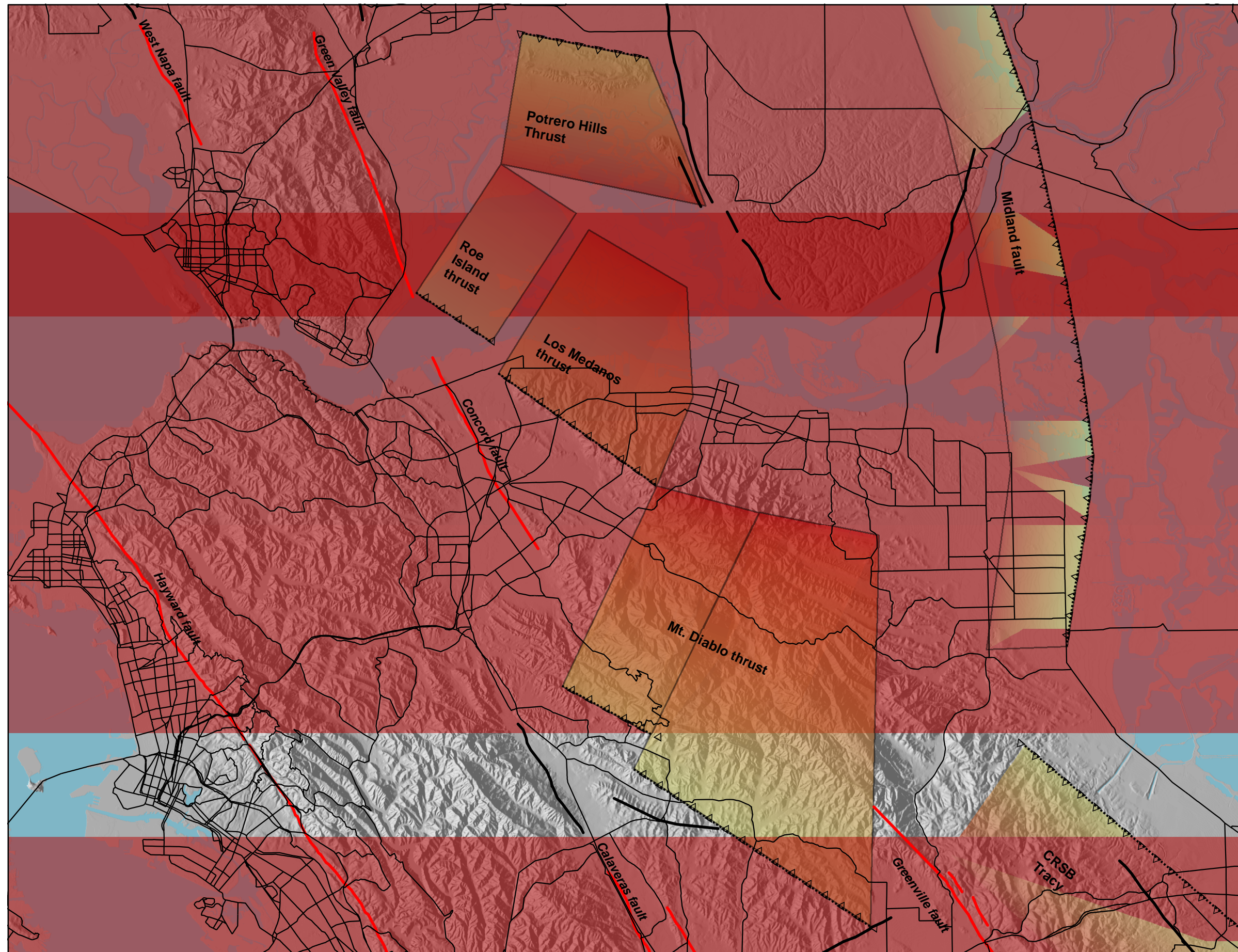
- Wells, D.L. and Coppersmith, K.J., 1994, New empirical relationships among magnitude, rupture length, rupture width, rupture area, and surface displacement, *Bulletin of the Seismological Society of America*, v. 84, p. 974-1002.
- Wesnousky, S.G., 1986, Earthquakes, Quaternary faults, and seismic hazard in California, *Journal of Geophysical Research*, v. 91, p. 12,587-12,631.
- Wills, C.J., Snyder, D.L. and Borchardt, G., 1994, Preliminary results of paleoseismic studies of the Concord fault at Galindo Creek, Concord, California, *in* Proceedings of the Workshop on Paleoseismology, 18-22 September 1994, Marshall, California, Prentice, C.S., Schwartz, D.P. and Yeats, R.S. (eds.), U.S. Geological Survey Open-File Report 94-568, p. 200-201.
- Wong, I.G., 1990, Seismotectonics of the Coast Ranges in the vicinity of Lake Berryessa, northern California, *Bulletin of the Seismological Society of America*, v. 80, p. 935-950.
- Wong, I.G., 1991, Contemporary seismicity, active faulting and seismic hazards of the Coast Ranges between San Francisco Bay and Healdsburg, California, *Journal of Geophysical Research*, v. 96, p. 19,891-19,904.
- Wong, I.G., Ely, R.W. and Kollmann, A.C., 1988, Contemporary seismicity and tectonics of the Northern and Central Coast Ranges-Sierran Block Boundary zone, California, *Journal of Geophysical Research*, v. 93, p. 7,813-7,833.
- Woodward-Clyde Consultants, 1994, Seismic hazard evaluation, geotechnical detailed design report, Utah Copper Tailings Modernization, North Expansion, Revision 6, Appendix A, unpublished report prepared for KUC and Morris Knudsen Corporation.
- Working Group on California Earthquake Probabilities, 1999, Earthquake probabilities in the San Francisco Bay region: 2000 to 2030 - A summary of findings, U.S. Geological Survey, Open-File Report 99-517, 38 p.
- Working Group on Northern California Earthquake Potential, 1996, Database of potential sources for earthquakes larger than magnitude 6 in northern California, U.S. Geological Survey, Open-File Report 96-705, 53 p.
- Wright, R.H., Hamilton, D.H., Hunt, T.D., Traubenik, M.L. and Shlemon, R.J., 1982, Character and activity of the Greenville structural trend, *in* Proceedings. Conference on Earthquake Hazards in the Eastern San Francisco Bay Area, Hart, E.W., Hirschfeld, S.E. and Schulz, S.S. (eds.), California Division of Mines and Geology, Special Publication 62, p. 187-196.
- Youngs, R.R. and Coppersmith, K.J., 1985, Implications of fault slip rates and earthquakes recurrence models to probabilistic seismic hazard estimates, *Bulletin of the Seismological Society of America*, v. 75, p. 939-964.
- Zoback, M.L., Jachens, R.C. and Olson, J.A., 1999, Abrupt along-strike change in tectonic style: San Andreas fault zone, San Francisco peninsula, *Journal of Geophysical Research*, v. 104, p. 10,719-10,742.



- 1. Sera Fault
- 2. Stanford Fault
- 3. Hayward Fault-SE Extension
- 4. Sacramento Delta Faults
- 5. Mt. Diablo Thrust Fault
- 6. Los Mendanos Thrust
- 7. Western East Bay Hills Domain
- 8. Southern East Bay Hills Domain
- 9. Northern East Bay Hills Domain

 Fault Domain Boundary  
 Fault



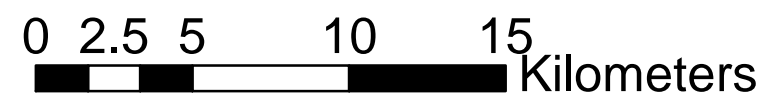
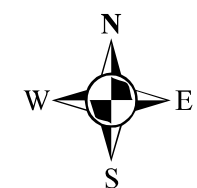


# Legend

## Thrust fault

Thrust fault:  
 ..▲.....▲  
 bars on hanging  
 wall. Darker shading  
 indicates down-dip  
 extent.

———— Strike-slip fault



In-Delta Storage  
 26814105

Local Seismic Sources

Figure  
 2

Table A-1. Fault Parameters

Fault Name	Probability of Activity <sup>1</sup>	Rupture Scenario <sup>2</sup>	Segment Name	Length <sup>3</sup>	Width <sup>4</sup>	Dip <sup>5</sup>	Direction of Dip <sup>6</sup>	Sense of Slip <sup>7</sup>	Magnitude <sup>8</sup>	Slip Rate <sup>9</sup>	Notes
San Andreas	1.0	Unsegmented (0.2)	1906	474 ± 25	15 ± 3	90	N/A	SS	8.1 7.9	24 ± 5	Characterization of the SAF based on Working Group on California Earthquake Probabilities (1999). Unsegmented rupture scenario is a repeat of the 1906 M <sub>w</sub> 7.9 San Francisco earthquake.
		Two Segments (0.05)	North Coast	327 ± 11	15 ± 3	90	N/A	SS	7.7 7.6	24 ± 5	
			Peninsula + Santa Cruz Mountains	147 ± 13	15 ± 3	90	N/A	SS	7.5 7.4	17 ± 4	
		Three Segments (0.6)	North Coast	327 ± 11	15 ± 3	90	N/A	SS	7.7 7.6	24 ± 5	
			Peninsula	85 ± 13	15 ± 3	90	N/A	SS	7.3 7.1	17 ± 4	
			Santa Cruz Mountains	62 ± 8	15 ± 3	90	N/A	SS	7.2 7.0	17 ± 4	
		Four Segments (0.1)	North Coast North	137 ± 11	15 ± 3	90	N/A	SS	7.5 7.3	24 ± 5	
			North Coast South	190 ± 11	15 ± 3	90	N/A	SS	7.7 7.5	24 ± 5	
			Peninsula	85 ± 13	15 ± 3	90	N/A	SS	7.3 7.1	17 ± 4	
			Santa Cruz Mountains	62 ± 8	15 ± 3	90	N/A	SS	7.2 7.0	17 ± 4	
		Floating Earthquake (0.05)	N/A	N/A	15 ± 3	90	N/A	SS	6.9	24 ± 5	
San Gregorio	1.0	Unsegmented (0.2)	Northern + Southern San Gregorio	175 ± 13	15 ± 3	90	N/A	SS	7.6 7.5	1 (0.2) 3 (0.4) 7 (0.4) 10 (0.1)	Characterization of SGF based on WGCEP (1999) model.
		Segmented (0.7)	Northern San Gregorio	109 ± 13	15 ± 3	90	N/A	SS	7.4 7.3	7 ± 3	
			Southern San Gregorio	66 ± 10	15 ± 3	90	N/A	SS	7.2 7.0	3 ± 2	
		Floating Earthquake (0.1)	N/A	N/A	15 ± 3	90	N/A	SS	6.9	1 (0.2) 3 (0.4) 7 (0.4) 10 (0.1)	
		Hayward – Rodgers Creek	1.0	Dependent (0.2)	Hayward + Rodgers Creek	150 ± 9	15 ± 3	90	N/A	SS	
North Hayward + Rodgers Creek	98 ± 9				15 ± 3	90	N/A	SS	7.4 7.2	9 ± 2	
Southern Hayward	52 ± 9				15 ± 3	90	N/A	SS	7.1 6.9	9 ± 2	
Independent (0.2)	Rodgers Creek			63 ± 9	15 ± 3	90	N/A	SS	7.2 7.0	9 ± 2	
	Hayward			87 ± 9	15 ± 3	90	N/A	SS	7.3 7.2	9 ± 2	

Table A-1. Fault Parameters

Fault Name	Probability of Activity <sup>1</sup>	Rupture Scenario <sup>2</sup>	Segment Name	Length <sup>3</sup>	Width <sup>4</sup>	Dip <sup>5</sup>	Direction of Dip <sup>6</sup>	Sense of Slip <sup>7</sup>	Magnitude <sup>8</sup>	Slip Rate <sup>9</sup>	Notes
		Independent – 2 Segment Hayward (0.4)	Rodgers Creek	63 ± 9	15 ± 3	90	N/A	SS	7.2 7.0	9 ± 2	
			North Hayward	35 ± 8	15 ± 3	90	N/A	SS	6.9 6.8	9 ± 2	
			Southern Hayward	52 ± 9	15 ± 3	90	N/A	SS	7.1 6.9	9 ± 2	
		Independent – 3 Segment Hayward (0.1)	Rodgers Creek	63 ± 9	15 ± 3	90	N/A	SS	7.2 7.0	9 ± 2	
			North Hayward	35 ± 8	15 ± 3	90	N/A	SS	6.9 6.8	9 ± 2	
			South Hayward	27	15 ± 3	90	N/A	SS	6.8 6.7	9 ± 2	
		Floating Earthquake (0.1)	N/A	N/A	15 ± 3	90	N/A	SS	6.8 6.6	9 ± 2	
		<b>Calaveras</b>	1.0	Unsegmented (0.05)	Northern + Central + Southern Calaveras	118 ± 5	15 ± 3	90	N/A	SS	
Two Segments (0.35)	Northern Calaveras			40 ± 5	15 ± 3	90	N/A	SS	7.0 6.9	6 ± 2	
	South + Central Calaveras			78 ± 5	15 ± 3	90	N/A	SS	7.3 7.1	15 ± 5	
Three Segments (0.45)	Northern Calaveras			40 ± 5	15 ± 3	90	N/A	SS	7.0 6.9	6 ± 2	
	Central Calaveras			59 ± 5	15 ± 3	90	N/A	SS	7.2 7.0	15 ± 5	
	Southern Calaveras			19 ± 5	15 ± 3	90	N/A	SS	6.6 6.5	15 ± 5	
Segment + Floating Earthquake (0.1)	Northern Calaveras			40 ± 5	15 ± 3	90	N/A	SS	7.0 6.9	6 ± 2	
	Floating Earthquake on Central + South Calaveras			78 ± 5	15 ± 3	90	N/A	SS	6.2	15 ± 5	
Floating Earthquake (0.05)	N/A			N/A	15 ± 3	90	N/A	SS	6.2	4 (0.2) 6 (0.4) 15 (0.3) 20 (0.1)	
<b>Concord – Green Valley</b>	1.0			Unsegmented (0.3)	Concord + Green Valley	56 ± 4	15 ± 3	90	N/A	SS	7.1 7.0
		Three Segments (0.1)	Concord	14 ± 4	15 ± 3	90	N/A	SS	6.5 6.4	4 ± 2	
			Southern Green Valley	22 ± 3	15 ± 3	90	N/A	SS	6.7 6.6	5 ± 3	
			Northern Green Valley	20 ± 4	15 ± 3	90	N/A	SS	6.7 6.5	5 ± 3	

Table A-1. Fault Parameters

Fault Name	Probability of Activity <sup>1</sup>	Rupture Scenario <sup>2</sup>	Segment Name	Length <sup>3</sup>	Width <sup>4</sup>	Dip <sup>5</sup>	Direction of Dip <sup>6</sup>	Sense of Slip <sup>7</sup>	Magnitude <sup>8</sup>	Slip Rate <sup>9</sup>	Notes
		Two Segments (0.1)	Concord	14 ± 4	15 ± 3	90	N/A	SS	6.5 6.4	4 ± 2	
			Green Valley	42 ± 4	15 ± 3	90	N/A	SS	7.0 6.8	5 ± 3	
		Two Segments (0.3)	Concord + Southern Green Valley	36 ± 4	15 ± 3	90	N/A	SS	6.9 6.8	5 ± 3	
			Northern Green Valley	20 ± 4	15 ± 3	90	N/A	SS	6.7 6.5	5 ± 3	
		Floating Earthquake (0.2)	N/A	N/A	15 ± 3	90	N/A	SS	6.2	5 ± 3	
<b>Cordelia</b>	1.0	Unsegmented (0.9)	Northern + Southern Cordelia	19 ± 2	15 ± 3	90	N/A	SS	6.6 6.5	0.05 (0.4) 0.6 (0.5) 1.0 (0.1)	Characterization based on paleoseismic data of Kieffer <i>et al.</i> (1994).
			Segmented (0.1)	Northern Cordelia	13 ± 2	15 ± 3	90	N/A	SS	6.5 6.4	
		Southern Cordelia		6 ± 2	15 ± 3	90	N/A	SS	6.2 6.0	0.05 (0.4) 0.6 (0.5) 1.0 (0.1)	
<b>Greenville</b>	1.0	Unsegmented (0.1)	Northern + Central + Southern Greenville	73 ± 8	15 ± 3	90	N/A	SS	7.2 7.1	4.1 ± 1.8	Characterization of the Working Group on California Earthquake Probabilities (1999) modified by paleoseismic data from Sawyer and Unruh (2002).
			Three Segments (0.4)	Northern Greenville	20 ± 8	15 ± 3	90	N/A	SS	6.7 6.5	
		Central Greenville		20 ± 8	15 ± 3	90	N/A	SS	6.7 6.5	4.1 ± 1.8	
		Southern Greenville		33 ± 8	15 ± 3	90	N/A	SS	6.9 6.7	4.1 ± 1.8	
		Two Segments (0.2)	Northern + Central Greenville	40 ± 8	15 ± 3	90	N/A	SS	7.0 6.8	4.1 ± 1.8	
			Southern Greenville	33 ± 8	15 ± 3	90	N/A	SS	6.9 6.7	4.1 ± 1.8	
		Two Segments (0.2)	Northern Greenville	20 ± 8	15 ± 3	90	N/A	SS	6.7 6.5	4.1 ± 1.8	
			Central + Southern Greenville	53 ± 8	15 ± 3	90	N/A	SS	7.1 6.9	4.1 ± 1.8	
Floating (0.1)	N/A	N/A	15 ± 3	90	N/A	SS	6.2	4.1 ± 1.8			
<b>Ortigalita</b>	1.0	Unsegmented (0.3)	Northern + Southern Ortigalita	100 ± 5	15 ± 3	90	N/A	SS	7.4 7.2	0.5 (0.15) 1.0 (0.35) 2.0 (0.35) 2.5 (0.15)	Characterization revised from Working Group on California Earthquake Potential (1996) using recent paleoseismic data from Anderson and Piety (2001).
			Segmented (0.35)	Northern Ortigalita	40 ± 5	15 ± 3	90	N/A	SS	7.0 6.8	
		Southern Ortigalita		60 ± 5	15 ± 3	90	N/A	SS	7.2 7.0	0.2 (0.5) 1.0 (0.5)	

Table A-1. Fault Parameters

Fault Name	Probability of Activity <sup>1</sup>	Rupture Scenario <sup>2</sup>	Segment Name	Length <sup>3</sup>	Width <sup>4</sup>	Dip <sup>5</sup>	Direction of Dip <sup>6</sup>	Sense of Slip <sup>7</sup>	Magnitude <sup>8</sup>	Slip Rate <sup>9</sup>	Notes
		Segmented + Floating Earthquake (0.35)	Northern Ortigalita	40 ± 5	15 ± 3	90	N/A	SS	7.0 6.8	0.5 (0.15) 1.0 (0.35) 2.0 (0.35) 2.5 (0.15)	
			Floating Earthquake on Southern Ortigalita	60 ± 5	15 ± 3	90	N/A	SS	6.7 6.5	0.5 (0.15) 1.0 (0.35) 2.0 (0.35) 2.5 (0.15)	
<b>Mt Oso</b>	0.5	Unsegmented (1.0)	Mt. Oso	25 ± 2	15 ± 2	20	NE	R	6.9 6.7	0.5 (0.15) 1.0 (0.2) 2.0 (0.4) 4.0 (0.2) 6.0 (0.05)	Inferred thrust fault occupying the contractional stepover between the Ortigalita and Greenville faults. NE-dipping geometry inferred from the SW-vergence of the Mt. Oso anticline (J. Unruh, Wm. Lettis and Associates, <i>Pers. Comm.</i> , 2002). Rupture geometry based on a Mt. Diablo analogue. Activity based on slip transfer from the northern Ortigalita to the southern Greenville.
<b>West Napa</b>	1.0	Unsegmented (0.5)	Northern + Southern West Napa	25 ± 2	15 ± 3	90	N/A	SS	6.8 6.6	0.5 (0.2) 1.0 (0.5) 2.0 (0.3)	Characterization based on Working Group on California Earthquake Potential (1996) with modifications based on recent data of J. Wesling, Geomatrix, Inc. ( <i>pers. Comm.</i> , 2001).
		Segmented (0.5)	Northern West Napa	15 ± 2	15 ± 3	90	N/A	SS	6.6 6.4	0.5 (0.2) 1.0 (0.5) 2.0 (0.3)	
		Segmented (0.5)	Southern West Napa	10 ± 2	15 ± 3	90	N/A	SS	6.4 6.2	0.5 (0.2) 1.0 (0.5) 2.0 (0.3)	
<b>Mount Diablo</b>	1.0	Unsegmented (0.5)	North + South Mount Diablo	25 ± 2	15 ± 2	20	NE	R	6.9 6.7	1.0 (0.3) 3.0 (0.5) 5.0 (0.2)	Characterization based on Unruh and Sawyer (1997).
		Segmented (0.5)	North Diablo	10 ± 2	10 ± 2	20	NE	R	6.2 6.1	1.0 (0.3) 3.0 (0.5) 5.0 (0.2)	
		Segmented (0.5)	South Diablo	15 ± 2	15 ± 2	20	NE	R	6.6 6.4	1.0 (0.3) 3.0 (0.5) 5.0 (0.2)	
<b>Los Medanos fold and thrust belt</b>	1.0	Unsegmented (0.2)	Roe Island + Los Medanos	15 ± 5	18 ± 2	30	NE	R	6.6 6.5	0.3 (0.3) 0.5 (0.4) 0.7 (0.3)	Characterization based on Unruh and Hector (1999).
		Segmented (0.8)	Roe Island	5 ± 2	5 ± 2	30	NE	R	5.5 (0.2) 5.75 (0.6) 6.0 (0.2)	0.3 (0.3) 0.5 (0.4) 0.7 (0.3)	
		Segmented (0.8)	Los Medanos	10 ± 2	10 ± 2	30	NE	R	5.75 (0.2) 6.0 (0.6) 6.25 (0.2)	0.3 (0.3) 0.5 (0.4) 0.7 (0.3)	
<b>Potrero Hills</b>	1.0	Unsegmented (1.0)	Potrero Hills	9 ± 2	9 ± 2	30 ± 10	SW	R	5.75 (0.3) 6.0 (0.6) 6.25 (0.1)	0.1 (0.2) 0.3 (0.6) 0.6 (0.2)	Characterization based on Unruh and Hector (1999).

Table A-1. Fault Parameters

Fault Name	Probability of Activity <sup>1</sup>	Rupture Scenario <sup>2</sup>	Segment Name	Length <sup>3</sup>	Width <sup>4</sup>	Dip <sup>5</sup>	Direction of Dip <sup>6</sup>	Sense of Slip <sup>7</sup>	Magnitude <sup>8</sup>	Slip Rate <sup>9</sup>	Notes
<b>Pittsburgh-Kirby Hills</b>	1.0	Strike-Slip Model (0.6)	PKHF	20 ± 5	20 ± 5	90	N/A	SS	6.6 6.7	0.3 (0.4) 0.5 (0.4) 0.7 (0.2)	Model includes both strike-slip (Unruh and Hector, 1999) and reverse (Weber-Band, 1998) models for fault activity. The former is given greater weight based on the focal mechanisms from contemporary seismicity. Seismogenic depth is significantly greater than elsewhere in the Bay Area.
		Reverse Model (0.4)	PFHF	20 ± 5	28 ± 4	60 ± 15	E	R	6.6 6.7	0.1 (0.2) 0.15 (0.6) 0.5 (0.2)	
<b>Midland</b>	0.7	Unsegmented (0.1)	Midland	60 ± 5	15 ± 5	70	W	R	7.1 7.0	0.1 (0.2) 0.15 (0.6) 0.5 (0.2)	Activity is inferred from displacement of late Tertiary (and possibly early Pleistocene) strata in seismic reflection profiles.
		Floating Earthquake (0.9)	Midland	20 ± 10	15 ± 5	70	W	R	6 (0.3) 6.25 (0.4) 6.5 (0.3)	0.1 (0.2) 0.15 (0.6) 0.5 (0.2)	
<b>CRSB North of Delta</b>	1.0	Multisegment (0.1)	Mysterious Ridge	35 ± 5	13 ± 2	25 ± 5	W	R	6.9 6.7	1.0 (0.7) 3.5 (0.3)	Characterization revised from Working Group on California Earthquake Potential (1996) using data from O'Connell <i>et al.</i> (2001).
			Trout Creek + Gordon Valley	38 ± 5	13 ± 2	25 ± 10	W	R	7.0 6.8	0.5 (0.3) 1.25 (0.6) 2.0 (0.1)	
		Independent (0.9)	Mysterious Ridge	35 ± 5	13 ± 2	25 ± 5	W	R	6.9 6.7	1.0 (0.7) 3.5 (0.3)	
			Trout Creek	20 ± 5	13 ± 2	20 ± 5	W	R	6.7 6.5	0.5 (0.3) 1.25 (0.6) 2.0 (0.1)	
			Gordon Valley	18 ± 5	13 ± 2	30 ± 5	W	R	6.5 6.4	0.5 (0.3) 1.25 (0.6) 2.0 (0.1)	
<b>Wragg Canyon</b>	1.0	Unsegmented (1.0)	Wragg Canyon	17 ± 2	15 ± 3	90	N/A	SS	6.6 6.5	0.1 (0.3) 0.3 (0.4) 0.5 (0.3)	Cryptic strike-slip fault inferred by O'Connell <i>et al.</i> (2001).
<b>CRSB South of Delta</b>	1.0	Unsegmented (0.1)	Tracy + Vernalis	69 ± 5	10 ± 2	15	W	R	7.0 6.9	0.7 (0.3) 1.5 (0.4) 2.3 (0.3)	Segmentation based on Wakabayashi and Smith (1994) as modified by Working Group on California Earthquake Potential (1996). Segment characteristics from Sowers and Ludwig (2000) and Wakabayashi and Smith (1994).
		Segmented (0.9)	Tracy	45 ± 5	10 ± 2	15	W	R	6.8 6.7	0.29 (0.1) 0.42 (0.3) 1.0 (0.2) 1.5 (0.2) 2.3 (0.1)	
			Vernalis	24 ± 5	10 ± 2	15	W	R	6.6 6.5	0.7 (0.3) 1.5 (0.4) 2.3 (0.3)	
<b>Foothill thrust belt</b>	1.0	Floating Earthquake (1.0)	N/A	N/A	N/A		SW	R	6.25 (0.3) 6.5 (0.3) 6.75 (0.3) 7.0 (0.1)	0.2 (0.2) 0.5 (0.6) 0.8 (0.2)	Simplified characterization based on WGCEP (1999). Incorporates Berrocal, Shannon-MonteVista, and Cascade faults.
<b>Sargent</b>	1.0	Entire Rupture (1.0)	Sargent	56 ± 5	15 ± 3	45 ± 15	SW	OR	7.1 6.9	1.5 (0.3) 3.0 (0.4) 4.5 (0.3)	Characterization based on Working Group on California Earthquake Potential (1996).

**Table A-1. Fault Parameters**

Fault Name	Probability of Activity <sup>1</sup>	Rupture Scenario <sup>2</sup>	Segment Name	Length <sup>3</sup>	Width <sup>4</sup>	Dip <sup>5</sup>	Direction of Dip <sup>6</sup>	Sense of Slip <sup>7</sup>	Magnitude <sup>8</sup>	Slip Rate <sup>9</sup>	Notes
East Bay Hills	0.5	Western East Bay Hills (1.0)	Floating Earthquake	N/A	N/A	70 ± 15	N/A	R	5.5 (0.4) 6.0 (0.45) 6.5 (0.15)	0.5 (0.2) 1.0 (0.65) 1.5 (0.15)	Characterization based on fault model of the Thrust Fault Sub-Group of the 1999 Working Group on California Earthquake Probabilities (Unruh, <i>unpublished memo</i> ). The WEBH includes the Miller Canyon fault (Wakabayashi and Sawyer (1998)). The NEBH includes the Franklin and Southampton faults; suspected of accommodating slip transfer from the northern Calaveras fault (approx. 3 mm/yr). SEBH incorporates the Mission fault, a blind seismogenic structure that appears to transfer strain between the Calaveras and Hayward faults.
	0.5	Southern East Bay Hills (1.0)	Floating Earthquake	N/A	N/A	45 ± 15	N/A	R	6.25 (0.6) 6.5 (0.4)	0.1 (0.3) 0.3 (0.4) 0.5 (0.2) 1.0 (0.1)	
	1.0	Northern East Bay Hills (1.0)	Floating Earthquake	N/A	N/A	90 ± 20	N/A	R	6.25 (0.3) 6.5 (0.4) 6.75 (0.3)	1.0 (0.6) 2.0 (0.2) 3.0 (0.2)	

<sup>1</sup> Probability of Activity: Holocene or historical activity (1.0); Late Pleistocene or inferred association with historical seismicity (0.7); activity inferred from fault geometry considered likely to move under current tectonic regime (0.5).

<sup>2</sup> Weight assigned according to likelihood of occurrence of rupture scenario.

<sup>3</sup> Rupture length in kilometers. Unless otherwise stated, weights are 0.4 for the best estimate and 0.3 for the upper and lower bound estimates.

<sup>4</sup> Down-dip width of fault rupture. Unless otherwise stated, weights are 0.4 for the best estimate and 0.3 for the upper and lower bound estimates.

<sup>5</sup> Inclination of fault plane, measured from the horizontal. Unless otherwise stated, weights are 0.4 for the best estimate and 0.3 for the upper and lower bound estimates.

<sup>6</sup> Direction of inclination of the fault plane. N/A infers a vertical fault plane.

<sup>7</sup> SS – strike-slip; R – reverse; OR – oblique-reverse.

<sup>8</sup> Unless otherwise stated, magnitude estimates are weighted equally (0.5 each).

<sup>9</sup> Slip rate based on paleoseismic data. Unless otherwise stated, weights are 0.4 for the best estimate and 0.3 for the upper and lower bound estimates.